Coordination Chemistry Reviews 445 (2021) 214008

Contents lists available at ScienceDirect

Coordination Chemistry Reviews

journal homepage: www.elsevier.com/locate/ccr

Review

Nuclear imaging for immune cell tracking *in vivo* – Comparison of various cell labeling methods and their application

Łukasz Kiraga [a,b], Paulina Kucharzewska [a,b], Stephen Paisey [c], Łukasz Cheda [d], Anita Domańska [e], Zbigniew Rogulski [d], Tomasz P. Rygiel [b,f], Alberto Boffi [g], Magdalena Król [a,b,*]

[a] Department of Cancer Biology, Institute of Biology, Warsaw University of Life Sciences, 02-787 Warsaw, Poland
[b] Cellis AG, Bleicherweg 45, 8002 Zurich, Switzerland
[c] Wales Research & Diagnostic PET Imaging Centre (PETIC), School of Medicine, Heath Park, Cardiff University, Cardiff CF14 4XN, UK
[d] Faculty of Chemistry, Biological and Chemical Research Centre, University of Warsaw, 02-089 Warsaw, Poland
[e] Centre of Postgraduate Medical Education, Department of Clinical Neuroendocrinology, 01-813 Warsaw, Poland
[f] Department of Immunology, Medical University of Warsaw, 02-097 Warsaw, Poland
[g] Department of Biochemical Sciences "Alessandro Rossi Fanelli", Sapienza University of Rome, 00-185 Rome, Italy

ARTICLE INFO

Article history:
Received 28 September 2020
Received in revised form 22 March 2021
Accepted 26 April 2021

Keywords:
Nuclear imaging
SPECT
PET
Radiotracers
Immune cell tracking
Cell labeling

ABSTRACT

There is currently great interest in the development of cell-based therapies, particularly those focused on the idea of exploiting systemically administered immune cells for therapeutic purposes in cancer (*e.g.*, CAR-T and CAR-NK cells). The ability to monitor the fate of cells *in vivo* after administration is vital for the assessment of therapeutic outcomes of immune cell-based therapies both in preclinical research and clinical practice. In this context, imaging techniques, which allow for noninvasive and real-time monitoring of the distribution and long-term viability of the adoptively transferred immune cells in the tissue of interest, are of paramount importance. Among clinically relevant *in vivo* imaging modalities, the nuclear imaging techniques, comprising planar scintigraphy, SPECT, and PET, are considered to be of pivotal importance to *in vivo* cell tracking and designing optimal treatment strategies for cell-based therapies. This review paper focuses on nuclear imaging and its role in the evaluation of immune cell-based therapies' effectiveness - tracking cells and their ability to home to the target tissue. We compare different types of radiotracers, outline various ways of immune cell labeling, and provide the latest examples for the use of nuclear imaging techniques both in preclinical studies and clinical settings.

Contents

* Corresponding author at: Department of Cancer Biology, Institute of Biology, Warsaw University of Life Sciences, Nowoursynowska 166, 02-787 Warsaw, Poland.
E-mail address: magdalena_krol@sggw.edu.pl (M. Król).

https://doi.org/10.1016/j.ccr.2021.214008
0010-8545/

1. Introduction

Adoptive transfer of immune cells for inflammatory and neoplastic diseases is the subject of intense clinical research. So far, methods involving the administration of different types of autologous lymphocytes have shown great potential to treat different diseases. Such a therapeutic approach is especially promising in the treatment of cancer [1,2] as well as other disease conditions, including allergies, infections, and inflammation [3–5]. The type of immune cells to be selected for the adoptive therapy depends on the treated pathology. Among diverse immune cells tested so far, T cytotoxic lymphocytes (CTLs), T regulatory lymphocytes (Tregs), natural killer (NK) cells, monocytes, macrophages, eosinophils, neutrophils, and dendritic cells (DCs) all appear to play an emerging role.

Inarguably, the efficacy of cell-based therapies depends on the successful targeting of pathological lesions by the adoptively transferred cells. When considering novel approaches to this kind of treatment, the targeting efficiency of selected cells to the pathological lesion should be evaluated first. In this context, molecular imaging techniques, which enable noninvasive and real-time monitoring of the cell distribution in the tissues of interest, take center stage, as they provide key information on the long-term survival of the adoptively transferred immune cells. Among clinically relevant *in vivo* imaging modalities, the nuclear imaging techniques, comprising planar scintigraphy, SPECT, and PET, are considered to be of pivotal importance to *in vivo* cell-tracking as they can afford the design of optimal treatment strategies for cell-based therapies. Tracking of immune cells with nuclear imaging has been used for a long time in routine medical practice for diagnostic purposes in infections and inflammation [5]. Immune cell labeling for cell tracking with nuclear imaging can be accomplished with direct or indirect methods. Direct methods involve the labeling of immune cells with radiotracers *in vitro* before cell transfer, whereas indirect labeling relies on the introduction of a reporter gene into immune cells to induce an additional function that makes the cells uniquely targetable by a specific radiotracer *in vivo* after cell transfer. In this Review, we provide the description of various nuclear imaging modalities in the context of live tracking of immune cells, outline immune cell labeling methods, and underline the latest examples for the use of nuclear imaging techniques both in preclinical and clinical research.

2. Nuclear imaging overview

Nuclear imaging is routinely employed in medical practice to assess disease severity and treatment effect. It involves oral, intravenous, or inhalation administration of small doses of a radiopharmaceutical (radiotracer), which consists of a short-lived gamma-emitting radionuclide conjugated to a chemical probe, capable of targeting the desired cellular or molecular process with high affinity and selectivity. The ionizing radiation thus emitted is then measured and imaged using an imaging device. The spatial resolution coupled to the capabilities of the probes to interact with specific cellular targets classify nuclear imaging among the molecular imaging techniques. Radioisotope-based imaging is commonly used for diagnostic purposes in cancer as well as in neurological, cardiovascular, gastrointestinal diseases, and cysts in kidneys [6–9]. In addition to diagnostic applications, nuclear imaging can also be selected to treat certain cancers such as non-Hodgkin lymphoma and thyroid-related tumors by radio-immunotherapy [10]. Nuclear imaging has become the most attractive and powerful modality for molecular imaging in personalized cancer therapy. Considering the type of image obtained, we can distinguish two groups of nuclear imaging techniques: planar (2D) gamma scintigraphy and spatial (3D) methods, including single-photon emission computed tomography (SPECT) and positron emission tomography (PET).

Nuclear imaging offers a range of important benefits in preclinical and clinical research, which lead to its routine use in many clinical applications. Primarily, nuclear imaging techniques are extremely sensitive to injected tracers compared to magnetic resonance imaging (MRI) and computed tomography (CT)-based techniques maintaining at least a similar level of sensitivity as optical imaging methods. Radiation detectors can detect picomolar concentrations of radiotracers. This sensitivity allows the use of subpharmacological quantities of radiotracers, avoiding the risk of biological side effects. Secondly, nuclear imaging is non-invasive and therefore can be applied in series to identify the longitudinal run of certain processes (*e.g.*, reaction to the implemented therapy). Thirdly, thanks to suitable image analysis techniques, both PET and SPECT allow quantitative data to be obtained, such as the concentration of radiotracers in certain regions or volumes of interest (ROI/VOI). Fourthly, a great number and diversity of radiopharmaceuticals such as metabolites and their analogs, ligands for specific receptors, or antibodies are still being developed to provide an ever more accurate and relevant characterization of biological phenomena *in situ* [11–13]. However, nuclear imaging has its flaws. One of them is a moderate spatial resolution that ranges from ~2 mm to ~6 mm for PET or more for SPECT and is much worse than that of CT and MRI. Furthermore, nuclear imaging, by definition, is based on radioactive decay, and provides patients with low, but probably not insignificant, doses of radiation [14,15]. Finally, nuclear imaging delivers images with imprecise anatomical information, which may make their interpretation and analysis difficult. However, nowadays this limitation can be overcome by combining it with different imaging techniques, such as CT or MRI, which show anatomical structures in greater detail. Thanks to the widespread use of hybrid imaging methods such as SPECT/CT, PET/CT, and even PET/MRI, which are currently accessible at the clinical and preclinical level, it is feasible to obtain detailed functional and anatomical information during one study.

2.1. Nuclear imaging modalities

Planar gamma scintigraphy measures and images the location of the radiotracer in one 2D image. The signals from an array of photomultipliers in a gamma detector are transmitted to the position-coding matrix and reconstructed on an oscilloscope screen. In such a manner, the distribution and accumulation of the radiolabeled probe in the organism are visualized [16]. For dynamic imaging, multiple "frames" of images between 1 s (beginning) and 1 min

(end) each, are usually obtained for 30–40 min following the radiotracer's injection [17]. Planar gamma scintigraphy, routinely employed in the last decades, is now commonly utilized in medical practice. In specific clinical scenarios, it is used for the diagnosis of patients with suspected infections and inflammatory processes. However, it has now been replaced to a large degree by the tomographic modalities: SPECT and PET.

SPECT is a modification of the classic gamma camera imaging. The SPECT principle is based on the detection of gamma rays with energy within a certain range (specific to each isotope), as opposed to PET, which only detects 511 keV gamma rays. The imaging is carried out by a gamma detector, which obtains a set of two-dimensional projection images at different angles. Typically, one, two, or three detectors or heads are slowly rotated around the patient's body, while acquiring the information needed to reconstruct 3D images. Usually, clinical cameras have a resolution between 7 and 15 mm and preclinical devices between 0.8 and 1.5 mm. Usually, the SPECT tool is combined with CT and it applies a specific algorithm to reconstruct the projection data, to generate a spatial image of the administered radioisotope distribution. Pinhole collimators at a distance of several centimeters from the detector are often used for imaging small animals as they enable magnification of the image on the detector achieving very high resolutions, even sub-millimeter: 0.25–0.6 mm [18], at the expense of a reduction in detector sensitivity. An important advantage of SPECT is the possibility that multiple radioisotopes can be imaged at the same time thanks to the ability to detect photons of different energies. Therefore, several different cell populations, each labeled with a different radioisotope, can be tracked during the same imaging procedure [19].

PET imaging records gamma photons generated during the annihilation of positrons (β^+). The sources of positrons are the β^+-decayed radioisotopes. Emitted positrons, after a free path of not more than a few millimeters, collide with electrons in body tissues, leading to the annihilation of the positron and the electron [20]. The annihilation event produces two photons, each of energy 511 keV, moving in opposite directions from each other (at an angle of 180°). The angle can be slightly different due to the result of kinetic motion (like Fermi motion). This has a significant impact on resolution, especially with large-diameter (distances between opposite detectors) scanners [21]. The photons are detectable by the use of a PET camera, which is composed of an array of crystal sensors usually in a ring configuration surrounding the sample or patient. The coincidence detection mechanism searches for pairs of photons detected within about a 10 ns coincidence window on opposing sections of the detector at different angles around the object, enabling the precise determination of the positron formation point. After reconstruction to localize the points where the annihilation occurred, the 3D visualization of the isotope distributed in the organism is possible. Importantly, PET acquisition time is shorter than in the case of SPECT, due to a combination of the static ring detector sampling all radial lines of response simultaneously, and the fact that sensitivity is increased as collimation is not required. This feature allows reliable dynamic imaging to be performed, which allows pharmacokinetic modeling of the radiotracer to calculate rates of uptake, binding affinities, and receptor densities in tissues. The spatial resolution, which is measured as total width at half maximum, is usually about 2–6 mm, while preclinical animal scanners reach a resolution of 0.3–2 mm [16]. According to the quantitative ability of imaging modalities, PET is considered as the most valuable technique in this regard. A very high level of signal quantification accuracy is required especially in the case of cell-tracking studies, therefore in this context PET seems to be the preferred tool [22]. However, although SPECT scanners usually have lower spatial resolution and sensitivity in comparison to PET and clinical applications of quantitative SPECT imaging are lacking due to the insufficient availability of accurately calibrated SPECT reconstructions, currently produced SPECT instruments often exhibit quantitative ability comparable to PET. Routine corrections for resolution recovery, photon attenuation and scattering, radioactive decay, cross-calibration, and instrumental dead time are applied to enable quantitative SPECT analyses [23,24]. Nevertheless, detailed quantitative studies are nowadays performed mainly by using PET. A schematic presentation of the SPECT and PET scanners and their imaging modalities is shown in Fig. 1. In Table 1, the schematic mechanisms of action and main differences between SPECT and PET imaging techniques are given. For a thorough comparison of SPECT and PET imaging, the interested reader is referred to the additional review articles [11,19,25].

The technique called "whole-body counter" also deserves mention, although it does not provide an image in the full sense of the word. In this method, high-sensitivity scintillation probes are moved along the patient's body, generating a quantitative profile of radioactivity from certain regions. The counter is isolated from the background radiation, which results in high sensitivity in the detection of photons, making it possible to administer radiotracers at very low activity.

2.2. Radioisotopes for nuclear imaging

There are a number of conditions that need to be satisfied for a radioisotope to be suitable for *in vivo* imaging. The unbound radioisotope and its decay products, which are commonly different elements from the parent isotope, must not exhibit any toxicity at clinical doses. The satisfaction of this criterion is helpfully aided by the extremely high sensitivity of nuclear imaging modalities, with just picomoles of radiotracer required for typical clinical doses. The radioisotope must also be capable of readily forming biologically active compounds or complexes that are soluble and chemically stable in biological conditions. In addition to these standard biochemical requirements for pharmaceutical agents, a radioisotope must also have favorable radioactivity properties. It must be possible to produce and isolate the radioisotope in high radiochemical purity with a high specific activity. The high radiochemical purity is important because any alternative radioisotopes present in the sample will cause spurious signals in the images and interfere with the interpretation of the images. The high specific activity is important because high levels of non-radioactive isotopes of the element can interfere with tracer synthesis and can lead to the inadvertent co-administration of non-radioactive versions of the tracer which are not detected by the scanner but act as 'cold' blocking agents hindering the uptake of the radiotracer. Also, the radioisotope must emit radiation that penetrates enough to leave the body to enable its external detection. These are most commonly single gamma rays in the case of planar gamma scintigraphy and SPECT imaging or the pair of 511-keV annihilation gamma rays emitted during positron (β^+) decay employed in PET imaging. Ideally, non-penetrating radiation, *i.e.* particulate radiation, including electrons (apart from positrons relevant for PET) and β^- particles, should only be emitted in small amounts by imaging radionuclides. This is because particulate radiation does not leave the body and cannot be measured with external detectors, but will still contribute to the radiation dose experienced by the tissues. Importantly, the imaging radioisotope should have a radioactive half-life comparable with the biological half-life of the probe, allowing for the radiotracer to reach the tissue of interest while still preserving an optimal imaging signal. In this way, patients can be exposed to minimal radiation dose. Table 2 summarizes the relevant physical properties of single-photon and positron-emitting radionuclides commonly used in nuclear imaging.

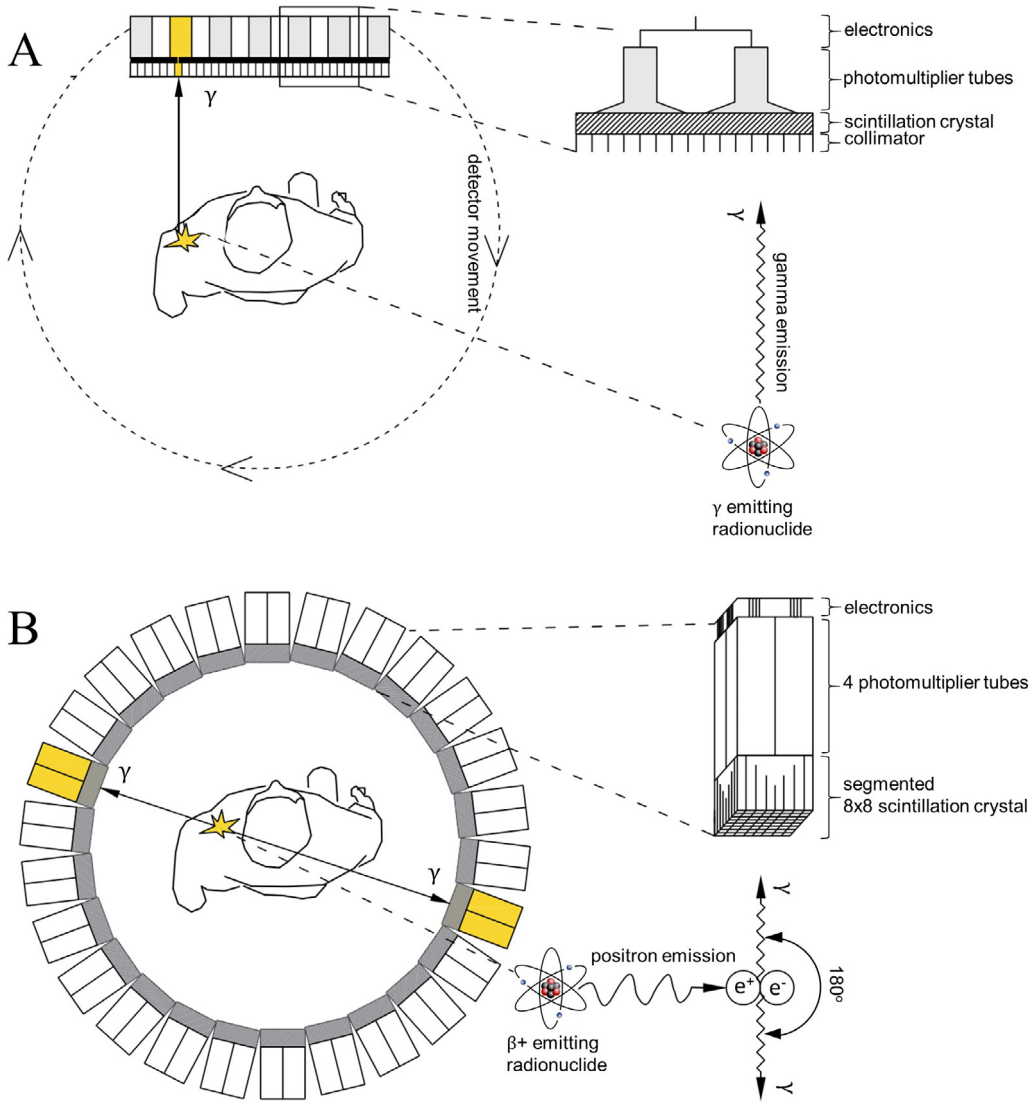

Fig. 1. Schematic presentation of the SPECT and PET scanners and their imaging modalities.

The ideal radioisotope for planar gamma scintigraphy and SPECT should emit gamma and X rays with 100–200 keV energies at 100% abundance. Additionally, it should emit only marginal amounts of particulate radiation or high energy gamma and X rays with energies above several hundred keV, which are not efficiently collimated and detected. By giving off only a 140-keV gamma-ray and few particulate radiations, technetium-99 m ([^{99m}Tc]) is an almost ideal radioisotope for planar gamma scintigraphy and SPECT imaging. The latest devices allow obtaining full-width at half-maximum (FWHM) value of less than 0.4 mm for [^{99m}Tc] in the center of Field of View (FOV) [18,26]. Unlike [^{99m}Tc], iodine-131 ([^{131}I]), for example, emits high-energy (364 keV) gamma rays and high amounts of β^- particles, allowing the compound to exhibit both diagnostic and therapeutic properties. The spatial resolution of SPECT images is influenced by many factors including the energy of photons emitted by the radioisotope, the number and shape of pinholes in collimators, and the type of detector. The use of radionuclides with energy values of gamma rays significantly different from technetium clearly affects the sensitivity of the device and parameters of the acquired image [26]. However, modern devices using collimators of greater thickness and varied geometry allow the use of isotopes with the higher energy of emitted gamma radiation, even exceeding the values used in PET technique. Thus, the proper selection of collimators makes it possible to keep the FWHM value at a relatively constant level when using radioisotopes emitting energies in the range 100–500 keV [27–29]. The relationship is not obvious when considering the influence of the emitted energy on the labeled cells. In addition to the value of the photon energy, the potentially harmful effect on cells is also influenced by the type of corpuscular radiation associated with the photon emission and the radio-sensitivity of the investigated cells.

The most frequently used SPECT radioisotopes have a half-life between 6 h and 8 days, which allows images to be acquired over a moderately long time scale. Additionally, SPECT radionuclides are more commonly available than PET radionuclides because SPECT radionuclides are usually eluted from a small portable generator. In turn, most PET isotopes can only be produced on a cyclotron, which means that large-scale infrastructure is required to produce them, making them much more expensive. The average cost of SPECT radiopharmaceuticals is about ten times lower than those for PET [30].

Numerous PET radionuclides may be incorporated into the imaging tracers. The ideal radionuclide for PET imaging should

Table 1
Differences in SPECT and PET imaging techniques with emphases on values of each one.

SPECT	PET
Resolution range of clinical devices: 7–15 mm	Resolution range of clinical devices: 2–6 mm ✓
Resolution range of preclinical devices: 0.25–1.5 mm ✓	Resolution range of preclinical devices: 0.3–2 mm
Long acquisition time – dynamic imaging/kinetic modeling is impractical	Short acquisition time – dynamic imaging/kinetic modeling is efficient ✓
Various values of gamma rays' energy can be detected (but in the range between 20 and 511 keV) - several radiotracers can be applied at one time (multi-tracer imaging) ✓	Only 511 keV radiation energy is detectable – only a single radiotracer can be applied
Most of the available radiotracers are long-lived ✓	Most of the radiotracers are short-lived, however, several long-lived are available too
Requires administration of higher radiotracer's radioactivity	Requires administration of lower radiotracer's radioactivity ✓
Relatively cheap ✓	Relatively expensive
Generator production of the most commonly used radioisotope (^{99m}Tc) make them widely available ✓	Cyclotron production of the most commonly used radioisotopes (including ^{18}F-FDG) limit the availability
Usually lower quantitative ability compared to PET	Excellent quantitative ability ✓

emit short-range, low-energy positrons with an abundance of 100%, and lack of gamma rays with energies close to the 511 keV, generated during positron annihilation. Fluorine-18 [^{18}F], for example, is such a PET radionuclide, and thus radiotracers tagged with this radioisotope exhibit the most favorable features for PET imaging, however, with a half-life of 109.8 min is only effective for imaging up to a few hours after administration. Thus, for specific applications that require longer term tracking of administered agents, including some which are routinely clinically applied for SPECT imaging, alternative isotopes with longer half-lives are required. When considering the choice of an isotope, it is important to consider the radiation dose to the patient, as longer exposure times to a given amount of radioactivity will lead to a higher overall radiation dose. As a result, the best practice is to select radioisotopes with half-lives that are tailored to the optimum biodistribution time of the proposed radiotracer. Additionally, overall patient radiation dose for tracers based on longer lived isotopes can be reduced by minimizing the total amount of injected activity although this requires compensation through the use of modern measuring devices or extension of scan acquisition time. Also - unlike [^{18}F], many radioisotopes, such as gallium-68 [^{68}Ga], zirconium-89 [^{89}Zr], and iodine-124 [^{124}I], release large amounts of high-energy prompt gamma rays that may cause scattering artifacts in the positron energy range thus leading to suboptimal overall quality and quantitative accuracy of PET imaging. Despite these drawbacks, there is still a role for radionuclides other than [^{18}F] and many have been successfully used in PET imaging [12,13,31,32]. Most commonly used PET isotopes are produced employing a cyclotron apparatus, and are usually short-lived isotopes in comparison to SPECT isotopes. Isotope lifetime may thus represent a key issue to be addressed as a function of the desired probe effect. Adequate time period must be provided for the radioisotopes in medicine for diagnostic tests in order to lose their radioactivity through natural decay, and the shorter the half-life the sooner this point will be achieved. In addition, it may be preferable to minimize the radiation dose delivered to the patient during the test or it might be desirable to repeating the test at intervals without concern for residual activity in the body from the previous test. On these accounts, a short-lived radioisotope might be preferable to a long-lived one. In contrast, in several specific cases, the short half-life of some of the most commonly exploited PET radioisotopes may hinder long-term monitoring of the radionuclide fate inside the body. The recent development of long-lived positron emitters, including copper-64 [^{64}Cu], [^{89}Zr], [^{124}I], and vanadium-48 [^{48}V] have paved the way for new applications of PET imaging such as the long term tracking radiolabeled cells to be explored.

3. Labeling strategies of immune cells for tracking *in vivo* with nuclear imaging

Live tracking of immune cells using nuclear imaging involves the detection of radioisotope-labeled cells. There are two major cell labeling techniques for nuclear imaging: i) direct cell labeling with radiotracers or ii) indirect cell labeling involving the expression of an imaging reporter gene in target cells.

3.1. Direct cell labeling

Radiotracer-based direct labeling of immune cells is usually applied in the context of nuclear imaging. It is a quite straightforward technique that is performed under *in vitro* conditions with little influence on cell behavior, including cell viability and migration [8,18,20,24]. There are different types of radiotracers suitable for cell labeling, sharing one basic physical property consisting of a radionuclide that emits externally detectable radiation. The radiotracers, used for direct cell labeling, may be incorporated into the

Table 2
List of radionuclides routinely used for planar gamma-scintigraphy/SPECT or PET and their characteristics.

	Radionuclide	$T_{1/2}$	Decay	E_{max} (keV)	Production method
planar gamma scintigraphy/SPECT(gamma emitters)	[^{99m}Tc]; Technetium-99 m	6.01 h	IT, β^-	140	Generator
	[^{123}I]; Iodine-123	13.22 h	EC, β^-	159	Cyclotron
	[^{111}In]; Indium-111	2.80 days	EC	171, 245	Cyclotron
	[^{131}I]; Iodine-131	8.02 days	β^-	364	Reactor
PET (positron emitters)	[^{11}C]; Carbon-11	20.38 min	β^+	961	Cyclotron
	[^{68}Ga]; Gallium-68	67.71 min	EC, β^+	1899	Generator + cyclotron
	[^{18}F]; Fluorine-18	109.77 min	EC, β^+	634	Cyclotron
	[^{64}Cu]; Copper-64	12.70 h	EC, β^+, β^-	656	Cyclotron
	[^{89}Zr]; Zirconium-89	78.41 h	EC, β^+	900	Cyclotron
	[^{124}I]; Iodine-124	4.18 days	EC, β^+	2100	Cyclotron

IT - isomeric transition; EC - electron capture; β^-- beta decay, β^+- positron decay.

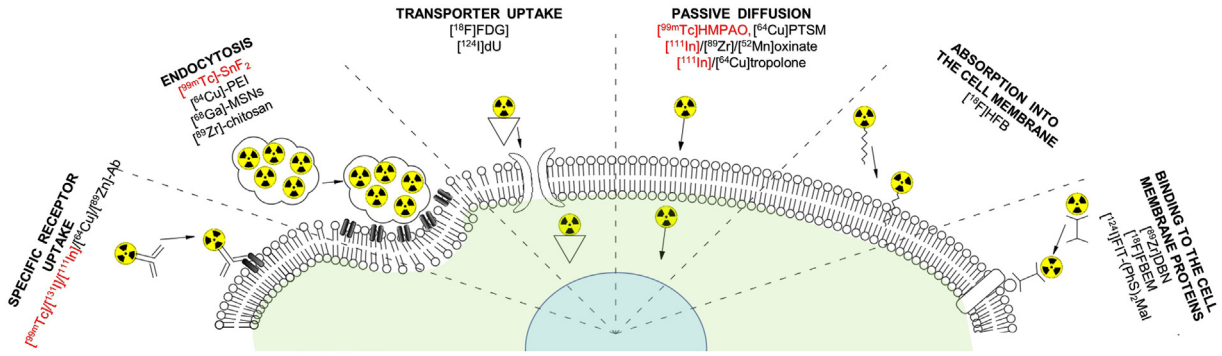

Fig. 2. Diagram of different direct cell labeling processes, with examples of radiotracers. SPECT radiotracers are listed in red font and PET radiotracers in black font.

cell through different processes, and under this criterion, we may divide them into a few groups [10,16,33,34]:

1) binding to a specific receptor
2) undergoing endo/phagocytosis
3) taken up via the pump or ion channel
4) undergoing passive transport across the membrane and trapping in the cytosol
5) being built-in the cell membrane
6) linking to cell membrane proteins

Different radiotracers grouped by the mechanism of direct cell labeling are presented in Fig. 2.

A number of agents for direct cell labeling have been generated, such as indium-111 [^{111}In]oxine, [^{111}In]tropolone, [^{99m}Tc]hexamethylpropylenamine oxime ([^{99m}Tc]HMPAO) for planar gamma camera scintigraphy and SPECT imaging, 2-[^{18}F]-fluoro-2-deoxy-D-glucose ([^{18}F]FDG), hexadecyl-4-[^{18}F]-fluorobenzoate ([^{18}F]HFB), N-succymidyl-4-[^{18}F]-fluorobenzoate ([^{18}F]FSB), [^{64}Cu]pyruvaldehydebis(N4-methylthiosemicarbazone) ([^{64}Cu]PTSM), [^{64}Cu]polyethyleneimine ([^{64}Cu]PEI) [35], 5-[^{124}I]-iodo-2′-deoxyuridine ([^{124}I]IdU) [36] for PET imaging, and [^{124}I]FIT-$(PhS)_2$Mal for both PET and fluorescence imaging. All these radiotracers directly label cells through one of the abovementioned mechanisms. Tracers such as [^{99m}Tc]HMPAO, [^{111}In]oxine, and [^{64}Cu]PTSM are nonspecific cell-labeling agents, which by their lipophilic nature, diffuse across the cell membrane and enter the cell [37–41]. Subsequently, these complexes dissociate and the released radionuclides become trapped within the cell by binding to intracellular proteins. Direct labeling of immune cells with radiolabels can also be achieved through the uptake of radiolabeled probes via a transporter mechanism, including a transmembrane receptor, a channel, or a pump, located on the membrane of the cell. As a single transporter located on a plasma membrane can transport many molecules of a radiotracer, this method of direct cell labeling may lead to amplification of the signal. A typical example of radiotracer-based direct cell labeling through this mechanism is [^{18}F]FDG, which enters the cell through glucose transporter (GLUT) transmembrane proteins and is retained in cells by hexokinase-mediated phosphorylation, causing entrapment of this tracer in the cytoplasm [42,43]. Finally, direct cell labeling can be achieved through direct binding of the radiotracer to the cell membrane. One example of such radiotracers is [^{18}F]HFB, which binds to cellular membranes via a lipophilic long-chain ester [44]. Another approach of direct cell labeling through the radiotracer anchoring to the cell membrane involves the chemical coupling of [^{89}Zr]desferrioxamine-NCS ([^{89}Zr]DBN] [45] or [^{124}I]FIT-$(PhS)_2$Mal [46] to cell membrane-bound proteins.

Direct immune cell labeling provides several benefits, which include fairly simple labeling protocols performed without the requirement of genetic cell manipulation and high sensitivity, enabling detection of small numbers of cells due to the minor background signal. Given these properties, direct labeling methods are easier to translate into clinical practice than indirect labeling approaches. Although direct cell labeling is fairly simple, it has some limitations. One disadvantage of this method is that the radiotracer becomes diluted upon each cell division, which leads to decreased concentrations of the probe per individual cell. Additionally, the radiotracer may be transferred asymmetrically to the daughter cells following cell division or may be released from the cells (*e.g.*, [^{111}In]oxine and [^{64}Cu]PTSM), eventually leading to the disappearance of the signal [12,39,47]. As a consequence, directly labeled cells can be tracked *in vivo* for only up to a few days. Furthermore, direct-labeling does not enable monitoring of cell biological functions, such as proliferation, activation, or viability, and may evoke changes of cellular characteristics after radiotracer uptake. Finally, the adoptively transferred, radiolabeled dead cells may be engulfed by the phagocytic cells leading to the generation of an unspecific signal. To overcome the limitations, reporter-based indirect labeling techniques for live-cell tracking have been developed. These approaches enable the detection of reporter gene-expressing, live immune cells with nuclear imaging techniques following administration of a specific radiotracer [12,13,48].

3.1.1. Tracking of directly labeled immune cells with planar gamma-scintigraphy and SPECT imaging

The use of immune cells directly tagged with radioisotopes for live tracking of immune cells with planar gamma scintigraphy and SPECT imaging is currently an accepted procedure, and many labeling techniques have been developed for this purpose [49]. Although live tracking of directly radiolabeled white blood cells with planar gamma scintigraphy is routinely used in clinical settings [6], recent progress has focused on the more technologically advanced SPECT imaging in the majority of preclinical and clinical immune cell tracking studies.

Immune cell labeling with direct methods for planar gamma scintigraphy and SPECT imaging relies on radiotracers that are mainly chemical complexes of two radionuclides, namely [^{111}In] and [^{99m}Tc].

Direct immune cell labeling with [^{111}In]-based radiotracers. [^{111}In] is a commonly used radioisotope, which, thanks to its long half-life, enables imaging for up to 96 h post-injection (Table 2). It is produced in a cyclotron via the ^{111}Cd(p,n)^{111}In or ^{112}Cd(p,2n)^{111}In reactions and decays with a 2.81 day half-life via electron capture to the nuclide [^{111}Cd]. [^{111}In] emits gamma radiation at 171.3 keV and 245.4 keV, which makes it applicable for both planar scintigraphy and SPECT. The only stable state of oxidation in aqueous conditions is In(+III), which is a hard Lewis acid preferring to coordinate to hard amine-N and carboxylate-O Lewis bases, and

it has a high affinity for water making its complexes susceptible to hydrolysis. As a result, high coordinate polyamino acids such as EDTA, DTPA, DOTA, TACN are most frequently used as In(+III) chelators for radiochemical applications to maximize complex stability. In(+III) complexes can form with coordination numbers varying from 4 to 8 and can exhibit a wide variety of coordination complexes and geometries as detailed in these excellent reviews [50,51]. However, for cell labeling tight irreversible binding of the radiometal by the chelating ligands is not always required. One established labeling strategy is to employ metastable lipophilic complexes, which diffuse across the cell membrane, carrying the radiometal with them, and then dissociate inside the cells causing the radiometal to become trapped intracellularly [37,52,53] (Fig. 2). With this approach, highly stable complexes are not desired as there would be no trapping mechanism and the activity would leak out of the cells after labeling.

As described above, [^{111}In] complexes have been at the forefront of the development of cell labeling for *in vivo* imaging using this strategy. The most prominent example is [^{111}In]oxine [54], which in 1985 was approved by the FDA for leukocyte scintigraphy. The oxine ligand (8-hydroxyquinoline) is lipophilic but retains enough water solubility to react with metal ions in an aqueous solution. It reacts by losing a proton to become an anionic N, O-chelate enabling the formation of neutral lipophilic complexes, which can be readily purified by biphasic extraction into organic solvents followed by solvent evaporation. In the case of In(+III) a hexadentate tris(oxinato)indium(+III) complex is formed with a pseudo octahedral geometry [55] (see Fig. 3).

Initial approaches of immune cell tracking with [^{111}In]-based radiotracers took place in the 70-ties. Segal *et al.* radiolabeled leukocytes *in vitro* with [^{111}In]oxine and administered them to patients with various inflammatory diseases: gut abscesses, bacterial endocarditis, rheumatoid arthritis, pyogenic infection. In each case, a high signal was detected in the inflammatory areas using a whole-body counter, and inflammatory tissues were visualized using planar gamma-scintigraphy [54]. This early study gave rise to further research, which established [^{111}In]oxine leukocyte scintigraphy or SPECT/CT as a practical and very accurate technique identifying inflamed tissues. Currently, not only rodents are used as an animal model in cell tracking studies employing this tracer. Afzelius *et al.* labeled a fraction of leukocytes with [^{111}In]oxine, yielding 57.7% – 69.7%, and administered it intravenously to pigs with inflammatory lesions caused by *Staphylococcus aureus*. The aim of the experiment was to compare the efficacy of osteomyelitis detection by radiolabeled leukocytes and several pure radiotracers. Although ^{111}In-leukocytes accumulated in 79% of inflammatory affected regions, the effectiveness in the case of ^{18}F-FDG PET was 100%, which made this method more reliable [40]. Nowadays, the [^{111}In]oxine labeled leukocyte method is used in humans, for example, to diagnose inflammatory conditions of the urinary bladder [41].

The development of successful immune cell-based anticancer therapies requires a deep understanding of *in vivo* biodistribution and antitumor activity of immune cells upon administration. Nuclear imaging research has significantly improved our knowledge about immune cell-based therapies against cancer by noninvasive and real-time tracking of immune cells and by visualization of their anticancer activity in numerous preclinical and clinical studies [2]. Noninvasive tracking of directly labeled immune cells using [^{111}In]oxine has been used to trace target tumors. For example, in 20 patients with different lymphatic malignancies and a perceptible lymph node enlargement, *in vivo* migration of leukocytes labeled with [^{111}In]oxine was studied in planar scintigraphy. Targeting of those cells to lymph nodes was observed in all patients suffering from Hodgkin's lymphoma or high-grade lymphoma, although, in the case of patients with low-grade lymphomas, effective targeting was observed in less than half of the patients [56]. SPECT imaging can also be useful for the evaluation of targeting directly radiolabeled adoptive T lymphocytes to tumors. CD8$^+$ Tc lymphocytes (CTLs) with affinity to the Melan-A melanoma antigen were labeled with [^{111}In]oxine, administered to patients, and their targeting was evaluated using whole-body counter and static gamma camera imaging. Nuclear imaging allowed the detection of CTLs at metastatic sites, but there was also a signal in the liver, lungs, and spleen [57]. In another study, Pittet *et al.* labeled mouse T-cells expressing the hyaluronan-characteristic T-cell receptor with [^{111}In]oxine and injected them intravenously to mice with HA$^+$ CT44 and HA$^-$ CT26 tumors. Labeled CTLs were detectable in HA$^+$ CT44 tumors within 24 h of administration, and their numbers increased throughout the study. By comparison, there was very little homing of the labeled CTLs to the HA$^-$ CT26 tumors, suggesting that the tumor-targeting of these T-Cells was mainly TCRs mediated [58]. In a different study, human CAR-T cells were radiolabeled with [^{111}In]oxine to evaluate their trafficking in mice using SPECT/CT when different routes of cell injection were used. Compared to subcutaneous (S.C.) and intraperitoneal (I.P.) injections, optimal biodistribution was obtained after intravenous (I.V.) administration [59]. Finally, γδ T cells, which are a specific type of T cells capable of identifying and killing neoplastic cells without involvement of MHC molecules, were directly labeled with [^{111}In]oxine and adoptively transferred to mice with 4 T1 mammary adenocarcinoma (a murine model of triple-negative breast cancer). SPECT and CT study of adoptively-transferred γδ T cells

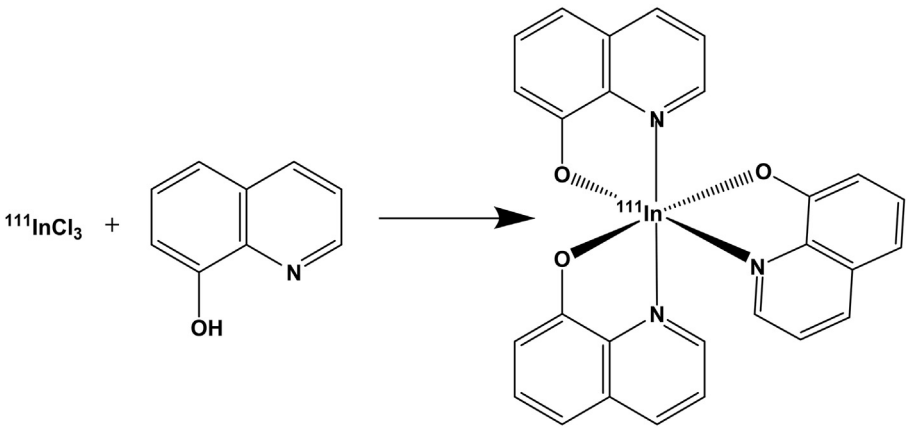

Fig. 3. [^{111}In]oxine formation reaction and structure.

has revealed that these cells targeted mouse tumors, and efficiently reduced their size [60].

NK cells are another type of immune cell with substantial antitumor activity, and thus NK cell-based anticancer therapies have emerged as a promising therapeutic approach for cancer treatment. Nuclear imaging has contributed to our understanding of therapeutic approaches focused on the administration of tumor-infiltrating NK cells [61]. In a study by Meller *et al.* SPECT imaging was employed to investigate the biodistribution and kinetics of *in vitro* expanded allogeneic NK cells [62]. For this purpose, NK cells were labeled with [^{111}In]oxine and administered with a ten-fold excess of unlabeled cells to three patients with renal cell carcinoma. SPECT imaging revealed that shortly after transfusion [^{111}In]oxine labeled NK cells were primarily detected in lungs, but within the first 24 h they were redistributed from lungs to liver, spleen, and bone marrow. Moreover, 24 h after transfusion [^{111}In]oxine labeled NK cells could be observed in two out of four large metastases, which were confirmed by high glucose uptake with [^{18}F]FDG-PET. In another study, SPECT imaging was used to compare the migration of [^{111}In]oxine-labeled autologous NK cells to liver metastasis in colon carcinoma patients upon administration either via the systemic (intravenous) or locoregional (intraarterial) routes [63]. SPECT imaging analysis revealed that NK cells injected intravenously localized primarily to the lung, whereas localization of intraarterially injected NK cells was limited to the spleen and liver. Moreover, migration of NK cells to liver metastasis was observed only after intraarterial injections. The [^{111}In]oxine radiotracer was also successfully used in the biodistribution and tumor targeting study of NK cells generated from umbilical cord blood hematopoietic progenitor cells (UCB-NK cells) and adoptively transferred in immunodeficient NOD/SCID/IL2Rgnull mice [64]. Using SPECT imaging, Cany *et al.* demonstrated that [^{111}In]oxine-labeled UCB-NK cells migrated to liver, spleen, and bone marrow within 24 h after transfusion, and most importantly a single administration of UCB-NK cell impaired the growth of bone marrow-residing human leukemia cells injected intra-femorally in mice, leading to increased mouse survival.

Dendritic cells (DCs) induce protective adaptive immunity and thus have been a focus of anticancer vaccines and immunotherapy treatments. SPECT imaging has contributed to our increased understating of DC biology and DC-based anticancer therapies. In a study by Prince *et al.* PET and SPECT imaging modalities were employed to track the *in vivo* migration of monocyte-derived nonmatured DC (nmDCs) or matured DC (mDCs). For this purpose, DCs were labeled with [^{18}F]FDG or [^{64}Cu]PTSM for PET imaging and [^{111}In]oxine for SPECT imaging and administered to patients with multiple myeloma via (I.V.), intradermal (I.D.), (S.C.), and intranodal routes [65]. Among tested radiotracers, [^{111}In]oxine showed reproducible tracking of both types of DCs to regional lymph nodes after either S.C. or I.D. administration, with mDCs showing superior migration to regional lymph nodes. [^{111}In]oxine-SPECT imaging was also successful in the *in vivo* monitoring of lymph node migration of [^{111}In]oxine labeled DCs in a murine breast cancer model (MMTV-Ras). Labeling of DCs with [^{111}In]oxine, had no adverse effect on DC phenotype or functionality, and most importantly SPECT imaging revealed the presence of [^{111}In]oxine-labeled DCs in both axillary and popliteal lymph nodes. These results were confirmed with immunohistochemistry and γ-counting analysis [66]. [^{111}In]oxine binds to the iron transport protein transferrin in blood plasma and so the blood plasma must be removed from patient samples before the cell labeling step, however, this process may affect cell viability. To overcome this problem, other [^{111}In]-based radiolabels such as [^{111}In]-2-mercaptopyridine-N-oxide ([^{111}In]Merc), [^{111}In]tropolone and [^{111}In]acetylacetone (ACAC) were developed [67,68]. Although these radiotracers exhibited effective labeling of leukocytes in a plasma, they did not become commonly applied agents for nuclear imaging of leukocytes *in vivo*. Nevertheless,It is worth mentioning an experiment in which human blood-derived $\gamma\delta$ T cells were labeled with [^{111}In] tropolone and then injected I.V. into NSG mice with A375Pβ6.luc cell tumors, inoculated I.V., S.C. and I.P. The I.P. model showed the highest $\gamma\delta$ T cell uptake of the three examined models [69].

Direct immune cell labeling with ^{99m}Tc-based radiotracers. The promising results obtained with [^{111}In]-labeled leukocytes studies inspired efforts to develop analogous methods of cell radiolabeling with [^{99m}Tc], which due to its unique physical properties is now the most commonly used radioisotope for gamma-based diagnostics [70]. Moreover, this radioisotope guarantees a high signal-to-noise ratio, enabling the detection of even small numbers of cells. Stable isotopes of technetium do not exist and so most of the Tc used in laboratories is freshly generated from nuclear reactions. The most commonly used isotope [^{99m}Tc] is produced in a generator by the decay of the longer-lived isotope – [^{99}Mo]. The half-life of [^{99m}Tc] is 6 h and it decays with 12% internal conversion and 88% gamma photon emission at 140 keV, making it excellent planar gamma scintigraphy and SPECT imaging isotope (Table 2). Technetium is available at oxidation states from (-I) to (+VII), but the most stable states are (+VII) and (+IV). The lower oxidation states (+I), (+II), and (+III) need to be stabilized with chelating ligands to prevent technetium hydrolysis products from forming, which interfere with subsequent labeling efficiencies. [^{99m}Tc] is eluted from a [^{99}Mo] generator as [$^{99m}TcO_4$-] (+VII). This needs to be reduced to lower oxidation states with an *in situ* reducing agent, commonly $SnCl_2$, to form coordination complexes with chelating ligands. Tc can form stable complexes with both hard and soft Lewis bases as demonstrated by the diversity of the commercially available [^{99m}Tc] imaging agents, such as Myoview P_4O_2, Sestamibi C_6, Draximage DTPA- N303, and Technescan MAG3-N3S.

Although a variety of chemical complexes of [^{99m}Tc] for direct cell labeling have been designed, the most commonly used [^{99m}Tc]-based radiotracer, initially dominating in planar scintigraphic techniques and now mainly used in SPECT imaging, is [^{99m}Tc]HMPAO. This N_4 coordinating ligand, also known as exametazine is sold in kit form with the $SnCl_2$ reducing agent under the trade name Ceretec®. The kit is reconstituted with freshly eluted [$^{99m}TcO_4$-] to form [^{99m}Tc]HMPAO via the reaction presented in Fig. 4. The resultant lipophilic complex is passively absorbed across the cell membrane and is trapped within cells via a combination of reduction to a hydrophilic complex and binding of the complex to non-diffusible proteins and cellular organelles [71].

Comparison of [^{99m}Tc]HMPAO and [^{111}In]oxine biodistribution shows significant differences. [^{99m}Tc]HMPAO has significant intestinal activity due to its biliary secretion route [71]. This makes [^{99m}Tc]HMPAO less effective in the case of cell tracking within the abdomen. The low energy emission properties of the radionuclide [^{99m}Tc] can be used at a higher dose than [^{111}In] which confers an advantage for imaging small parts of the body. The disadvantage is its relatively short half-life giving only a short period for the tracking of immune cells. [^{99m}Tc]HMPAO is mainly applied in imaging of infections [6]. In 1990, 19 patients suffering from inflammatory diseases were injected with leukocytes labeled with [^{99m}Tc]HMPAO and imaged with a gamma camera [72]. This study achieved 100% specificity, 93% sensitivity, and 95% accuracy. This was later repeated by Reynolds *et al.* who obtained similar results: sensitivity 92.8%, specificity 93,3%, and accuracy 93,2% [73]. In 1994 Peters *et al.* concluded that injection of autologous [^{99m}Tc] HMPAO-labeled white blood cell fraction should be the top compound for the diagnosis of inflammatory bowel disease (IBD) and most forms of acute sepsis [74]. Mansfield *et al.* attempted to compare the diagnostic potential of autologous leukocytes labeled with [^{111}In]tropolone and [^{99m}Tc]HMPAO for IBD [75]. They observed a

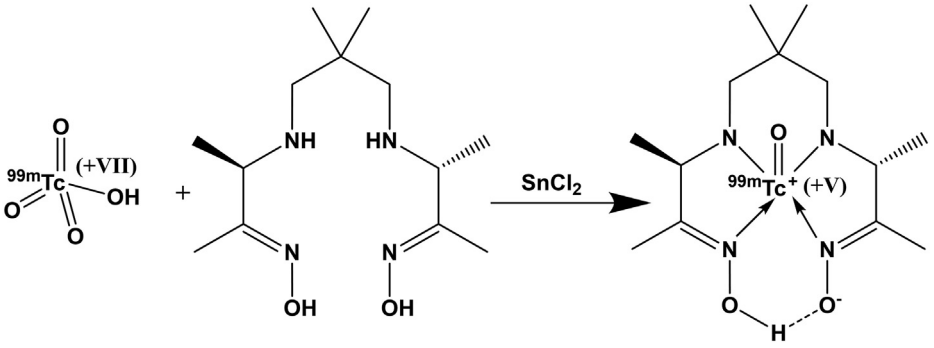

Fig. 4. [^{99m}Tc]HMPAO formation reaction and structure.

close correlation between the fecal excretion of [^{111}In] and the result of the [^{99m}Tc] image analysis, which confirms the usefulness of these radiotracers in the context of determining inflammatory bowel activity. A diagnostic method involving the venous leukocyte fraction is also used today in the clinics. Migliari *et al.* reviewed 490 studies with labeled leukocytes in the context of infection diagnosing (mainly bone and orthopedic implant infections). They concluded, that this method is characterized by its ease of application in routine clinical practice, good cell labeling efficiency (72%) and high-quality images [76]. Jorgensen *et al.* have approached the radiolabeling of the pure lymphocyte fraction and confirmed the effectiveness of lymphocytes for targeting arthritic joints [38]. The research aimed at rheumatoid arthritis (RA) visualization was also performed with the use of autologous blood-derived monocytes which upon labeling with [^{99m}Tc]HMPAO, were re-infused to RA patients. Scintigraphy [77] or SPECT imaging [78] of the hands and feet of RA patients revealed clear images of re-infused, radiolabeled monocytes localized to the inflamed joints. Importantly, the biodistribution of [^{99m}Tc]HMPAO-labeled monocytes is similar to that of [^{99m}Tc]HMPAO-labeled white blood cells and might therefore be employed for live monitoring of antirheumatic therapy in patients [79]. In 2011 Ruparelia *et al.* showed significant migration of [^{99m}Tc]-labeled neutrophils to the target tissue in patients suffering from a chronic obstructive pulmonary disease (COPD). [^{99m}Tc]-labeled neutrophils were administered and tracked using sequential SPECT imaging in six COPD patients and three volunteers. The obtained images demonstrated significant levels of neutrophil migration to the lungs in COPD patients. The results corresponded well with a whole-body counter quantitative analysis of [^{111}In]tropolone radiolabeled neutrophils [80]. Lukawska *et al.* compared the kinetics of autologous granulocytes and eosinophils in healthy human patients. These two populations of leukocytes were radiolabeled with [^{99m}Tc]HMPAO, administered intravenously and SPECT images were taken after 1, 5, 15, 25, and 120 min. Granulocytes and eosinophils showed different distribution patterns to the liver, lungs, and mediastinum. Favorable trafficking of eosinophils to the spleen and bone marrow and neutrophils to the liver was proven [81]. The same team evaluated the targeting properties of neutrophils and eosinophils to the lungs of patients suffering from asthma [82]. The patients were divided into three groups: (1) early allergic responders, (2) early/ late allergic responders pre-treated with antigen, and (3) allergic patients treated with steroids. Using the gamma camera, a higher net retention time of eosinophils was observed in the first group of asthma individuals than the non-smoking group from the previous study. Further development of this technique may bring the discovery of a key tool for asthma phenotyping. This observation corresponds with the recent study, in which autologous venous blood eosinophils radiolabeled with [^{99m}Tc]HMPAO were I.V. injected to healthy and obese asthmatic patients, showing higher eosinophil trafficking in the lungs of asthma group patients [83]. Interestingly, it was acknowledged that treating leukocytes with [^{99m}Tc]HMPAO results in the preferential labeling of granulocytes, with the strongest selectivity of eosinophils over other leukocytes, which indicates the utility of this radiotracer application during eosinophil-labeling studies [84]. Pillay *et al.* observed, that the trafficking of autologous neutrophils labeled with [^{99m}Tc]HMPAO initially occurred in the lungs, over time their number in the lungs decreased and after 24 h they were detectable only in the liver and spleen. Interestingly, the administration of C-X-C chemokine receptor type 4 (CXCR4) antagonist did not affect neutrophils' distributions [85].

[^{99m}Tc]HMPAO was also successfully used for *in vivo* tracking of specific populations of immune cells such as T cells, DCs, and NK cells in the context of cancer immunotherapy. Sharif-Paghaleh *et al.* employed SPECT/CT analysis to evaluate the efficacy of DC vaccination by early detection of [^{99m}Tc]HMPAO-labeled CD4 + T cells in draining lymph nodes [86]. Another [^{99m}Tc]HMPAO/SPECT imaging study investigated the lymph node migration of mDCs and immature DCs (iDCs) and the impact of administration route (intradermal versus subcutaneous) on this process. SPECT analysis showed that intradermal administration of [^{99m}Tc]HMPAO-labeled DCs resulted in about a threefold higher migration to lymph nodes than subcutaneous administration, and mDC exhibited higher migration than iDC. DCs were first detected in lymph nodes just 20–60 min after inoculation and the maximum numbers were detected at 48–72 h post inoculation [87]. The [^{99m}Tc]HMPAO radiotracer was also used for labeling and *in vivo* tracking of lymphokine (IL-2)-activated killer (LAK) cells induced from T cells (T-LAK) and NK cells (NK-LAK) isolated from patients with head and neck carcinoma [88]. [^{99m}Tc]HMPAO-labeled LAK cells were administered back into the respective patients locally into the tumor tissue or via the superficial temporal artery. The administered LAK cells were tracked using a gamma camera. T-LAK cells were retained longer in the tissue than NK-LAK cells, because T-LAK cells were less adherent and less chemotactic to endothelial cells, and exhibited decreased migration through endothelium as compared with NK-LAK cells.

Another method of leukocyte labeling with [^{99m}Tc] involves the phagocytic engulfment of a radiolabel being in the form of a colloid. An attempt has been made to label blood cells with [^{99m}Tc]-stannous oxide colloid ([^{99m}Tc]-SnF_2). Although the labeling efficiency was between 80 and 90%, most of the radiolabel was accumulated in phagocytic cells: neutrophils and monocytes. The radiolabeled monocytes were reinjected to the patients with the tentative diagnoses of an abdominal abscess or septic loosening of an endoprosthesis, resulting in visualization of local inflammatory foci [89].

3.1.2. Tracking of directly labeled immune cells with PET imaging

Direct cell labeling with [^{18}F]-based radiotracers. [^{18}F] is the isotope, which is the most commonly exploited for various PET studies. [^{18}F]-based radiotracers generate images of high-resolution due to the high β^+ decay ratio (97%) and low positron energy (maximum 0.634 MeV). Its main drawback for cell tracking concerns its short half-life of 109.8 min, which impairs complex radiosynthesis, the performance of extended *in vivo* studies, and delivery to PET centers with no radiochemistry facilities. It entails the necessity of easy access to the freshly synthesized radiocompound. The most widely applied radio-compound both in medicine (tumor diagnosis) and cell labeling studies, is [^{18}F]FDG. This molecule is an analog of glucose with a positron-emitting [^{18}F] atom connected to the 2 carbon instead of a hydroxyl group. It is absorbed by live cells, via the GLUT transporters. The family of these membrane-bound proteins consists of 5 subtypes, however, GLUT-1 and GLUT-3 are considered to contribute to the *in vivo* accumulation of FDG in malignant tumors [90]. In the cytosol, it enters the glycolytic pathway, which leads to its phosphorylation by hexokinase to [^{18}F]FDG-6-phosphate. This molecule is not capable of leaking out from the cell, causing a metabolic trap. But elution of unphosphorylated [^{18}F]FDG which is initially taken up, is a major drawback that results in continuous retention and loss of cell radioactivity. For instance, the cell labeling efficiency decreased in two hours from 89.9% to 62.1% in human stem cells, and from 91.6% to 68.6% in porcine stem cells [91]. In a different study, the labeling efficiency of the fraction of human blood-derived leukocytes decreased from 64 to 75% to 39%–44% after 90 min and eventually to 19% after 240 min [92].

Many types of white blood cells as well as mixed fractions of leukocytes were radiolabeled with [^{18}F]FDG and tracked *in vivo*. Forstrom *et al.* showed [^{18}F]FDG uptake mainly by the granulocyte fraction (78.5 ± 1.4%), with significantly lower uptake by the lymphocytes and platelets (12.6 ± 1.9%) [93]. Most studies regarding the tracking of [^{18}F]FDG labeled cells concerned imaging of infections. Pio *et al.* have proven the feasibility of autologous leukocyte application for visualization of inflammatory foci, both in mice and human patients with inflammatory bowel disease [94]. During another study, a similar method was applied to 49 human patients suffering from various inflammatory diseases. The radiolabeled leukocyte-based PET/CT was more valuable than the conventional [^{18}F]FDG PET/CT in the context of imaging of infection, as this approach reached higher values of specificity and sensitivity [95]. Bhattacharya *et al.* have proven that [^{18}F]FDG labeled autologous leukocytes efficiently target infected fluid accumulations in acute pancreatitis, finding this method reliable in diagnosing this disease in human patients [96]. In a systematic review, Meyer *et al.* summarized the effectiveness of [^{18}F]FDG labeled leukocytes in diagnosing infections. It has been concluded, that when comparing the effectiveness of this method to classical techniques: CT, MRI, and even [^{18}F]FDG-based PET, the obtained results indicate higher diagnostic performance and claim, that [^{18}F]FDG labeled leukocyte-based method should be routinely applied in the clinics. Importantly, no adverse effects were observed in any human patient [97].

In our research, we studied the ability of mouse macrophages (the mouse macrophage cell line RAW 264.7) to migrate to metastases-bearing lungs (4T1 model). Plain [^{18}F]FDG was injected into the mice that were subjected to the PET study within 1 h. The short decay time of [^{18}F] allowed us to administer macrophages labeled with [^{18}F]FDG intravenously into the same mice on the same day and track their distribution. PET analysis showed focal signal from the lungs in mice with lung tumors that received labeled macrophages and no signal in the lungs in mice that received [^{18}F]FDG (Fig. 5) [98].

Another [^{18}F]-based radiotracer is [^{18}F]4-fluorobenzamido-N-ethylamino-maleimide ([^{18}F]FBEM). This compound undergoes a completely different labeling reaction - unlike [^{18}F]FDG, it covalently binds to functional groups of the cell membrane surface and more specifically – to exofacial protein thiols (EPT). The limitation of this method is that was found to be a large variation in the labeling efficiency between cell types that couldn't be explained by the variation in EPT levels alone. Jurkat and SaOS-2 cells were radiolabeled at a fairly low level (7.7 and 7.1% respectively), whereas primary T lymphocytes at a relatively high level – 60.5% [99]. The *in vivo* PET tracking of these cells was performed

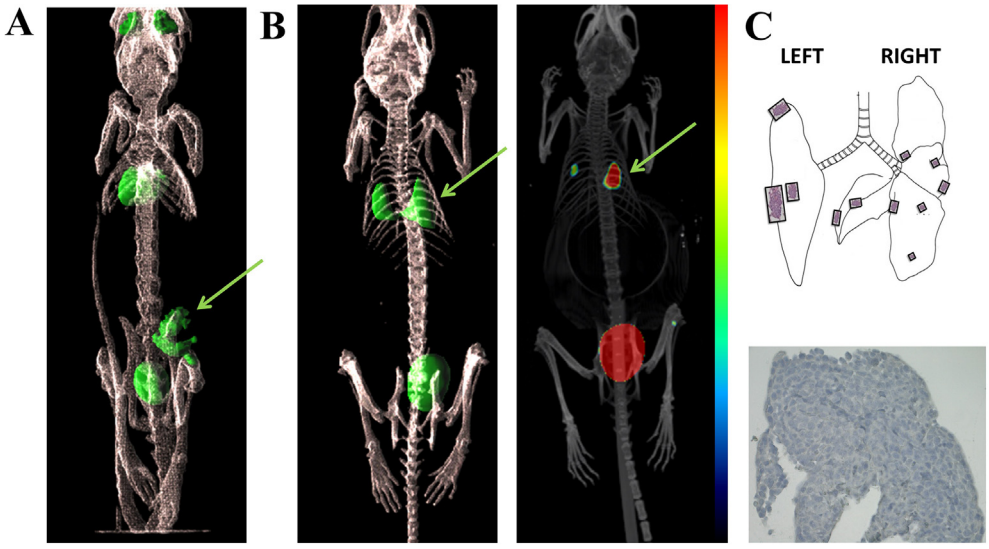

Fig. 5. Fused PET/CT images presenting the distribution of intravenously injected [^{18}F]FDG and RAW264.7 macrophages radiolabeled with [^{18}F]FDG in breast cancer lung metastases. A - surface rendering (SR) of fused PET/CT images obtained after [^{18}F]FDG administration (imaged 1 h post-injection); primary tumor (arrow), bladder, heart, and eyes are visible; the signal was not detected in lungs. B – SR (left) and maximum intensity projection (MIP) (right) of PET/CT images followed prior administration of RAW264.7 macrophages radiolabeled with [^{18}F]FDG (3 h post-injection); in SR images, green color represents PET signal; in the MIP image, PET signal intensity is reflected by the color bar; the tumor was not visualized, but strong, the asymmetric signal from lungs was detected; the signal from the bladder indicates that part of the radiotracer was eluted. C - schematic location of lung metastases (upper image) and representative histopathological image of the tumor focus from examined sample (lower image). The PET/CT images were generated using PMOD software (PMOD Technologies LLC, Zurich, Switzerland).

successfully, following intravenous injection of the cell suspension to the naïve C57BL/6 mice, and the signal was detected mainly in the spleen. Thus, this method has promise for certain cell types evaluation of labeling efficiency and label retention is required for each new cell type to be labeled. The most important feature of this method compared to [^{18}F]FDG labeling is distinctly lower radiotracer retention. There was also an approach of labeling murine spleen-derived leukocytes with [^{18}F]FBEM and evaluation of their recruitment to the lungs with fibrosis in mice. Interestingly, PET images showed greater and faster trafficking of leukocytes in the mice treated with bleomycin than control mice [100]. An efficient and quick procedure of automated radiosynthesis of [^{18}F]FBEM was recently introduced by Lim *et al.* [101]

The [^{18}F]-containing radiolabel that demonstrates a cell incorporation mechanism similar to that observed for fluorescent dyes, is hexadecyl-4-[^{18}F]fluorobenzoate ([^{18}F]HFB). It is a novel, lipophilic ester derivative, which is incorporated into the cell membrane but does not enter the cytoplasm. The labeling efficiency was evaluated so far only in rodent mesenchymal stem cells - after 30 min it reached 25% and cell viability was found to be > 90%, furthermore, there was a retention of radiotracer in the cells > 90% over 4 h. The labeling procedure was quick and simple [44]. However, Kiru *et al.* observed a certain drawback of this method. Although bulk gamma counting showed higher MDA-MB-231 labeling efficiency comparing to [^{18}F]FDG (it was 2.5 fold greater), the single-cell imaging with radioluminescence microscope revealed relatively weak binding of [^{18}F]HFB to living cells and high binding to membrane fragments from dead cells [102]. Zhang *et al.* compared labeling of the human circulating progenitor cells (CPC) with this radiotracer and [^{18}F]FDG and found that the cell labeling with [^{18}F]HFB as compared with [^{18}F]FDG was more efficient (23.4% ± 7.5% vs 7.6% ± 4.1%) and stable (88.4% ± 6.0% vs 26.6% ± 6.1% after 4 h). The CPC radiolabeling with [^{18}F]HFB resulted in a more effective, accurate, and stable way of quantifying cell migration as shown in a rat myocardial infarction model *in vivo* [103].

Direct cell labeling with [^{64}Cu]-based radiotracers. [^{64}Cu] is a theranostic radionuclide endowed with the remarkable property of releasing both β^+ (17.6%) decay for PET imaging and β^- (38.5%) decay for therapeutic applications [104,105]. The maximum β + emission energy (656 keV) and the mean positron range (0.7 mm) compare favorably to [^{18}F] (250 keV, 0.6 mm) [106]. [^{64}Cu] has a half-life of 12.7 h allowing for the tracking of longer-lived biological processes over 1 to 2 days. Copper is a group 11 transition metal element that is capable of accessing oxidations states (+I), (+II), and (+III) although in aqueous solutions Cu(+II) predominates. Copper is a borderline Lewis acid [107], meaning it is a versatile metal that can form stable complexes with a wide variety of donor atoms including hard Lewis bases such as nitrogen and oxygen, and soft Lewis bases such as phosphorus and sulfur. Cu(+II) complexes commonly take a distorted octahedral form with a coordination number of 6. Cu(II) complexes are typically very labile meaning ligands can rapidly exchange [108,109] leading to a breakdown of complexes and release of the metal ion from labeled constructs. As a result, careful design of multidentate and macrocyclic ligands are required for [^{64}Cu] radiolabeling strategies when metal ion release is not desired such as in the radiolabeling of antibodies, peptides, or other targeting moieties. This an extremely broad topic and has been the subject of many recent comprehensive reviews [52,34,105,109–114]. For cell labeling applications alternative strategies can be applied where the release of the metal from the ligand can be of benefit. For example, [^{64}Cu]PTSM, due to its lipophilic properties, passively diffuses through the cell membrane. When it enters the cytoplasm, the [^{64}Cu]PTSM breaks down releasing free [^{64}Cu], which is bound by cellular proteins and the neutral PTSM disperses back out of the cells [34]. Adonai *et al.* performed efficient murine splenic lymphocyte labeling and tracked their systemic migration in a mouse model. Cell monitoring for over 18.9 h revealed that the lymphocytes initially traveled through the lungs and then accumulated in the spleen and liver [39]. Park and co-workers compared two radiolabels in the context of leukemia cells (K562-TL): [^{124}I]FIAU and [^{64}Cu]PTSM claiming that the second one is more efficient, because of its markedly higher labeling efficiency and lower *in vitro* but also *in vivo* efflux [115]. Griessinger and collaborators labeled *in vitro* murine OVA Th1 lymphocytes, reaching labeling efficiency of 6.5% – 9%, however, retention studies indicated that only after 5 h, 47% of added [^{64}Cu]PTSM was still observed in the cells, however, after 24 h it was only 14%. They injected cells I.P. or I.V. to mice with airway hyperreactivity (AHR) induced by OVA and also to naïve control mice. The cells were targeted specifically to the hyperactive sites and remained visible for over 48 h. These authors were able to detect 60 000 [^{64}Cu]-labeled Th1 lymphocytes in a single lymph node 20 min after intraperitoneal administration [116]. In an alternative study [^{64}Cu]tropolone was evaluated as a radiolabel for the human WBC fraction. Although the initial labeling efficiency was encouragingly high (83%), the rapid elution of radionuclide (nearly 50% after 4 h and > 70% after 24 h) makes it impractical for potential application in this setting [117]. Similar approach to white blood cell tracking was introduced by Socan *et al.* Various radiotracers, including [^{64}Cu]oxinate and [^{64}Cu]tropolone were synthesized using specific anion-exchange cartridges. This novel method allows for the synthesis of oxinate and tropolonates in small volumes, suitable pH and the reaction is characterized by high yield (94.8% ± 2.4 for tropolone and 76% ± 20.3 for oxine) and high extraction efficiency (>94%). In this study, the animal model was BALC/c mouse and the targeted pathologies were muscle infection caused by intramuscular (I.M.) inoculation of *P. aeruginosa* and muscle sterile inflammation induced by I.M. injection of turpentine oil. WBC fraction isolated from BALB/c mice was successfully radiolabeled with [^{64}Cu]oxinate and [^{64}Cu]tropolone, reaching 57.1% ± 8.6 and 95.6% ± 2.6 labeling efficiency, respectively. The fractions of radiolabeled WBC were reto-orbitally injected and the series of PET scannings was performed. Clear signal indicating the presence of labeled leukocytes was detectable at sites of infection and inflammation [118].

To label cells with the [^{64}Cu]-containing radiolabel, another mechanism was employed. An organic polymer, polyethylenimine (PEI) was used to create a stable complex with [^{64}Cu]. Interestingly, this reaction was feasible without using a metal chelator. PEI binds to anionic heparin sulfate proteoglycans presented on the cell membrane and is transported into the cell via endocytosis [119]. Li *et al.* synthesized [^{64}Cu]PEI and managed to radiolabel U87MG cells, however, the labeling efficiency was low (20.5% compared to 42.8% using [^{64}Cu]PTSM in the same study), moreover, the efflux reached 61% at 27 h. In general, [^{64}Cu]PEI demonstrated a comparable cell distribution pattern to [^{64}Cu]PTSM - initially, the cells were retained in the lungs, after 20 h redistributed to the liver but radioactivity was also found in the kidneys [35].

To overcome the problem of low radiotracers' retention, we developed a system in which [^{64}Cu] was incorporated within the apoferritin cage and this complex was subsequently loaded by endocytosis to macrophages to track their distribution in lung-tumor-bearing mice. We called this diagnostic conjugate "MRIC" – macrophage radioisotope conjugate. The [^{64}Cu] apoferritin incorporation procedure was previously proposed by Wang *et al.* [120]. Briefly, 1 ml apoferritin solution in acetate buffer 50 mM at 2 mg/mL concentration, pH 6.0, was mixed with 1 ml of a [^{64}Cu] solution (about 1 GBq/mL, in 0.5 M HCl) neutralized with concentrated sodium carbonate (Na_2CO_3). The solution was placed under stirring (Vortex) for 2 min and then 30 min in a shaking heater at 45 °C. Thereafter, 100 μl of a 0.1 M sodium sulfite solution was added to the reaction and warmed again at 50 °C for half an hour. Finally,

the reaction mixture was exchanged for PBS buffer using a Vivaspin 500 concentrators PM30 in an Eppendorf centrifuge at 2000 g (4500 rpm for rotor MSC-6000) for 10 min. This was repeated two further times and the protein was recovered, diluted to the desired concentration for cell loading, and sterile filtered (overall protein recovery about 1 mg). Such method allowed for safe and fast labeling of the apoferritin protein with [^{64}Cu] with negligible leaking of the isotope, which was rendered water-insoluble inside the cavity after transformation onto its sulfide derivative. Further optimized human apoferritin mutants have been recently obtained that allow for faster and efficient [^{64}Cu] incorporation [121].

To be able to track RAW264.7 macrophages longitudinally in tumor-bearing mice (CT26 colon cancer cells injected on the thigh according to the procedure already described [122]), we loaded them with the complex of apoferritin and [^{64}Cu] and injected them into the tail vein. Using PET/CT we observed a specific accumulation of the radioactive signal in the tumor in a time-dependent manner showing macrophage trafficking to this site (Fig. 6). This study showed that even a single administration of autologous or allogeneic macrophages loaded with apoferritin-[^{64}Cu] significantly reduced the number of lung tumors in mice.

Direct cell labeling with [^{89}Zr]-based radiotracers. [^{89}Zr] is a PET radioisotope with a distinctly longer half-life (78.41 h) than those previously mentioned. However, only 22.7% of its radiation is β^+. The mean β^+ emission energy is 396 keV and the mean positron range (1.3 mm) is higher than for [^{18}F] (0.6 mm) [106]. Besides, [^{89}Zr] also exhibits a 77.6% electron capture decay pathway to [^{89m}Y] which decays by emission of a single gamma quantum at 909 keV. Despite the slightly less favorable imaging properties of [^{89}Zr], its long half-life makes it a very useful tool for immuno-PET imaging, and efficiently performed labeling procedures allow *in-vivo* cell tracking for up to 15 days [123].

Zirconium is a group 4 transition metal element, existing mainly in the (+IV) oxidation state. Because of its small size and high charge, Zr(+IV) is considered to be a hard Lewis acid meaning it preferentially coordinates to hard Lewis bases like oxygen and nitrogen [107]. Zr(+IV) has a preference for 8 coordinate complexes as demonstrated by Kathirgamanathan and co-authors who prepared and crystallized zirconium tetrakis(8-hydroxyquinolinolate) for the preparation of organic light-emitting diodes [124]. The formation reaction and structure of [^{89}Zr]oxinate$_4$ [125] is given in the Fig. 7.

This work was of interest to the nuclear medicine community as 8-hydroxyquinolinoline (oxine) has been employed since the mid-1970 s for radiolabeling cells with [^{111}In]oxine for scintigraphy studies and SPECT imaging. In the case of this compound, the cell labeling procedure is analogous to the other lipophilic agents (HMPAO, PTSM, tropolone). They passively diffuse across the cell membrane, and then the isotope-chelator complex breaks down in the cytosol in a reduction reaction and the isotope binds to intracellular proteins. [^{89}Zr]oxinate$_4$ was firstly synthesized by Charoenphun *et al.* in 2014 and the first approach of cell labeling with [^{89}Zr]oxinate$_4$ was performed using human leukocytes and the following cell lines: breast cancer cells (MDA-MB-231), murine macrophages (J774), and murine myeloma cells (eGFP-5 T33). Labeling efficiency of these cell lines was in the range of 40 – 61%, the retention measured after 24 h upon labeling was high (from 71% to 90%) and cell viability > 90%, without a significant decrease after 24 h [126]. In another study, Sato *et al.* attempted to label BMDCs and naïve splenic T lymphocytes to evaluate their tumor-targeting properties in the mouse model. Interestingly, DC labeling efficiency was twice higher (>40%) than for lymphocytes (10% for naïve and > 20% for activated by TCR stimulation). PET tracking of intravenously injected cells was performed for 7 days.

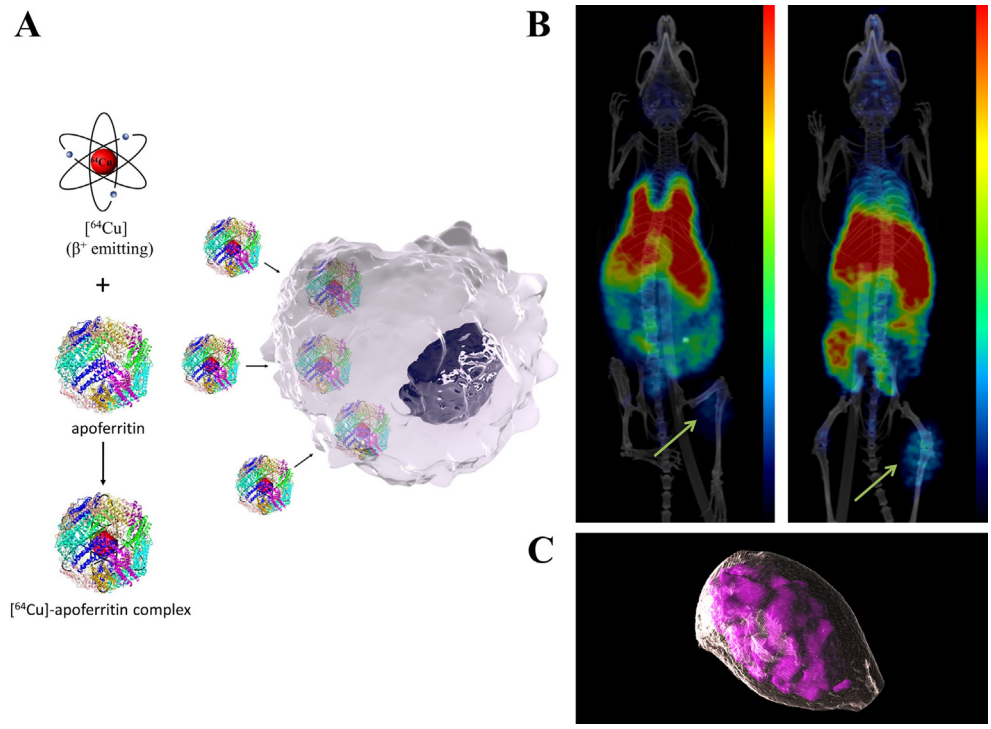

Fig. 6. A – schematic presentation of MRIC preparation: [^{64}Cu] encapsulation in apoferritin (left) and loading of the obtained complex to macrophage (right). B – MIP of fused PET/CT images presenting the distribution of RAW264.7 macrophages loaded with apoferritin-[^{64}Cu] complex; left - time-point 1 (3 h post-injection) and right - time-point 2 (16,5h post-injection). CT26 tumor was visualized (arrows); PET signal intensity is reflected by the color bars. C - SR image of CT26 tumor targeted by radiolabeled macrophages at time-point 2. The apoferritin scheme was generated from the NCBI Structure - online Protein Data Bank. The macrophage image was created in Dimension software (Adobe Inc., San Jose, CA) with the use of an external template. The MIP images were generated using PMOD software. The motion GIF of the mouse scanned at time-point 2 is presented in the supplementary material (Supplementary File 1).

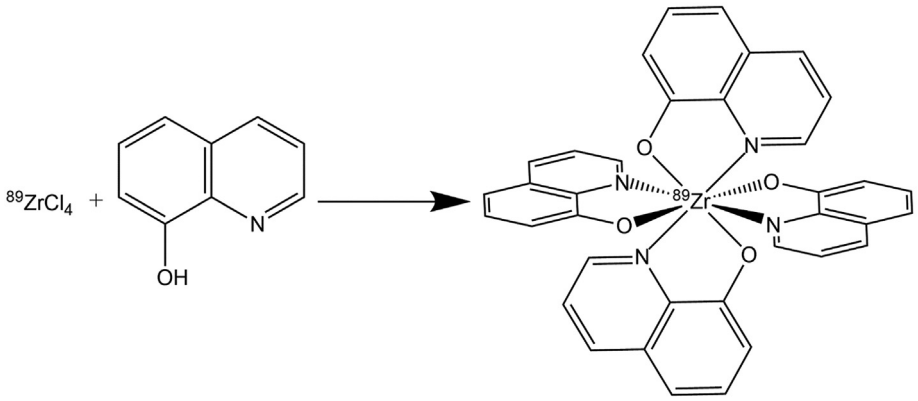

Fig. 7. The formation reaction and structure of coordinate zirconium-89 tetrakis (8-hydroxyquinolinolate).

PET images showed that DCs were mainly distributed to the liver and spleen after passing through the lungs and Tc lymphocytes were mostly trafficked in the lymph nodes and spleen. The most interesting outcome from this study was that only a small fraction of these lymphocytes targeted the tumor [127]. A similar distribution was also observed in our studies [123,128], which corresponded well with recent outcomes. Watson *et al.*. isolated murine spleen and lymph node-derived CD8 + T cells and radiolabeled them with freshly synthesized [^{89}Zr]oxinate$_4$ reaching 18–20% labeling efficiency and > 90% cell viability. After intravenous injection of 8 – 17 mln lymphocytes to C57BL/6J mice with subcutaneously inoculated B16F10 tumors, PET imaging was performed. The signal from the tumors was observed within the first-hour post-injection and was gradually increasing alongside the tumor growth until reaching the final time-point of imaging, which was 188 h. This shows immediate diapedesis of T cells from the vascular system and their migration to solid tumors. This phenomenon also gradually increases over time [123].

Recently, Man *et al.* evaluated the targeting of γδ T cells to engrafted mouse breast tumors. This specific subtype of lymphocytes acts as a very promising agent in adoptive immunotherapy when considering their tumor-infiltrating abilities, cytotoxicity, and antigen-presenting properties. The [^{89}Zr]-labeled cells were administered to the tail vein of female SCID/Beige and NOD SCID GAMMA (NSG) mice inoculated with cancer cells (MDA-MB-231. hNIS-GFP) via intramammary administration. Tumor targeting of lymphocytes was significantly increased in the case of injection of alendronate-loaded liposomes, suggesting that they increase leukocytes' migration to the tumor [129]. Adoptive therapy with chimeric antigen receptor T cells (CAR-T) has recently become a very exciting clinical concept in human oncology [130]. Weist *et al.* conducted a preclinical study involving the transplantation of [^{89}Zr]oxinate$_4$-labeled human CAR-T cells to NSG mice, to evaluate their targeting of glioblastoma brain tumors (cells administered intraventricularly) and subcutaneously inoculated prostate tumors (cell administered intravenously). That was the first approach of human lymphocytes radiolabeling with this tracer. As expected, cell labeling efficiency was high (75%) and radionuclide retention measured after 6 days was satisfying (60%). The cells injected intravenously were distributed to the tumor over 6 days as shown with PET imaging, and the ones that were intratumorally injected were visible only in the region of the tumor for the whole study [131]. Concluding, the efficacy of this radiotracer in tracking many types of cells have been confirmed in numerous preclinical studies, not only in mice models but also in non-human primates [132]. Together these exciting preclinical results have focused efforts to translate [^{89}Zr]oxinate$_4$ cell labeling techniques to the clinic as exemplified by the development of a kit formulation for the preparation of [^{89}Zr]oxinate$_4$ [133] and the publication of a guide to producing [^{89}Zr]oxinate$_4$ labeled WBC to US Pharmacopea standards [134]. An unconventional approach to using [^{89}Zr]oxinate$_4$ in cell tracking studies was taken by Sato *et al.* who chose the rhesus macaque as an experimental model. Macaques' autologous NK cells were *ex vivo* radiolabeled with [^{89}Zr]oxinate$_4$. Importantly, the labeling step did not affect the phenotype, function nor viability of the cells. The macaques were intravenously injected with radiolabeled NK cells, which were PET tracked for 7 days of the experiment's duration. Significantly, the monkeys were treated with a continuous I.V. infusion of deferoxamine, starting just before the cells' administration. The role of deferoxamine was to chelate the eluted zirconium what leads to the renal excretion of the radionuclide and prevents its accumulation in the bones. PET imaging revealed the initial accumulation of NK cells in the lungs and subsequently, they were distributed to the liver, spleen, and to a lesser extent, bone marrow. The most important observation from this study appears to be the confirmed safety of this type of adoptive cell transfer method. The fact of finding no side effects in a species close to humans allows us to consider this method as applicable in medicine [135].

The development of chelator chemistries for [^{89}Zr] to enable the radiolabeling of antibodies for immuno-PET imaging is an extremely fertile field of research and there have been several excellent reviews covering recent developments in this area [109,112,136–139]. The most commonly used methodology is a two-step process whereby a deferoxamine based bifunctional chelator (DFO-Bz-NCS) is covalently bound to amine groups of lysine side chains on the surface of the antibody through NCS coupling followed by [^{89}Zr] chelation to the DFO in aqueous conditions at neutral pH [140]. Interestingly, DFO has also found application in the effective radiolabeling of human hemoglobin, where the chelator is bound to a cysteine residue at position β93 [141]. The formation reaction and structure of [^{89}Zr]DBN (or [^{89}Zr]DFO-NCS) is presented in the Fig. 8. Notice that as a hexadentate ligand DFO does not fully satisfy the 8 membered coordination sphere of Zr.

One interesting adaptation of this chemistry is to reverse the order of the process and form [^{89}Zr]DBN and then covalently bind this to the lysine residues of proteins presented on a cell's outer membrane as a novel approach to cell labeling [45]. In the first study applying this method, murine melanoma cells, murine DCs, and human mesenchymal stem cells (hMSCs) were radiolabeled with [^{89}Zr]DBN with an efficiency of 30% to 50%. Importantly, this method of labeling did not affect cell viability and their ability to proliferate, however, the most important outcome was no efflux observed for over 7 days post labeling. Radiolabeled hMSCs were

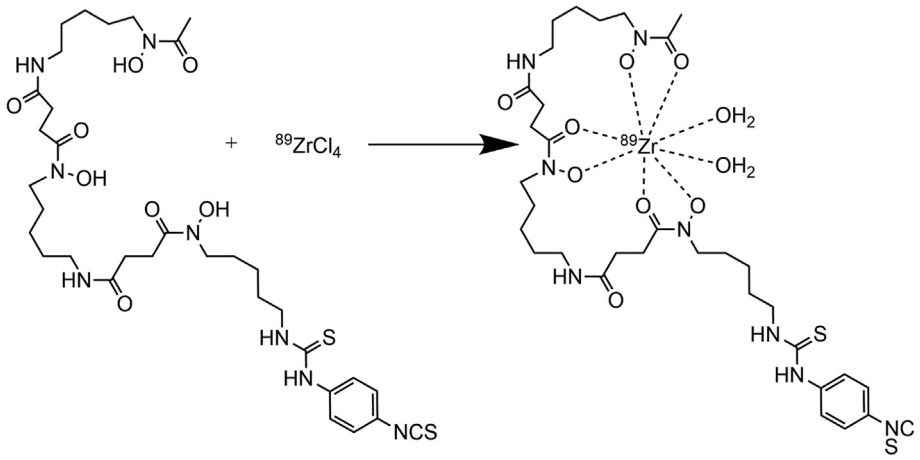

Fig. 8. Formation reaction and structure of [^{89}Zr]DBN.

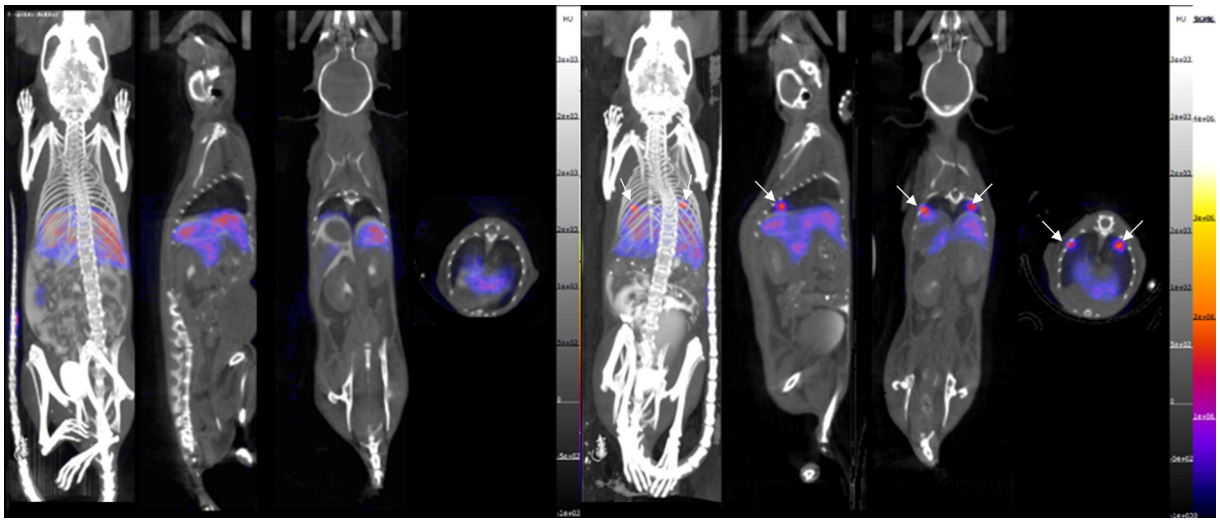

Fig. 9. Focal hotspots of [^{89}Zr]DBN labeled macrophages in naive mice. Left - representative image of [^{89}Zr]oxinate$_4$ labeled RAW264.7 cells 44 h after tail vein injection showing normal liver distribution. Right - example of misleading activity hotspots in lungs of[^{89}Zr]DBN labeled RAW264.7 cells 44 h after tail vein injection in WT mouse; white arrows denote focal hotspots of activity in lungs; subsequent histology showed no biological reason for the accumulation of activity. The images were created using VivoQuant software (Invicro LLC, Boston, MA). The motion GIF (created using PMOD) can be found in the supplementary material (Supplementary File 2).

intravenously injected into athymic mice and their migration was tracked by PET imaging for 7 days. They were also injected into the myocardium within the ischemic regions of a reperfusion mouse model, being retained in ischemic lesions for the whole imaging period.

Lee *et al.* performed a similar study – they radiolabeled Jurkat/CAR-T cells with [^{89}Zr]DBN, reaching 70 – 79% of labeling efficiency and > 95% of cell viability after the procedure. Subsequently, the cells were I.V. injected into mice bearing Raji and K562 cell-tumors, inoculated on the left and right flanks. The mice were PET imaged for 7 days post-injection, revealing that the CAR-T cells progressively migrated from the lungs and trafficked mainly in the liver and in part the spleen. However, an unexpected result was, that cell targeting to the tumors was not observed on PET scans [142]. The radiolabeling of human cardiopoietic stem cells (CPs) using this radiotracer was also successfully performed [143].

This is the only one known radiolabel that does not exhibit significant leaking out of the cells and thus indicates a high potential and wide use in future studies. However, our research results suggest that lymphocytes and macrophages labeled with [^{89}Zr]DBN may non-specifically create *in vivo* focal shaped clusters in murine lungs, which may lead to false-positive results in PET studies concerning cell targeting to pathological lesions, such as lung tumors (Fig. 9).

[^{89}Zr] can also be applied in the form of chitosan-conjugate. Chitosan is a biocompatible copolymer of glucosamine and N-acetylglucosamine which can chelate metal ions. This nanoparticle can be incorporated through phagocytosis, therefore the phagocytic capacity of treated cells is essential. Nevertheless, Fairclough *et al.* performed the labeling of the blood-derived leukocyte fraction, reaching an efficiency of 82.7% after 10 min of incubation, however, continuous, gradual efflux was observed and it reached 53.3% after 2 h [144]. Another method of labeling with [^{89}Zr] harnessing phagocytosis is the treatment of cells with [^{89}Zr]dextran nanoparticles. Wilks *et al.* introduced a few reports concerning PET tracking of [^{89}Zr]dextran-labeled B lymphocytes [145] and T lymphocytes [146,147] in murine models.

Other radiotracers in direct PET imaging. An unusual approach to cell tracking was presented by Pham *et al.* They introduced a dual PET and fluorescent labeling reagent, [^{124}I]FIT-(PhS)$_2$Mal, with an excellent radiochemical yield and confirmed cell conjugation. [^{124}I]FIT-(PhS)$_2$Mal efectively radiolabeled different cell lines via

their membrane thiols with 22%–62% labeling efficiency with extended radiotracer retention. Due to its fluorescent characteristics, the cell membrane localization of [^{124}I]FIT-$(PhS)_2$Mal was proved by confocal fluorescence microscopy. Prolonged monitoring of the *in vivo* distribution of [^{124}I]FIT-$(PhS)_2$Mal-labeled Jurkat cells showed that it can be monitored with PET for over 7 days [46]. The same radionuclide is also applied as a conjugate with deoxyuridine ([^{124}I]dU). The cell penetration of uridine is based on the principle of transporter uptake – via the concentrative nucleoside transporters (CNT1) [148] and it is incorporated into DNA [149,150]. Although the conjugates of deoxyurudine with various radioisotopes have been used in diagnostics for a long time, they have been mainly used for cancer detection due to their high uptake by the proliferating cells [151]. However, there was an approach in which OVA-specific CD8 + T cells were *in vitro* radiolabeled with [^{124}I]dU. Because the results showed a distinctive accumulation of injected radiolabeled T cells in B16-OVA-cell melanoma tumors of C57BL6 mice, it was confirmed that this method is effective for the labeling and long-term tracking of T cells [36]. Jung *et al.* reported the feasibility of a technique termed "CellGPS", which allows a single radiolabeled cell to be tracked *in vivo* using PET imaging. Mesoporous silica nanoparticles (MSNs) concentrating high amounts of [^{68}Ga] were loaded into MDA-MB-231 breast cancer cells. Subsequently, an isolated single cell was I.V. administered into an athymic nude mouse. Using PET, it was possible to detect and visualize that single cell. As expected, the arrest of the cell was eventually observed in the lungs [152]. [^{68}Ga] was also used in connection with oxine ([^{68}Ga]oxinate$_3$) to radiolabel and track CAR-T lymphocytes in NSG mice, however, their targeting to CD19-K562-luc and Raji tumors was slow and no significant accumulation was reported. The authors claim, that although [^{68}Ga] allows performing shorter study comparing to [^{89}Zr], it has a better safety profile what suggests, that it could be safely translated into human studies [153].

3.1.3. Tracking of immune cells with radiolabeled antibodies – SPECT and PET

Another interesting approach of nuclear imaging is cell labeling with radionuclide-conjugated antibodies. In contradiction with the direct cell labeling methods, when tracking cells via this strategy the radioisotopes must be tightly bound to the targeting antibody, particularly if the antibody targets a non-internalizing cell surface receptor, as any released radiometal will no longer be cell-associated. As a result, different chemical strategies are required from the direct cell labeling methods discussed above. Radioisotopes may be connected to antibodies directly (*e.g.*, [^{99m}Tc] and the various iodine radioisotopes) or by bifunctional chelating agents linked to antibodies ([^{99m}Tc], [^{111}In], [$^{89/90}$Y], [^{89}Zr], [^{64}Cu]), with a variety of chelators: DFO, DTPA, DOTA, NOTA, NODAGA, HYNIC, N2S2, N3S [154,155] and potentially - recently synthesized 4HMS [156]. Depending on the radioisotope that is coupled with the antibody, both PET and SPECT techniques may be used to track cells via this labeling method.

Direct antibody radiolabeling methods have the advantage of the radioisotope being covalently bound to the targeting vector reducing the likelihood of loss of the radioisotope from the antibody. In the case of [^{99m}Tc], reduction of the [^{99m}Tc]pertechnetate in the presence of antibodies will produce [^{99m}Tc] labeled antibodies but the [^{99m}Tc] is bound to low-affinity binding sites and is easily lost from antibodies. However, Rhodes *et.al* showed that pre-tinning the antibodies reduces its disulfide bridges to free thiol groups creating high-affinity binding sites for [^{99m}Tc] labeling [157]. Paik *et al.* have shown that the [^{99m}Tc]-thiol bond is stronger than [^{99m}Tc]DTPA binding [158], and Hawkins *et al.* have shown high resistance to transmetallation of [^{99m}Tc] from the antibodies labeled via this method [159]. Further developments and refinements of [^{99m}Tc] direct labeling methodologies have been excellently explained and reviewed by Rhodes *et al.* [160]

Bifunctional chelator-based labeling strategies rely upon the formation of coordination bonds which individually are weaker than covalent bonds and are prone to exchange in aqueous solution, hence appropriate chelator design is vital to minimize loss of radiotracer *in vivo* when employing this strategy. Guiding principles that apply to chelator design for all radiometals are the chelate and macrocyclic effects whereby multidentate and macrocyclic ligand complexes are vastly more stable than the equivalent monodentate complexes of the same coordination number and donor atom type. The strength of the chelate effect increases as chelate denticity increases, which explains the preponderance of high denticity chelates in radiochemistry applications. The primary driving force behind the chelate effect is the entropy increase caused by displacing multiple coordinated monodentate ligands with a single multidentate chelator ligand leading to an increase in the total number of individual molecules upon complex formation. Additionally, metal complexes are at high dilution compared to the competing coordinating solvent molecules meaning monodentate molecules will be readily diluted out during ligand exchange equilibria in solution whereas multidentate chelating ligands will remain tied in close vicinity to the metal ion maintaining competition until all the coordinating bases have been exchanged from the metal. As discussed by Martel *et al.* [161], numerous additional elements also influence the chelator effect to greater or lesser degrees depending on the characteristics of the chelating ligand and the metal ion. Each radiometal has its own unique set of chemical properties such as preferred- oxidation state, coordination number, coordination geometry, donor ligands, and ionic radius. Ignoring steric hindrance, small monodentate coordinating ligands are free to conform to the preferences of the coordinated metal ion whereas macrocyclic or multidentate coordinating ligands need to be pre-formed with the correct charge, number, and type of coordinating bases and have the conformational flexibility to satisfy the preferred coordination geometry of the metal to be coordinated. As a result chelators need to be designed and optimized specifically for each radiometal and it is crucial to match the appropriate chelator to the adequate radiometal. The design and development of chelators for individual radiometals is an extremely fertile field that has been the topic of many excellent recent reviews and the reader is directed to these for further details [50,51,109,111,112,138,153].

A unique aspect of the antibody-based labeling technique is the possibility to label cells in two different ways: *in vivo* - after intravenous administration of the antibody, and in *in vitro* conditions - before administration of the cells. Although the first method has the drawback of non-specific labeling of body cells that have the same receptor as the cells to be tracked, it is much more commonly applied. First attempts of using radiolabeled antibodies are dated back to the 1950s but the development of imaging methods allowed their effective detection only in the 70s [162]. Radiolabeled therapeutic or imaging antibodies approved by FDA and EMA are as follow:

1) compounds for tumor imaging: [^{111}In]satumomab pendetide (approved in 1992), [^{111}In]capromab pendetide (approved in 1996), [^{99m}Tc]arcitumomab (approved in 1996), [^{99m}Tc]nofetumomab merpentan (approved in 1996), [^{111}In]igovomab (approved in 1996), [^{99m}Tc]-murine antimelanoma fragments (approved in 1996), [^{99m}Tc]votumumab (approved in 1998), [^{111}In]ibritumomab tiuxetan (approved in 2002) [163,164].

2) compounds for tumor therapy: [^{90}Y]ibritumomab tiuxetan (approved in 2002) [165], [^{131}I]tositumomab (approved in 2003) [166]. In these groups, many compounds may be potentially used in cell radiolabeling and tracking trials.

Table 3
Examples of targets and radioisotopes examined in preclinical and clinical trials.

Agent	Linked isotope	Target molucule	Target cell	Target pathology (for antibody or radiolabeled cells)	Source
Visilizumab	[^{99m}Tc]	CD3	HuT78, human lymphoma (ATCC® TIB-161™)	T-cells – to autoimmune diseases	[167]
DAbR1	[^{177}Lu] [^{86}Y]	CD4	CAR-DAbR1 T cells	T cells - to U373 glioma and Nalm-6 cell line	[168]
Anti-ICO-80	[^{188}Re]	CD5	Jurkat, T-lymphoblastic lymphoma (ATCC®, TIB-152™)	adenocarcinoma, T-Lymphoblstic lymphoma	[169]
rat anti-mouse αCD11b mAb (isotype: IgG2b)	[^{64}Cu]	CD11	Myeloid-derived suppressor cells (MDSCs)	MDSC - to PyMT breast cancer and B16F10 melanoma.	[170]
Rituximab	[^{131}I]	CD20	n/a	non-Hodgkin's lymphoma	[171,172,173,174,175]
Lym-1	[^{131}I] [^{67}Cu] [^{90}Y] and [^{111}In]		n/a n/a n/a	non-Hodgkin's lymphoma non-Hodgkin's lymphoma non-Hodgkin's lymphoma	[176,177,171] [176,177,171] [177]
Epratuzumab (hLL2)	[^{90}Y] and [^{111}In]	CD22	Ramos, human B-cell lymphoma (ATCC® CRL-1596™) CaPan1 human pancreatic carcinoma (ATCC® HTB-79™)	non-Hodgkin's lymphoma	[171,178,179,180,181]
Lintuzumab (HuM195)	[^{213}Bi] [^{225}Ac] [^{131}I]	CD33	n/a n/a n/a	myeloid leukemia myeloid leukemia myeloid leukemia	[182,183,184] [185] [186]
9E7.4	[^{64}Cu] [^{89}Zr]	CD138	5 T33 murine multiple myeloma	myeloma	[187]
IgG2a k rat anti-mCD138	[^{213}Bi]		5 T33 murine multiple myeloma	myeloma	[188]
syndecan-1	[^{131}I]		n/a	multiple myeloma	[189]
J591	[^{177}Lu]	PSMA	LNCaP human prostatę cancer (ATCC® CRL1740™)	prostate cancer	[190]
	[^{89}Zr] [^{124}I]		LNCaP human prostatę cancer (ATCC® CRL1740™)	prostate cancer	[191]
Cetuximab	[^{89}Zr] [^{88}Y] [^{177}Lu] [^{125}I]		A431, human squamous cell carcinoma (ATCC® CRL-1555™)	squamous carcinoma	[192]
Trastuzumab	[^{111}In]	HER2	n/a	breast cancer	[193,194,195]
ABY-025	[^{111}In]		n/a	breast cancer	[196]
$Z_{HER2:342-pep2}$	[^{111}In]		SKOV-3, human ovary adenocarcinoma (ATCC® HTB-77™)	ovary ascites adenocarcinoma mammary gland adenocarcinomas	[197]
$Z_{HER2:342}$	[^{99m}Tc]		SKOV-3, human ovary adenocarcinoma (ATCC® HTB-77™)	ovarian carcinoma	[198]
	[^{111}In]		SKOV-3, human ovary adenocarcinoma (ATCC® HTB-77™)	adenocarcinoma	[199]
	[^{18}F]		SKBR-3, Human parental breast cancer (ATCC® HTB-30™) MCF-7, Human parental breast cancer (ATCC® HTB-22™) SKOV-3, human ovary adenocarcinoma (ATCC® HTB-77™)	adenocarcinoma glioblastoma	[201]
2Rs15d	[^{131}I]		BT474/M1, human breast cancer cell (ATCC® CRL-3434™) JIMT-1, human breast cancer (AddexBio C0006005) SKOV-3, human ovary adenocarcinoma (ATCC® HTB-77™)	ductal carcinoma	[201]
$Z_{HER3:8698}$	[^{89}Zr]	HER3	MCF-7, Human parental breast cancer (ATCC® HTB-22™) BT-474 Human mammary gland adenocarcinoma cancer (ATCC® HTB-20™) MDA-MB-468, Human mammary gland adenocarcinoma(ATCC® HTB-132™) MDA-MB-231, Human mammary gland adenocarcinoma (ATCC® HTB-26™)	breast adenocarcinoma	[202]
cT84.66	[^{90}Y] [^{111}In]	CEA	n/a n/a	colorectal cancer colorectal cancer	[203,204,205] [203,206]

Table 3 (*continued*)

Agent	Linked isotope	Target molucule	Target cell	Target pathology (for antibody or radiolabeled cells)	Source
A5B7	[^{131}I] [^{90}Y] [^{125}I]		n/a n/a LS174T, human colorectal adenocarcinoma (ATCC® CL-188™) SW1222, human colorectal adenocarcinoma	gastrointestinal adenocarcinoma colorectal cancer liver metastases	[207,208] [208] [209]
$Z_{EGFR:03115}$	[^{89}Zr] [^{18}F]	EGFR	CAL27, human tongue squamous carcinoma (ATCC® CRL-2095™) Detroit562, human pharynx carcinoma (ATCC® CCL-138™) MCF7, Human parental breast cancer (ATCC® HTB-22™)	head and neck squamous cell cancer	[210]
$Z_{EGFR:955}$	[^{111}In]		A-431, human skin epidermoid carcinoma (ATCC® CRL-1555™)	squamous carcinoma	[211]
PAM4	[^{111}In] [^{131}I] [^{99m}Tc]	MUC-1	CaPan1 human pancreatic carcinoma (ATCC® HTB-79)	pancreatic cancer	[181]
PR81	[^{131}I] [^{99m}Tc]		MCF7, Human parental breast cancer (ATCC® HTB-22™) n/a	breast cancer breast cancer	[212] [213]
Anti-ICO-25	[^{188}Re]		SKOV-3 (ATCC® HTB-77™)	adenocarcinoma; T-Lymphoblstic lymphoma	[169]
KJ1-26	[^{64}Cu]	TCR	Th1 cells	lymphocytes to airway delayed-type hypersensitivity reaction	[116,214]

Table 4
Benefits and drawbacks of cell labeling by different mechanisms.

Mechanism of cell labeling	Benefits	Drawbacks	Sample references
Specific receptor uptake	• Possibility to label cells *in vivo* by intravenous administration of antibodies	• Non-specific *in vivo* labeling of body cells that share a common receptor with target cells	[167,170,214]
Endocytosis	• Quick labeling process, high labeling efficiency	• Only phagocytic cells can be labeled • Usually, high efflux of a radiotracer	[144,215,216]
Transporter uptake	• Inexpensive and readily available radiotracer ([^{18}F]FDG) • Quick labeling process not affecting cell viability	• Only short-term studies (T1/2 of [^{18}F] = 109.8 min) • Labeling efficiency depends on the expression level of transporter proteins • Typically quick elution of a radiotracer	[42,43,93,97]
Passive diffusion	• Various radiotracers available, both for SPECT and PET imaging • Quick labeling process with high efficiency, not affecting cell viability	• Typically rapid elution of a radiotracer	[45,71,77,115,131]
Absorption into the cell membrane	• The labeling process does not affect cell viability, phenotype, or migration potential • Low elution of radiotracer	• Typically low labeling efficiency	[44,34,103,117]
Binding to the cell membrane proteins	• No cellular efflux of a radiotracer – stable retention	• In theory, binding of a radiotracer to membrane proteins, has the potential to affect cell functionality	[45,46,99,100,200]

A novel approach involving the use of antibodies has been proposed by Pham *et al.* - a dual iodinated-fluorescent reagent for cancer PET imaging and fluorescence-guided surgery has been developed. The A5B7 carcinoembryonic antigen (CEA)-specific antibody was conjugated to [^{124}I]-Green. The compound was tested *in vivo* using the SW1222 xenograft model (CEA-expressing) where it was visualized by both PET/CT and *ex vivo* fluorescence imaging. CEA [^{124}I]-Green had relatively high tumor uptake of 20.21 ± 2.70, 13.31 ± 0.73, and 10.64 ± 1.86% ID/g at 24, 48, and 72 h post intravenous injection, respectively [46].

The examples of radionuclide-conjugated antibodies with their affinity to certain molecular targets and the isotopes that they are conjugated are given in Table 3.

In summary, many types of radiotracers are used in immune cells labeling. It is important to be aware that many molecules combined with the radioisotope to form the radiotracer were not originally designed to track cells, so some of them have significant limitations. Using radiotracers that are taken up by the cells that express the specific receptor, in the case of *in vivo* efflux of the radiotracer, may lead to the undesirable labeling of other cells of the organism. Some macromolecular radiotracers are characterized by a great capacity for radioisotope particles, what reduces their molar concentration in *in vitro* cell labeling step, however, they may be applied mainly in the case of phagocytic cells. Radiotracers that depend on transporter-mediated uptake are usually associated with their quick elution, furthermore, most of them have a relatively short half-life. In case of the radiotracers capable of passive diffusion across the cell membrane, low retention is also a big concern, however, their ability of unspecific labeling of different kind of cells regardless of their receptor profile is undoubtedly a big value. Fortunately, some compounds are devoid of the efflux effect, such as those labeling cells by absorption into the cell membrane, however with relatively low efficiency, or those binding to the cell membrane proteins, but with a risk of impairing cell

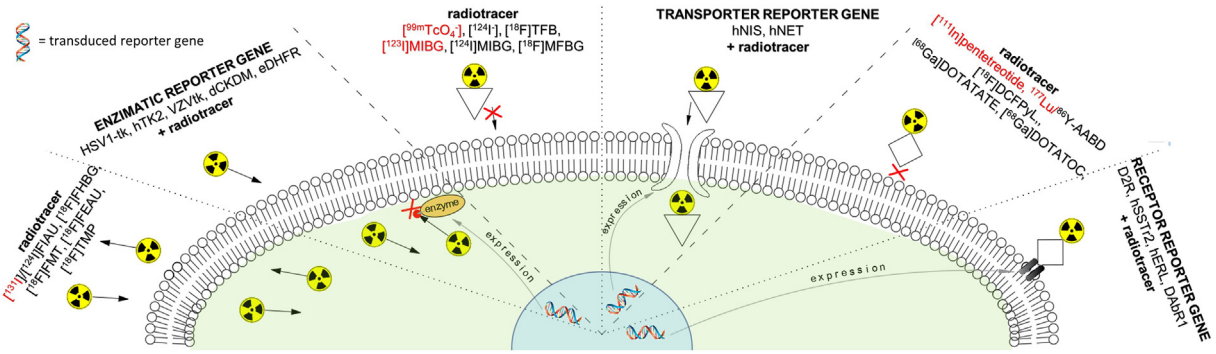

Fig. 10. Diagram of different indirect cell labeling processes, with examples of radiotracers and reporter genes. SPECT radiotracers are listed in red font and PET radiotracers in black font.

function. Nevertheless, the correct choice of radioactive agent should depend on the cell type intended to be labeled and the duration of the cell tracking study. The advantages and disadvantages of each direct labeling process are listed in Table 4.

3.2. Indirect cell labeling

Indirect labeling with reporters involves the introduction of a reporter gene to the immune cells under *in vitro* conditions before cell transplantation. Alternatively, immune cells isolated from transgenic animals that express a reporter gene of interest can be used [217]. These reporter genes are designed to induce an additional function to the cells to make them uniquely targetable *in vivo* by a chosen radiotracer. Reporter genes typically encode for enzymes or proteins capable of binding with high specificity and affinity to a particular radiotracer that may be administered repetitively at any time following cell transplantation. The indirect cell labeling provides several advantages as compared with the direct techniques, including the possibility of longitudinal monitoring of labeled immune cells over their entire lifetime, as well as tracking of proliferating and viable cell populations that express the imaging reporter genes. However, transcription of the reporter genes may be compromised by gene silencing through epigenetic mechanisms such as histone deacetylation or DNA methylation, leading to suppression of the reporter gene expression [218]. Treatment of cells with a DNA methyltransferase inhibitor may overcome this problem [219].

Both viral and non-viral methods have been used for the successful introduction of reporter genes to cells. Viral gene transfer makes use of viruses to introduce the reporter gene into the genome of the target immune cell and does not require any transfection reagents. Nowadays, lentiviruses and retroviruses are most commonly employed for genetic manipulation of immune cells [168,220–223]. Reporter gene transfection with non-viral methods

Table 5
List of reporter genes and radiotracers.

Reporter gene	Reporter probe	PET/ SPECT	Advantages	Disadvantages
Herpes simplex virus type 1 thymidine kinase (**HSV1-tk**) and mutants	[^{18}F]FHBG - 9-[4-[^{18}F]fluoro-3-(hydroxymethyl)butyl] guanine	PET	• lack of the reporter gene in mammalian cells • relatively high sensitivity • a few probes with good pharmacokinetics • dual activity as a molecular imaging gene and a suicide gene • enzymatic signal amplification through phosphorylation and trapping of a specific radiolabeled probe	• immunogenic viral protein, evoking immune-dependent recognition and elimination of immune cells transduced with HSV1-tk • induced expression of the reporter gene may change cell biological function • reporter probes do not cross the blood-brain barrier (BBB) • deiodination of the radio-iodine labeled probes
E. coli dihydrofolate reductase (**eDHR**)	[^{18}F]TMP – [^{18}F]fluoropropyl-trimethoprim	PET	• lack of the reporter gene in mammalian cells • high sensitivity • enzymatic signal amplification through phosphorylation and trapping of a specific radiolabeled probe	• immunogenic bacterial protein, potentially evoking immune-dependent recognition and elimination of immune cells transduced with eDHR • defluorination of the radiotracer → notable radioactivity in bones
Varicella-Zoster Virus thymidine kinase (**VZV-tk**)	[^{18}F]BCNA – p[^{18}F]fluoroethoxyphenyl bicyclic nucleoside analog	PET	• lack of the reporter gene in mammalian cells • relatively high sensitivity • enzymatic signal amplification through phosphorylation and trapping of a specific radiolabeled probe	• immunogenic viral protein, potentially evoking immune-dependent recognition and elimination of immune cells transduced with VZV-tk • reporter probe does not cross the BBB
Human mitochondrial thymidine kinase (**hmTK2**) and mutants	[^{124}I]FIAU – [^{124}I]2′ -deoxy-2′ -fluoro-β-d-arabinofuranosyl-5-iodouraci	PET	• a human protein → substantially reduced risk of inducing an immune response against cells transduced with this reporter gene • dual activity as a molecular imaging gene and a suicide gene	• reporter probes do not cross the BBB • high activity in organs engaged in clearance • deiodination of the radio-iodine labeled probes • possible disturbance of cell function

Table 5 (*continued*)

Reporter gene	Reporter probe	PET/ SPECT	Advantages	Disadvantages
			• probes with good pharmacokinetics • enzymatic signal amplification through phosphorylation and trapping of a specific radiolabeled probe • may be used in patients treated with Penciclovir • reporter system combined of a double mutant of the truncated hmtk2 with [^{18}F] L-FMAU has a sensitivity comparable to HSV1-tsr39tk/[^{18}F]FHBG	
Human deoxycytidine kinase (**hdCK**) double and triple mutants	[^{18}F]FEAU – 2′-[^{18}F]fluoro-5-ethyl-1-beta-D-arabinofuranosyluracil	PET	• a human protein → substantially reduced risk of inducing an immune response against cells transduced with this reporter gene • may be used in patients treated with Penciclovir • enzymatic signal amplification through phosphorylation and trapping of a specific radiolabeled probe	• reporter probe does not cross the BBB • potential modification of cell characteristics like all other reporter genes
Human dopamine receptor type 2 (**D2R**) and its mutant	[^{18}F]FESP – 3-(2′-[^{18}F]-fluoroethyl)-spiperone [^{11}C]RAC – [^{11}C]raclopride	PET PET	• a human protein → substantially reduced risk of inducing an immune response against cells transduced with this reporter gene • [^{18}F]FESP probe clinically approved and has good pharmacokinetics • probes can cross BBB • binding of the probe to mutant D2R does not initiate signal transduction	• high background in pituitary and striatum due to D2R expression in these tissues • slow clearance of [^{18}F]FESP
Human somatostatin receptor subtype 2 (**hSSTR2**)	[^{111}In]-pentetreotide [^{68}Ga]DOTATATE - [^{68}Ga] 1,4,7,10-tetraazacyclododecane-1,4,7,10-tetraacetic acid-(Tyr3)-octreotate [^{68}Ga]DOTATOC – [^{68}Ga]1,4,7,10-tetraazacyclododecane-1,4,7,10-tetraacetic acid-(Phe1-Tyr3)-octreotide	SPECT PET PET	• a human protein → substantially reduced risk of inducing an immune response against cells transduced with this reporter gene • reporter probes have good pharmacokinetics and have already undergone clinical testing	• binding of somatostatin to hSSTr2 may cause cell signaling → transgene overexpression may perturb cell function • hSSTr2 expressed on some tumors and tissues
Human estrogen receptor α ligand binding domain (**hERL**)	[^{18}F]FES – 16α-[^{18}F]-fluoro-17-β-estradiol	PET	• a human protein → substantially reduced risk of inducing an immune response against cells transduced with this reporter gene • reporter probe clinically approved • probe can cross BBB • hERL has no transcription factor activity	• tissue background due to expression in uterus, ovaries, mammary gland and breast cancer cells
Engineered DOTA antibody reporter 1 (**DAbR1**)	[^{177}Lu]AABD – [^{177}Lu]-(S)-2-(4-acrylamidobenzyl)-DOTA [^{86}Y]AABD – [^{86}Y]-(S)-2-(4-acrylamidobenzyl)-DOTA	SPECT PET	• humanized molecular imaging reporter gene • lack of the reporter gene in mammalian cells • relatively high sensitivity	• possibly immunogenic protein • [^{86}Y] is not a good PET radioisotope
Cannabinoid receptor type 2 (**CB2R**) and its mutant	[^{11}C]GW405833 – [^{11}C]-1-(2,3-Dichlorobenzoyl)-5-methoxy-2-methyl-3-[2-(4-morpholinyl)ethyl]-1H-indole	PET	• a human protein → substantially reduced risk of inducing an immune response against cells transduced with this reporter gene • reporter probe can cross BBB • a mutant CB2R possesses wild-type ligand recognition and binding but does not initiate signal transduction	• tissue background due to expression in spleen, cells of the immune system and brain under inflammatory conditions
Human sodium iodide symporter (**hNIS**)	[^{124}I$^-$] [^{18}F]TFB – [^{18}F]-tetrafluoroborate [^{99m}TcO$_4$] – [^{99m}Tc]-petrechnetate	PET PET SPECT	• a human protein → substantially reduced risk of inducing an immune response against cells transduced with this reporter gene • dual activity as a reporter gene and a therapeutic transgene	• tissue background due to hNIS expression in normal tissues, such as thyroid, stomach, salivary glands, mammary glands • radioprobes can efflux since they are not trapped in cells → short imaging window
Human norepinephrine transporter (**hNET**)	[^{123}I]MIBG – [^{123}I]-metaiodobenzyl - guanidine [^{124}I]MIBG – [^{124}I]metaiodobenzyl-guanidine [^{18}F]MFBG – [^{18}F]-meta-fluorobenzylguanidine	SPECT PET PET	• a human protein → substantially reduced risk of inducing an immune response against cells transduced with this reporter gene • probes clinically approved • small size of the hNET gene cassette allows it to be easily integrated into the delivery vehicle	• high tissue background due to hNET expression in many normal tissues • induced expression of this transgene may affect cell biological function

involves the use of electroporation, polymers, chemical vectors, nanoparticles, or cationic transfection agents [224]. Gene transfer with non-viral techniques is rarely used for genetic manipulation of immune cells. In general, three major groups of imaging reporter genes can be distinguished [10,225,226]:

1) enzymes - resulting in metabolic entrapment of the radiotracer inside the cell,
2) transmembrane receptors - binding radiolabeled probes,
3) transporters - actively pumping the radiotracer into the cytoplasm.

Different radiotracers grouped by the mechanism of indirect cell labeling are presented in Fig. 10.

Many imaging reporter genes exist for immune cell tracking, such as non-human reporter genes (herpes simplex virus type 1 thymidine kinase (HSV1-tk), *E. coli* dihydrofolate reductase (eDHFR) and Varicella-Zoster Virus thymidine kinase (VZV-tk)) as well as human reporter genes, including human deoxycytidine kinase (hdCK), human mitochondrial thymidine kinase (hmTK2), human dopamine receptor type 2 (D2R), human somatostatin receptor subtype 2 (hSSTR2), human estrogen receptor α ligand binding domain (hERL), human norepinephrine transporter (hNET), and human sodium-iodide symporter (hNIS) [12,13,16,226]. Table 5 lists the imaging reporter gene/radioprobe systems that have so far been studied and provides advantages and disadvantages of using of each reporter system for immune cell tracking.

One of the most broadly evaluated imaging reporter enzymes for nuclear imaging is HSV1-TK and its many variants, which mediate the uptake of substrates tagged with radioisotopes suitable for SPECT or PET analysis. Radioactively labeled nucleoside analog substrates are phosphorylated by thymidine kinases. The examples are 2′-[^{18}F]fluoro-5-ethyl-1-beta-D-arabinofuranosyluracil ([^{18}F]FEAU),2′-fluoro-2′-deoxy-1β-D-arabinofuranosyl-5-[^{124}I]iodouracil ([^{124}I]FIAU), 9-(4-[^{18}F] fluoro-3-hydroxymethylbutyl) guanine ([^{18}F]FHBG), providing them with a negative charge, which results in the entrapment of these substrates inside the cell [227,228]. Several studies have shown that tumor-infiltrating lymphocytes can be successfully tracked with the HSV1-TK reporter enzyme in mice [229,230] or in humans [231]. However, immune cells expressing HSV1-TK may evoke potential immune reactions due to the viral origin of this reporter enzyme. Similar immune reactions are expected to occur in response to cells expressing other non-human reporter genes, such as eDHFR and VZV-tk. Immunogenicity against non-human reporter proteins may lead to major problems in cell kinetics monitoring studies due to eradication of cells expressing the reporter gene. Thus, to overcome this shortcoming and to reduce immunogenicity, various human-derived reporter genes have been developed. However, the exploitation of such endogenous human genes for *in vivo cell* tracking has three potential problems: first, the reporter probes may also accumulate in cells expressing the endogenous gene causing high tissue background; second, the imaging reporter gene may act like the endogenous gene and thus affect the functioning of the cell in which it is expressed; third, there is still limited knowledge concerning the immunogenicity of these human imaging reporter genes. To overcome some of these problems mutations have been introduced in some of these genes to either eliminate their function [232] or to increase their detection sensitivity with a specific reporter probe [233]. Two human-derived, enzyme-based reporter genes, hmTK2 and hdCK, represent attractive nuclear imaging reporter genes for live cell tracking imaged with pyrimidine-based radiotracers [229]. The second group of reporter genes used for tracking live immune cells with nuclear imaging are receptors, including human dopamine receptor type 2 (D2R) and hSSTR2, which bind their radiotracers on the outside of the cell. The hSSTR2 is a non-immunogenic protein that has been used as an imaging reporter receptor for immune cell tracking using its ligand [^{68}Ga] DOTATOC [234,235]. Selective radiotracer import through transporters, such as hNIS and hNET, is another method for live immune cell tracking with nuclear imaging. hNIS is a glycosylated ion channel present on the cell membrane and is expressed in salivary and thyroid glands, but also in the stomach, where it transports iodine to the cells for sodium exchange. Its expression in target immune cells enables the receptor-dependent uptake of numerous radiotracers, such as radioiodine ([^{123}I], [^{124}I] and [^{131}I] and [^{99m}Tc]-pertechnetate ([$^{99m}TcO_4^-$]). The major advantage of using hNIS for immune cell tracking is the fact that some radiolabeled probes taken up by this receptor, such as [$^{99m}TcO_4$-], are already used for PET and SPECT imaging in the clinic [236,237]. Additionally, hNIS does not evoke an immune response, because of its human origin, and thus may be potentially used in clinical settings. hNET is another non-immunogenic reporter gene encoding a transmembrane protein that transports clinically approved analogs of noradrenaline, such as metaiodobenzylguanidine (MIBG) or metafluorobenzylguanidine (MFBG) across the cell membrane. MIGB can be radiolabeled with [^{123}I] and [^{131}I] for planar gamma scintigraphy and SPECT imaging, and with [^{124}I] for PET imaging [238,239]. It was also possible to synthesize a complex of different guanidines with ^{11}C as an indirect PET radiotracer [240]. A recently developed group of reporters used for indirect immune cell labeling are genetically introduced radiotracer-detectable surface tags. One such example is the DOTA antibody reporter 1 (DAbR1) that is a fusion of a single-chain fragment of a-Y-DOTA Ab 2D12.5/G54C and transmembrane domain of human T-cell. This cell surface tag may be visualized with PET and SPECT imaging following irreversible coupling of lanthanoid (S)-2-(4-acrylamidobenzyl)-DOTA (AABD) radiolabeled with yttrium-86 [^{86}Y] or lutetium-177 [^{177}Lu], respectively [168].

3.2.1. Tracking of indirectly labeled immune cells with SPECT imaging

As described earlier, indirect cell labeling requires genetic modification of the cells for the expression of reporter genes encoding enzymes, receptors, or importers, that induce accumulation of the radiolabeled probe inside the cell. Unlike direct labeling methods, this strategy enables longitudinal immune cell tracking following cell administration. Various reporters, including hNIS, hNET, and SSTR2 have been tested for adoptive cell therapy monitoring with SPECT imaging. In a preclinical study by Emami-Shahri *et al.*, the PSMA-specific P28ζ CAR-T cells were genetically modified to co-express hNIS, and then administered to mice with PSMA-expressing tumors [221]. Following the adoptive transfer, repetitive imaging with SPECT was employed to track [$^{99m}TcO_4^-$] uptake via the hNIS transporter in the CAR-T cells for up to 21 days. Tumor infiltration by T cells shown with SPECT imaging was confirmed by immunohistochemistry analysis of tumor tissue. This study showed that adoptive T cells expressing hNIS reporter gene could be tracked *in vivo* longitudinally with nuclear imaging, enabling analysis of the correlation between tumor infiltration by CAR-T cells and tumor growth. *In vivo* monitoring of Tregs seems to be of great importance for checking the biodistribution of these immune suppressive cells in patients with autoimmune disorders or after organ transplantation. To track the migration of Tregs *in vivo*, autologous Tregs were expanded under *ex vivo* conditions and then genetically modified with the hNIS reporter system for the [$^{99m}TcO_4^-$] radiotracer detection by SPECT/CT imaging [241]. Imaging analysis revealed increased infiltration of the spleen by Tregs as compared with other organs. This preclinical study demonstrated that adoptively transferred Tregs can be tracked *in vivo* in a time-dependent manner with SPECT/CT imaging, as this approach does not affect Treg function and viability. Future research will show whether this approach

may be exploited in the context of inflammatory or autoimmune diseases.

hNET, which binds and takes up clinically approved radiotracers such as MIBG or MFBG, is another reporter gene option for indirect immune cell tracking with SPECT. In a study by Doubrovin *et al.* human EBV-specific T lymphocytes were transduced to express hNET, and then injected intratumorally into EBV$^+$ tumors. After intravenous administration of radiotracers specific for the hNET reporter probe ([^{123}I]MIBG for SPECT or [^{124}I]MIBG for PET), as little as 10^4 hNET-expressing T cells injected intratumorally were detected by SPECT or PET imaging. For longitudinal studies, hNET-expressing EBV-specific T cells were administered intravenously and then tracked for accumulation in EBV$^+$ tumors for up to 28 days with SPECT or PET imaging. This study showed that the hNET reporter system is safe and non-immunogenic, and thus potentially may be used for longitudinal *in vivo* imaging of genetically modified immune cells in humans [238]. In another study, Moroz *et al.* directly compared various reporter systems for *in vivo* T cell detection. To this end, mice were injected subcutaneously with various numbers of T cells transduced with one of the following reporter genes hNET, hNIS, hdCKDM, and HSV-tk, followed by SPECT or PET detection using various radiotracers [242]. SPECT imaging with hNET and [^{123}I]MIBG tracer was the least effective as it required more than 10^7 T cells to generate a signal. The highest sensitivity, allowing for detection of only 40 000 injected cells, was observed for hNET and [^{18}F]MFBG radiotracer among various reporter gene-radiotracer combinations for PET that were evaluated.

Analogous to the reporter genes mentioned previously, efforts have been made to transduce immune cells for the expression of a surface tag-detected with a radiotracer for nuclear imaging. One such example is DAbR1 marker, which is made up of a single-chain fragment of the anti-lanthanoid-DOTA 2D12.5/G54C antibody linked to the CD4-transmembrane domain, which attaches covalently to AABD tracer. This tag has been recently successfully expressed in CAR-T cells and primary human T cells [168], and these cells not only showed efficient radiotracer uptake *in vitro* but also, could be tracked with AABD tracer labeled with [^{86}Y] (PET) or [^{177}Lu] (SPECT) upon intravenous administration to mice. Nuclear imaging analysis showing the highest radiotracer activity in the areas infiltrated by CAR-DAbR10-modified T cells was additionally corroborated with autoradiography and CD3 IHC staining.

3.2.2. Tracking of indirectly labeled immune cells with PET imaging

PET imaging has been successfully employed to track indirectly labeled immune cells with high sensitivity both in preclinical and clinical settings. Enzyme-mediated substrate alteration is commonly used for specific radiotracer entrapment in immune cells expressing enzymatic reporter genes. Up till now, various reporter enzymes and their substrates have been investigated in the context of *in vivo* immune cell tracking. The most extensively evaluated PET reporter gene, as mentioned in a previous paragraph, is HSV1-tk with its product HSV1-TK. Substrates of this enzyme are pyrimidine nucleoside analogs (*e.g.*, FIAU: 5-iodo-2-fluoro-2-deoxy-1-D-*arabino*-furanosyluracil; FEAU: 2-fluoro-2-deoxyarabinofuranosyl-5-ethyluracil), or acycloguanosine derivatives (*e.g.,* FPCV: fluoropenciclovir; FHBG: 9-[4-fluoro-3-(hydroxymethyl) butyl] guanine), which upon labeling with ^{18}F or ^{124}I can be used for *in vivo* PET imaging, however radiolabeled FHBG ([^{18}F]FHBG) is more sensitive than the other radiotracers [243]. This reporter system has been employed to track human T cells in a mouse tumor model. Koehne *et al.* transduced Epstein-Barr virus (EBV)-specific human T cells with the HSV1-TK reporter enzyme and observed with PET imaging that following administration of [^{131}I]FIAU or [^{124}I]FIAU radiotracers, adoptively transferred HSV1-TK-expressing T cells located to EBV-positive tumor xenografts in mice [229]. Importantly, exposure of transduced T cells to the radiotracer did not affect their cytolytic activity. In another study, PET imaging of T cells upon [^{18}F]FHBG radiotracer administration allowed quantification of their homing during inflammation [244]. Clinical use of this technology is reported in the study by Yaghoubi *et al.* [230,245]. Using PET, Keu *et al.* studied glioblastoma homing of CD8$^+$ CTLs expressing CAR IL-13, and HSV1-TK reporter enzyme that facilitated [^{18}F]FHBG uptake. The analysis of [^{18}F]FHBG signal on PET images performed before and after CLT-injection was very useful to show CTLs trafficking, survival, and proliferation [231].

The viral origin of the HSV1-tk reporter gene is its major limitation, as it can evoke potential immune reactions against cells carrying this gene. This limitation has been overcome by the generation of different mutants of human dCK, which selectively phosphorylate fluorinated thymidine analogs. Human prostate-specific membrane antigen (PSMA)-specific CAR-T cells have been successfully transduced with the human dCK double mutant (dCKDM) reporter gene before transplantation and then visualized in PSMA-positive prostate metastases in the lungs with [^{18}F]FEAU radiotracer and PET imaging within 6 h after T cell administration [233]. In another study, tumor infiltration by T cells co-expressing the triple mutant hdCK3mut with a melanoma antigen-specific T cell receptor was studied with [^{18}F]L-FMAU (1-(2-deoxy-2-fluoro-β-l-arabinofuranosyl) thymidine) radiotracer and PET imaging [246]. PET analysis showed that human leukocyte antigen (HLA)-matched tumors had higher T cell-associated radioisotope signal as compared with HLA-mismatched tumors. Importantly, the expression of various mutants of human dCK did not evoke any changes in behavior and viability of transduced cells, supporting the utility of monitoring adoptive cell transplantation with human dCK mutants and PET reporter imaging.

Selective radiotracer import via importers encoded by reporter genes such as hNIS, hNET, and SSTR2 is another common approach for tracking live immune cells with PET imaging. Ahn *et al.* studied trafficking of bone marrow-derived DC (BMDC) transduced with luciferase/hNIS reporters for bioluminescence imaging (BLI) and PET imaging using [^{124}I] as a radiotracer, respectively [247]. After 7 days of BMDC injection into a footpad, both imaging modalities showed enhanced signal in the draining lymph nodes, suggesting DC trafficking. In another study, the lymph node homing of the murine DC line DC2.4, transduced with the same luciferase/hNIS reporter system, was successfully visualized using BLI and PET/CT imaging with another probe for hNIS reporter gene, [^{18}F]-tetrafluoroborate ([^{18}F]TFB), in live mice [237], supporting the use of hNIS/[^{18}F]TFB reporter system in conjunction with PET imaging for monitoring immune cells in live animals. This approach has also found application in autologous human CAR-T cells tracking. Volpe *et al.* developed a novel platform to induce co-expression of both CAR and hNIS-RFP – a fused radionuclide-fluorescence reporter gene. The introduction of this unique set of genes induces human T lymphocytes to express CAR, red fluorescent protein, and transporter for [^{18}F]TFB and [$^{99m}TcO_4^-$], allowing the cells to be detected by fluorescence imaging, PET, and SPECT. The cell tracking to triple negative breast cancer (established by orthotopic human MDA-MB-436 and MDA-MB-231 cells inoculation into NSG mice) was evaluated. Interestingly, significant retention of CAR-T cells was observed only in MDA-MB-436 tumors. It appeared that CAR-T targeting to tumors was inversely correlated with immune checkpoint expression in triple negative breast cancer (TNBC) models [248]

SSTR2 is another human reporter gene that has been successfully employed to monitor in a quantitative and time-dependent manner the biodistribution and antitumor effects of CAR-T cells using the [^{68}Ga]-labeled somatostatin analog ([^{68}Ga]DOTATOC) and PET reporter imaging in a preclinical mouse tumor model

[235]. This study showed that low numbers of CAR-T cells could be visualized with high sensitivity and specificity, and [^{68}Ga]DOTATOC uptake in the tumor tissue correlated with tumor development. This PET analysis was successfully validated by the immunohistochemistry analysis of tumor tissues showing the correlation between the uptake of [^{68}Ga]DOTATOC and percent of CAR-T cell homing into the tumor.

A very novel approach to indirect cell labeling was implemented by Minn *et al.* Taking advantage of the fact that PSMA has limited expression in human tissue almost only to the prostate, they created transgenic human blood-derived CD19-tPSMA$^{(N9del)}$ CAR-T cells. Prostate-specific membrane antigen (PMSA) expressed on the cell surface of those cells was exploited as a target for [^{18}F]DCFPyL, which acted as an indirect radiolabel. The experimental model was NSG mice with S.C. inoculated Nalm6-eGFP-fLuc cell tumors. On the 12th-day post CAR-T cells I.V. injection, a clear PET signal at the tumor side was detected, which indicated that most of the injected cells infiltrated tumor tissue [249].

The aforementioned labeling methods are powerful tools for monitoring immune cells *in vivo*, although they all have both advantages and disadvantages. The application of genetically modified cells in patients can lead to severe regulatory complications and may increase the cost of diagnostics. On the other hand, it is easier to perform direct labeling from a technical standpoint - the method does not require an *in vitro* labeling step - instead, the radiolabel can be administered to the patient intravenously. Furthermore, the possibility of continuous monitoring of labeled immune cells over their entire lifetime is undoubtedly of great value. Hence, it is of great importance to appropriately match the cell labeling strategy with the purpose of the immune cell tracking study. Importantly, to date, there are no reports that would indicate impaired immune cell function caused by any of these approaches.

4. Cell tracking in clinical practice

Implementation of cell tracking methods in clinical practice still needs to face many regulatory and practical issues. Based on the preclinical data, indirect cell labeling has many advantages over the direct method. The possibility of longer cell tracking, the ability to monitor cell proliferation, and fate are the most important advantages. However, several issues need to be solved.

First of all, the range of available radioisotopes is limited. The development of reporter genes expressed in tracked cells that require already clinically approved and nontoxic radioisotope is an ongoing fast and efficient solution. Otherwise, the search for new labels will need to undergo the whole regulatory path.

Another aspect concerns the genetic engineering of the cells. The development of CAR-T technology gives the possibility to use gene-editing approaches in cell labeling for clinical use. Of course, the use of new vectors needs to face many regulatory issues, increasing cost and logistics of preparation of the cell-based product. However, one solution for that might be the co-delivery of the reporter gene in the same vector as the therapeutic gene [226].

The next aspect that cell labeling methods will face is the need for method tailoring. Different cells and different labels should be employed depending on the type of disease and its location. Different diseases attract different leukocyte populations. This is particularly true in oncology, as cancers are located at different sites, have different features (*e.g.* 'cold' vs. 'hot' tumors), and different neighboring tissues that may limit the selection of the proper radioisotope.

The unwanted accumulation of radioactivity in normal immune organs and tissues is also related to the previous comments as isotope carrying cells may certainly be endowed with preferred tropism towards selected tissues, independent of the tumor environments. This aspect is of particular concern in the case of cells carrying long half-life radionuclides.

A specific issue that must also be addressed concerns the stability of labeled cells. In the case of direct methods, the chemical stability of the isotope chelator moiety towards intralysosomal enzymes is an important experimental variable to be considered. In the case of indirect labeling, also the half life of the reporter gene product must be assessed with certainty. In fact, most reporter genes, even when fused with long lived protein moieties, may be targeted by the ubiquitin system and degraded at the proteasome intracellular sites. In both cases (direct and indirect), the degradation of the carrier inside the cell will lead ultimately to the leakage of the isotope outside the cell. As the last issue, the viability of the whole cell itself must be considered given possible intrinsic toxicity of the isotope label at a high concentration within the tracked cell.

Last but not least, before the cell labeling will be a routinely implemented method into clinical practice, the precise biological mechanisms of cell labeling and its effect on the cells and the whole organisms need to be studied [250].

Therefore, from a regulatory and technical point of view, direct cell labeling methods appear to be the most convenient ones in terms of costs and time and also the safest ones in clinical routine, especially when used for short-term cell tracking for diagnostic purposes.

5. Summary

In recent years nuclear imaging methods have been established for noninvasive and real-time monitoring of the long-term distribution and viability of adoptively transferred immune cells, including T cells, B cells, DCs, macrophages, and NK cells, both in preclinical and clinical settings. The most important studies, which were cited in this manuscript, are listed and summarized in Supplementary Table 1. Tracking of immune cells with nuclear imaging has been used for a long time in routine medical practice for diagnostic purposes in infections and inflammatory processes. Radioisotope-based imaging provides numerous advantages in basic research and clinical practice as compared with other molecular imaging modalities. Nuclear imaging modalities are exceptionally sensitive allowing for the use of sub-pharmacological amounts of radiotracers for cell labeling, that will not evoke any biological reactions. Furthermore, these imaging modalities provide quantitative analysis, *e.g. in vivo* concentration of the radiotracer in the tissue region of interest. Besides, the development of multimodal cameras (PET/CT, SPECT/CT, PET/MRI) provides detailed molecular information at both functional and anatomical levels, which overcomes the major shortcoming of nuclear imaging that is the absence of anatomical information. Finally, a great number of novel radiotracers for direct and indirect labeling strategies are being developed, and the growing availability of radiopharmaceuticals and imaging cameras will eventually broaden our understanding of immunological processes in living organisms. The summary of the currently used radiotracers in cell tracking studies containing valuable information concerning their dosage, normal systemic distributions and safety is provided in Table 6.

Immune cell labeling for nuclear imaging, which is essential for live-cell tracking, may be accomplished with direct or indirect labeling techniques. Direct labeling of immune cells, which is performed under *in vitro* conditions with radiotracers before cell transplantation, gives specific images of low cell numbers with no need for genetic manipulation. Hence, immune cell labeling with direct methods using radiotracers approved for clinical use may be potentially translated into the clinic. Indirect labeling, which involves the introduction of a reporter gene (*e.g.*, HSV-TK, hNIS, hNET, and SSTR2) into host cells provides the highest sensitivity and can be employed for longitudinal studies of immune cell

Table 6
The summary of the radiotracers used for immune cell tracking and data concerning their dosages, safety and systemic distribution.

Radiotracer	Cell type + radioactivity of dosage (administered *in vitro* in direct and *in vivo* in indirect cell labeling)	Safety; reported side effects	Data on systemic distribution; absorption coefficient in normal organs
	SPECT radiotracers for direct cell labeling through the mechanism:		
passive diffusion			
[^{111}In]oxine	• $CD8^{+}$Tc lymphocytes (CTLs) with affinity to the Melan-A melanoma antigen. Cells were resuspended in 1 ml of [^{111}In]oxine with a total radioactivity of 2 μCi/10^6 T cells [75] • γδ T cells labeled with the standard nuclear pharmacy ^{111}In-oxine method at 5 pCi/cell [60] • allogeneic NK cells [62] • umbilical cord blood hematopoietic progenitor cells (UCB-NK cells) 2 MBq of [^{111}In]oxinate was added per 10^6 cells [64] • monocyte-derived nonmatured DC (nmDCs) or matured DC (mDCs) – from 0,7 MBq to 20 MBq [82]	• it is reported that ^{111}In is secreted in human milk following administration [251] • sensitivity reactions (urticaria) have been reported [251] • recent studies have found no evidence of carcinogenicity in either rats or mice given oxyquinoline in feed at concentrations of 1500 or 3000 ppm for 103 weeks [251] • it has been denoted, that human lymphocytes labeled with recommended concentrations of [^{111}In]oxine showed chromosome aberrations consisting of gaps, breaks and exchanges that appear to be radiation induced [252]	• administration of [^{111}In]oxine is followed by excessive accumulation of radioactivity in kidneys [253] • [^{111}In]oxine bioaccumulation is observed mainly in liver, spleen, kidneys, bone marrow, stomach, intestine, lungs and muscles [254]
[^{111}In]tropolone	• 1.99 – 7.38 x10^8 human blood-derived WBC + 400 μCi (containing 25 ug tropolone and 37 MBq [^{111}In] per ml) [67] • human blood derived granulocytes + 500–600 μCi [68] • 5 × 10^6 human blood-derived γδ T cells + 1 or 10–15 MBq [69] • 5 × 10^6 human blood-derived γδ T cells + 10–15 MBq [69]	• extensive studies of cellular viability of cells using [^{111}In]tropolone do not report any adverse effects [255] • no adverse effects on animals or patients have been denoted	• distribution studies in animals with tropolone demonstrated an increased concentration in tissues of high lipid content when compared with appropriate controls [256]
[^{99m}Tc]HMPAO	• radiolabeling of the human mononuclear cell fraction derived from 120 ml whole blood + 280 MBq [^{99m}TcHMPAO] [38] • autologous granulocytes and eosinophils were incubated with up to 700 MBq of [^{99m}TcHMPAO] [81] • autologous venous blood eosinophils (mean, 120 MBq; range, 46–199 MBq injected/subject) [83] • CD4 + T cells were directly radiolabelled with ~5 MBq of [^{99m}TcHMPAO] [86] • a part of both mature and immature DCs (about 9 × 106) + 20 mCi [87]	• non-specific activity is oftentimes seen in kidneys, thus causing false-positive results [49] • a very few cases of mild hypersensitivity evidenced by the development of an urticarial erythematous rash have been reported following direct intravenous injection; no serious adverse effects on animals or patients have been denoted [257]	• uptake in the brain reaches a maximum of 3.5–7.0% of the injected dose within one minute of injection; about 20% of the injected dose is removed by the liver immediately after injection and excreted through the hepatobiliary system; about 40% of the injected dose is excreted through the kidneys and urine over the 48 h after injection resulting in a reduction in general muscle and soft tissue background [257]
endocytosis			
[^{99m}Tc]SnF_2	• human blood leukocytes (585 MBq, labeling efficiency 36% – 99,7%) [89]	• no adverse effects on cells nor patients have been denoted	• high uptake in the liver of healthy rats (85.7% of injected dosage), lower in lungs (3.1%) and spleen (7.6%) [258]
	PET radiotracers for direct cell labeling through the mechanism:		
transporter uptake			
[^{18}F]FDG	• 6.6 × 10^7–1.5 × 10^8 human DCs per sample + 84.7 MBq [65] • mixed leukocyte fraction from human blood + 3.7–74 Mbq [93] • autologous leukocytes + 314.5–555 MBq (8.5–15 mCi) [96]	• [^{18}F]FDG for imaging requires the patient to fast before injection and in the case of diabetic patients, blood glucose levels should be monitored before the administration of [^{18}F]FDG [259] • the amounts of [^{18}F]FDG excreted in breastmilk are below the level of concern for the breastfed infant and most international radiation safety organizations state that no interruption of breastfeeding is necessary [260] • overdoses of [^{18}F]FDG injection have not been reported [261]	• excessive and oftentimes non-specific [^{18}F]FDG uptake has been observed in many organs such as the heart, brain, and muscle, and kidneys [49] • [^{18}F]FDG accumulates mainly in the bladder, heart, pancreas, spleen, lungs, and kidneys [261]
[^{124}I]dU	• OVA-specific CD8 + T cells (no data available on the cell number and radioactivity of the compound) [36]	• no adverse effects on animals or patients have been denoted • however, it has been known, that the precorson - deoxyuridine exhibits dose dependent antifolate toxicity leading to perturbation of chromatine [149]	• in humans, marked accumulation of radioisotopes in the thyroid, salivary glands, intenstines, stomach, esophagus and along with elevated uptake in the bone marrow and liver and overall moderate enhancement in the mediastinum and throughout the abdominal cavity [150]

(*continued on next page*)

Table 6 (*continued*)

Radiotracer	Cell type + radioactivity of dosage (administered *in vitro* in direct and *in vivo* in indirect cell labeling)	Safety; reported side effects	Data on systemic distribution; absorption coefficient in normal organs
passive diffusion			
[^{64}Cu]PTSM	• murine splenic lymphocytes (2.8×10^7 - cells) were labeled with 72 μCi of ^{64}Cu–PTSM in 1 ml of medium [39] • 1×10^6 murine OVA Th1 lymphocytes; 0.7–2.2 MBq of [^{64}Cu]PTSM [116]	• no adverse effects on animals or patients have been denoted	• excellent uptake in the brain, liver, and heart after intravenous injection [262]
[^{64}Cu]tropolone	• human white blood cell fraction (derived from 40 ml venous blood) was incubated in saline with 74–185 MBq [^{64}Cu]tropolone [117]	• no adverse effects on cells, animals or patients have been denoted	• no data on bioaccumulation of the radiotracer administered to a healthy organism
[^{68}Ga]oxinate$_3$	• CAR-T lymphocytes in NSG mice; 1×10^6 CAR-T cells were incubated with 1.11 MBq [^{68}Ga]oxinate$_3$ solution [153]	• no adverse effects on animals or patients have been denoted	• most likely - analogous to other oxine-based radiotracers; in rat, fast accumulation of the radiotracer in the liver (SUV 6.8) [263]
absorption into the cell membrane			
[^{18}F]HFB	• human circulating progenitor cells (CPC); different dose ranges of [^{18}F]HFB (0.4–0.6, 1.5–2.5, or 5.0–7.0 mCi) [103]	• no adverse effects on animals or patients have been denoted	• the labeling efficiency was evaluated so far only in rodent mesenchymal stem cells - after 30 min it reached 25% and cell viability was found to be > 90%; furthermore, there was a retention of radiotracer in the cells > 90% over 4 h [44] • predominant uptake of free [^{18}F]HFB is observed in the liver [102]
binding to the cell membrane proteins			
[^{18}F]FBEM	• 1.3×10^7 splenic T lymphocytes from C57Bl/6 mice + 33 MBq [99]	• no adverse effects on animals or patients have been denoted	• in mouse - increased uptake in the lungs, no uptake in the spleen and significant presence in the kidneys and bladder [99]
[^{89}Zr]DBN	• 6×10^6 of mouse-derived melanoma cells (mMCs) or mouse derived DCs or human MSCs + 6 MBq in volume of 100 μl solution [45] • 6×10^6 human cardiopoietic stem cells (CPs) + 6 MBq in volume of 100 μl solution [143] • 5×10^6 Jurkat/CAR-T cells + 185 kBq/100 μl (500 μl in total) [142]	• the effects of intravenously administered radiotracer have not been described yet • however, during our own study, sudden death of BALB/c mice was observed after intravenous administration – the detailed studies on the toxicity of this tracer is required	• the biodistribution of pure radiotracer has not been described yet – the studies on the pharmacokinetics of this tracer is required
[^{124}I]FIT-(PhS)$_2$Mal	• Jurkat cells; (~100 KBq/10^6 cells) [46]	• no adverse effects on animals or patients have been denoted	• mainly liver and kidneys [264]
endocytosis			
[^{64}Cu]PEI	• U87MG cells (1×10^7) were incubated with 18.5 MBq of [^{64}Cu]PEI; the labeling efficiency was low (20.5% and the efflux reached over 60% in 27 h [35]	• no adverse effects on cells, animals, or patients have been denoted	• accumulates mainly in the liver, kidney, but also intestine, lungs, heart, spleen, muscle, pancreas, and brain [265]
[^{89}Zr]chitosan	• blood-derived leukocyte fraction; specific radioactivity of 24.7 MBq/mg chitosan nanoparticle [144]	• no adverse effects on animals or patients have been denoted	• accumulates in kidneys [266]
[^{89}Zr]dextran Ns	• the cell labeling procedure resulted in the proportion of 15 μCi of activity per 8×10^6 murine B cells [145] and 11.2 ± 3.25 MBq per $8.4 \pm 2.4 \times 10^6$ murine T cells [147]	• no adverse effects have been denoted	• after I.V. injection to mice, it was found to be located primarily in tissue resident-macrophages; pharmacokinetics depends on the size of Ns; in mouse, after I.V. injection, the total activity of 13 nm Ns was 22 ± 3% in liver, 19 ± 2% in circulating cells and 2 ± 0.1% in spleen, and the remainder was distributed in other organs, including high uptake in lymph nodes [216]
[^{68}Ga]MSNs	• 100 (one hundred) MDA-MB-231 breast cancer cells + 323 Bq [^{68}Ga]-MSN [152]	• no adverse effects on animals or patients have been denoted	• no data were found regarding [^{68}Ga] MSNs bioaccumulation
SPECT radiotracers for indirect labeling of cells expressing:			
enzymatic reporter gene			
[^{131}I]FIAU	• intravenous injection (0.01 mCi/animal) via the tail vein [267]	• no toxicity from the diagnostic dose reported	• clearance through urinary excretion (clearance from blood was completed in 24 h); high radioactivity accumulation observed in kidneys and blood in the early phase (1, 4 h); the low radiotracer uptake in non-target tissue; the high tumour/blood ratios enables tumor imaging [267]

Table 6 (*continued*)

Radiotracer	Cell type + radioactivity of dosage (administered *in vitro* in direct and *in vivo* in indirect cell labeling)	Safety; reported side effects	Data on systemic distribution; absorption coefficient in normal organs
transporter reporter gene [$^{99m}TcO_4^-$]	• intravenous injection of 340 MBq ± 10% of [$^{99m}TcO_4^-$] in a man [268]	• no clinically detectable pharmacologic effects caused by the administration of the diagnostic dose [268]	• clearance through urinary excretion; the highest radiotracer uptake in the thyroid, salivary glands, stomach, and urinary bladder [268]
[^{123}I]MIBG	• intravenous injection of 400 MBq (10.8 mCi) of [^{123}I]MIBG in man [269]	• no clinically detectable pharmacologic effects caused by the administration of the diagnostic dose	• clearance through urinary excretion (~50% of the administered radioactivity appears in the urine within 24 h and 70–90% within 48 h after administration); the tracer accumulates in the liver, salivary glands, nasal mucosa, heart, lungs and bowel; high *in vivo* stability (metabolites that account for <10% of the injected dose are m-iodohippuric acid, m-iodobenzoic acid, and 4-hydroxy-3-iodobenzylguanidine and free radioiodide); accumulation of unbound ^{123}I in the thyroid occurs only with inadequate blockade; the effective dose – 0.013 mSv/MBq [269,270]
receptor reporter gene [^{111}In]-pentetreotide	• intravenous injection of 120 to 220 MBq (3.2–5.9 mCi) of [^{111}In]-pentetreotide in man [271]	•no clinically detectable pharmacologic effects caused by the administration of the diagnostic dose	• rapid blood clearance: 35% of the administered activity remains in the blood at 10 min and only 1% at 20 h after injection; clearance through urinary excretion: (~50% of the administered activity is in the urine by 6 h and 85% within 24 h; the tracer accumulates in liver, spleen, pituitary, thyroid and kidneys, bladder, gall bladder; the organs exposed to the highest doses are the kidneys (0.52 mGy/MBq), urinary bladder wall (0.35 mGy/MBq) and spleen (0.34 mGy/MBq); the effective dose: 0.054 mSv/MBq [271,272]
PET radiotracers for indirect labeling of cells expressing:			
enzymatic reporter gene [^{124}I]FIAU	• intravenous injection of 77.7 MBq (2.1 mCi) of [^{124}I]FIAU in a man [273] • intravenous bolus injection of a dose of 74 MBq (2 mCi)) of [^{124}I]FIAU [274,275] (to limit radiation exposure of thyroid tissue from the formation of free [^{124}I]iodide from the metabolism of [^{124}I]FIAU, patients were given potassium iodide tablets)	• no clinically detectable pharmacologic effects caused by administration [274,275]	• clearance through urinary excretion [274,275] • organs with the highest radiation exposure are kidney, liver, spleen, and urinary bladder (doses to most organs ranged from 0.11 to 0.76 mGy/MBq); the effective dose – 0.16 to 0.20 mSv/MBq [274] • an exponential washout from the different organs during several hours followed by a late peak (>15 h) in the bladder • no penetration across the blood–brain barrier (however some accumulation observed within intact glioma tumor, probably due to a compromised BBB [273] → possible detection of HSV1-tk or hmTK2 expressing immune cells within these tumors)
[^{18}F]FHBG	• injection of 70.3–229.4 MBq of [^{18}F]FHBG into a hand vein of a man [230,276]	• the phase I study showed the safety of, and lack of toxicity of intravenously injected [^{18}F]FHBG tracer for imaging purposes [276]	• rapid blood clearance (8.42% ± 4.76% of the peak blood activity remained at 30 min following injection); primary routes of clearance are renal and hepatobiliary (high activities observed in the bladder, gut, liver, and kidney → possibly not suitable for imaging HSV1-tk gene expression in the lower abdomen); bladder absorbs the highest radiation dose; rapid clearance from all other tissues → low background signal; high *in vivo* stability (in the urine, 83% of activity 180 min following administration was stable [^{18}F]FHBG); no penetration across the blood–brain barrier (however some accumulation observed within intact glioma tumors or tumor resection sites, probably due to a compromised BBB [230] → possible detection of HSV1-tk expressing immune cells within these tumors)

(*continued on next page*)

Table 6 (*continued*)

Radiotracer	Cell type + radioactivity of dosage (administered *in vitro* in direct and *in vivo* in indirect cell labeling)	Safety; reported side effects	Data on systemic distribution; absorption coefficient in normal organs
[^{18}F]FEAU	• mice injected *retro*-orbitally with 29.6 MBq (800 μCi) of [^{18}F]FEAU [277]	• no safety data in man	• both renal and hepato-biliary clearance; high activities observed in large intestine, gallbladder, small intestine and kidney [277]
[^{18}F]L-FMAU	• bolus intravenous injection of ~56 MBq (1.5 mCi) sterile l-[^{18}F]L-FMAU in man [278]	• no safety data in man	• biliary excretion of the radiotracer; in man high signals observed in liver, kidneys, gall bladder, bladder, the GI tract and myocardium → the accumulation of the radiotracer in liver and myocardium may compromise its use for PET imaging of therapeutic cells at these sites [278]
transporter reporter gene			
[^{18}F]TFB	• intravenous injection of [^{18}F]TFB (333–407 MBq) in healthy volunteers [279]	• safe and non-toxic probe - no immediate or delayed adverse reactions were observed in volunteers after the radiotracer administration; the estimated absorbed radiation doses are acceptable for clinical imaging purposes [279]	• a multi-phasic blood clearance of the radiotracer (two rapid clearance phases during the first 20 min, followed by a slower clearance phase); clearance through urinary excretion • high uptakes observed in thyroid, stomach, salivary glands, and bladder; the highest radiation doses were observed in the thyroid, urinary bladder wall, intestine wall, heart wall, kidneys, liver, pancreas and spleen; high *in vivo* stability of the radiotracer (minor ^{18}F-labeled metabolites in the blood and urine during 4 h analysis) [279]
[^{124}I]MIBG	• intravenous administration of 3.07–4.84 MBq of [^{124}I]MIBG via tail vein of athymic mice [280]	• safe and non-toxic probe [280]	• high uptake in heart and bladder before the 2 h time point; thyroid uptake increases after the 24 h time point, whereas uptake in liver, kidneys, and lungs decreases with time; the highest mean equivalent dose is observed in the thyroid; the estimated mean human-equivalent effective dose – 0.25 mSv/MBq [280]
[^{18}F]MFBG	• intravenous bolus injection of a dose of 148–444 MBq (4–12 mCi) of [^{18}F]MFBG [281]	• first-in-human study showed the safety of, and lack of toxicity of intravenously injected [^{18}F]MFBG tracer for imaging purposes (no side effects seen in any patients after [^{18}F]MFBG injection); the estimated absorbed radiation doses are acceptable for clinical imaging purposes [281]	• rapid and biexponential blood clearance (mean biologic $T_{1/2}$ of 18 min for rapid phase and 6 h for slower phase); mono-exponential whole-body clearance, with a mean biologic $T_{1/2}$ of 1.95 h, enabling early imaging at 1 – 2 h after injection; clearance through urinary excretion (45% of the administered activity in the bladder by 1 h after injection) • high activity in blood, liver, and salivary glands, and mild uptake in kidneys and spleen, that decreases with time; urinary bladder receives the highest radiation dose; the effective dose – 0.023 ± 0.012 mSv/MBq [281]
receptor reporter gene			
[^{68}Ga]-DOTATOC	• intravenous injection of 86.9 ± 16.4 MBq (range, 62–112 MBq) of the radiotracer in man [282] • intravenous injection of 242.39 ± 53.38 MBq (range 156.5–334.2 MBq) of the radiotracer in man [283]	• safe and non-toxic probe - no immediate or delayed adverse reactions were observed in volunteers during the one week follow up after the radiotracer administration; the estimated absorbed radiation doses are acceptable for clinical imaging purposes [283]	• clearance through urinary excretion (at 4 h after injection 18.8 ± 1.0% ID of the injected activity was eliminated in the urine) [283] • the highest uptake at 1, 2, and 3 h after administration observed in spleen, kidneys and liver; the highest absorbed organ doses observed in urinary bladder, followed by spleen, kidneys, adrenals and liver [282] • the effective dose from 2.1 [282] to 4.8 mSv [283] from 100 MBq injected activity

Table 6 (*continued*)

Radiotracer	Cell type + radioactivity of dosage (administered *in vitro* in direct and *in vivo* in indirect cell labeling)	Safety; reported side effects	Data on systemic distribution; absorption coefficient in normal organs
[^{18}F]DCFPyL	• intravenous administration of 3.6 ± 0.18 MBq/Kg of [^{18}F]DCFPyL [284] • intravenous administration of 320.6 MBq (8.66 mCi, range 310.8–327.1 MBq (8.40–8.84 mCi)) of [^{18}F]DCFPyL [285]	• safe and non-toxic probe - no immediate or delayed adverse reactions were observed in volunteers after the radiotracer administration [285]	• rapid blood clearance [285] • clearance through urinary excretion [284,285] • high *in vivo* stability [285] • the highest activities were observed in the kidneys and bladder, followed by the salivary glands, liver, spleen and proximal small bowel [284] • the highest radiation dose observed in kidneys (0.0945 mGy/MBq), followed by urinary bladder wall (0.0864 mGy/MBq), submandibular glands (0.0387 mGy/MBq), and liver (0.0380 mGy/MBq); no radiotracer uptake in brain; the effective radiation dose – 0.0139 mGy/MBq from an injected dose of 370 MBq (10 mCi) [285]

distribution, activation, proliferation, and survival. Although indirect labeling of immune cells for reporter gene-based tracking in the clinical settings may be considered for adoptive cell therapies, such as CAR-T cells, that are already genetically modified, the genetic modification of primary immune cells for *in vivo* tracking purposes in humans probably will not be routinely used in the clinical practice. Limited use of reporter genes in man is caused by the fact that genetic modification of the target cell genome with viruses can lead to harmful effects owing to uncontrolled insertional mutagenesis. Genome editing methods, allowing for the reporter gene integration to precise genomic loci, may potentially circumvent this limitation and increase the safety of reporter gene imaging. Currently, available cell labeling techniques do not meet all expectations as they all have advantages and disadvantages. Key issues concerning the fate and distribution of labeled cells to unwanted sites in the body and consequent accumulation of radioactivity or undesirable leakage of radiotracer due to tracked cell premature degradation or simple biochemical degradation of the chelator molecule must be addressed. Consequently, a suitable strategy for immune cell labeling needs to be chosen for each experimental setup.

Despite the above-mentioned hurdles, nuclear imaging-based *in vivo* tracking of immune cells is a valuable technique that may provide us with a noninvasive way of studying the functioning of the immune system and contribute to the development of therapies using or targeting immune cells.

The room for improvement, besides the current biological and physical limits of the PET scanners, are proper approaches for data acquisition and algorithms for data analysis. The recent interesting study [152] showed that a very short acquisition timeframe and a reconstruction algorithm used for tracking single-cell radioactivity required a limited number of photon-coincidence detections and a spline method to track the cell. Importantly, the authors were able to track a single cell after *i.v.* injection. It was shown that a proper algorithm for a digital PET scanner with sensitive and excellent time-of-flight properties would limit the necessary radioactivity of the cell for its localization [286]. The cell tracking study utilizing PET, recently conducted by Sato et al. on the rhesus monkeys, was fully successful and importantly, no side effects were observed. That would give a potential clinical translation of this excellent preclinical method [135].

However, before the widely implementation of cell tracking methods in clinical practice will be possible, this method needs to face many regulatory and practical issues. The most important issues to solve seems to be the selection of the proper radioisotopes, genetic engineering of the cells, tailoring of cell-labeling methods to particular disease and site, as well as validation of the safety of such approaches.

Funding sources

This paper and research cited in this article are founded by the European Research Council Starting Grant McHAP: 715048 (MK). The contribution of Łukasz Cheda was realized within Project No POWR.03.02.00-00-I009/17-00 (Operational Project Knowledge Education Development 2014-2020 co-financed by European Social Fund) (ŁCh) and the National Science Centre, PRELUDIUM 18 Grant: contract no. UMO-2019/35/N/ST4/01987 (ŁCh). The research described in this paper has been founded by the NCN SONATA BIS: UMO-2015/18/E/N26/00642 grant given to MK from the National Science Centre (Poland).

Declaration of Competing Interest

The authors declare that they have no known competing financial interests or personal relationships that could have appeared to influence the work reported in this paper.

Acknowledgments

We would like to kindly acknowledge Dr. Marta Kiraga from Institute of Civil Engineering, Department of Hydrotechnics, Technology and Management. Warsaw University of Life Sciences, and Msc. Dariusz Zielonka from Institute of Biology, Department of Biochemistry and Microbiology, Warsaw University of Life Sciences, for technical support in the creation of figures. We are grateful to Dr. Elisabetta Manuali and Dr. Silvia Pavone from Istituto Zooprofilattico Sperimentale dell'Umbria e delle Marche, Italy, for the histopathological examination of murine organ samples.

Appendix A. Supplementary data

Supplementary data to this article can be found online at https://doi.org/10.1016/j.ccr.2021.214008.

References

[1] M.W. Rohaan, S. Wilgenhof, J.B.A.G. Haanen, Adoptive cellular therapies: the current landscape, Virchows Arch. 474 (2019) 449–461, https://doi.org/10.1007/s00428-018-2484-0.

[2] F. Galli, J.V. Aguilera, B. Palermo, S.N. Markovic, P. Nisticò, A. Signore, Relevance of immune cell and tumor microenvironment imaging in the new era of immunotherapy, J. Exp. Clin. Cancer Res. 39 (2020) 89, https://doi.org/10.1186/s13046-020-01586-y.
[3] E. Compalati, M. Penagos, F. Tarantini, G. Passalacqua, G.W. Canonica, Specific immunotherapy for respiratory allergy: state of the art according to current meta-analyses, Ann. Allergy Asthma Immunol. 102 (2009) 22–28, https://doi.org/10.1016/S1081-1206(10)60103-2.
[4] J.E. Cohen, S. Merims, S. Frank, R. Engelstein, T. Peretz, M. Lotem, Adoptive cell therapy: past, present and future, Immunotherapy. 9 (2017) 183–196, https://doi.org/10.2217/imt-2016-0112.
[5] A. Manohar, J. Ahuja, J.K. Crane, Immunotherapy for Infectious Diseases: Past, Present, and Future, Immunol. Invest. 44 (2015) 731–737, https://doi.org/10.3109/08820139.2015.1093914.
[6] C.M. Connolly, K.J. Donohoe, Nuclear Medicine Imaging of Infection, Semin. Roentgenol. 52 (2017) 114–119, https://doi.org/10.1053/j.ro.2016.07.001.
[7] M. Roca, E.F.J. de Vries, F. Jamar, O. Israel, A. Signore, Guidelines for the labelling of leucocytes with 111In-oxine, Eur J Nucl Med Mol Imaging. 37 (2010) 835–841, https://doi.org/10.1007/s00259-010-1393-5.
[8] O. Israel, O. Pellet, L. Biassoni, D. De Palma, E. Estrada-Lobato, G. Gnanasegaran, T. Kuwert, C. la Fougère, G. Mariani, S. Massalha, D. Paez, F. Giammarile, Two decades of SPECT/CT – the coming of age of a technology: An updated review of literature evidence, Eur J Nucl Med Mol Imaging. 46 (2019) 1990–2012, https://doi.org/10.1007/s00259-019-04404-6.
[9] M.S. Guy, A. Kardan, 111In WBC SPECT/CT Detection of a Radiographically Occult Solitary Infected Renal Cyst in Polycystic Kidney Disease, Clinical Nuclear Medicine 40 (2015) 542–544, https://doi.org/10.1097/RLU.0000000000000771.
[10] M. Krekorian, G.O. Fruhwirth, M. Srinivas, C.G. Figdor, S. Heskamp, T.H. Witney, E.H.J.G. Aarntzen, Imaging of T-cells and their responses during anti-cancer immunotherapy, Theranostics. 9 (2019) 7924–7947, https://doi.org/10.7150/thno.37924.
[11] S.L. Pimlott, A. Sutherland, Molecular tracers for the PET and SPECT imaging of disease, Chem. Soc. Rev. 40 (2011) 149–162, https://doi.org/10.1039/B922628C.
[12] J. Perrin, M. Capitao, M. Mougin-Degraef, F. Guérard, A. Faivre-Chauvet, L. Rbah-Vidal, J. Gaschet, Y. Guilloux, F. Kraeber-Bodéré, M. Chérel, J. Barbet, Cell Tracking in Cancer Immunotherapy, Front. Med. 7 (2020) 34, https://doi.org/10.3389/fmed.2020.00034.
[13] C.E. McCarthy, J.M. White, N.T. Viola, H.M. Gibson, In vivo Imaging Technologies to Monitor the Immune System, Front. Immunol. 11 (2020) 1067, https://doi.org/10.3389/fimmu.2020.01067.
[14] M.G. Stabin, A.B. Brill, Radiation Dosimetry and Exposure in Nuclear Medicine, Semin. Nucl. Med. 38 (2008) 306–307, https://doi.org/10.1053/j.semnuclmed.2008.05.009.
[15] P. Zanzonico, Principles of Nuclear Medicine Imaging: Planar, SPECT, PET, Multi-modality, and Autoradiography Systems, Radiat. Res. 177 (2012) 349–364, https://doi.org/10.1667/RR2577.1.
[16] E. Wolfs, C.M. Verfaillie, K. Van Laere, C.M. Deroose, Radiolabeling Strategies for Radionuclide Imaging of Stem Cells, Stem Cell Reviews and Reports. 11 (2015) 254–274, https://doi.org/10.1007/s12015-014-9575-3.
[17] N. Farahi, C. Loutsios, N. Tregay, C. Summers, L.S.C. Lok, P. Ruparelia, C.K. Solanki, D. Gillett, E.R. Chilvers, A.M. Peters, Radiolabelled leucocytes in human pulmonary disease, Br. Med. Bull. 127 (2018) 69–82, https://doi.org/10.1093/bmb/ldy022.
[18] O. Ivashchenko, F. van der Have, J.L. Villena, H.C. Groen, R.M. Ramakers, H.H. Weinans, F.J. Beekman, Quarter-Millimeter-Resolution Molecular Mouse Imaging with U-SPECT +, Mol Imaging. 14 (2015) 7290.2014.00053. https://doi.org/10.2310/7290.2014.00053.
[19] A. Rahmim, H. Zaidi, PET versus SPECT: strengths, limitations and challenges, Nucl. Med. Commun. 29 (2008) 193–207, https://doi.org/10.1097/MNM.0b013e3282f3a515.
[20] L. Jødal, C. Le Loirec, C. Champion, Positron range in PET imaging: an alternative approach for assessing and correcting the blurring, Phys. Med. Biol. 57 (2012) 3931–3943, https://doi.org/10.1088/0031-9155/57/12/3931.
[21] National Research Council, Mathematics and Physics of Emerging Biomedical Imaging, National Academies Press, Washington, 1996.
[22] D.L. Bailey, K.P. Willowson, An Evidence-Based Review of Quantitative SPECT Imaging and Potential Clinical Applications, J Nucl Med. 54 (2013) 83, https://doi.org/10.2967/jnumed.112.111476.
[23] D.L. Bailey, K.P. Willowson, Quantitative SPECT/CT: SPECT joins PET as a quantitative imaging modality, Eur. J. Nucl. Med. Mol. Imaging 41 (2014) 17–25, https://doi.org/10.1007/s00259-013-2542-4.
[24] E.C. Frey, J.L. Humm, M. Ljungberg, Accuracy and precision of radioactivity quantification in nuclear medicine images, Semin Nucl Med. 42 (2012) 208–218, https://doi.org/10.1053/j.semnuclmed.2011.11.003.
[25] J.J. Vaquero, P. Kinahan, Positron Emission Tomography: Current Challenges and Opportunities for Technological Advances in Clinical and Preclinical Imaging Systems, Annu. Rev. Biomed. Eng. 17 (2015) 385–414, https://doi.org/10.1146/annurev-bioeng-071114-040723.
[26] S. Deleye, R. Van Holen, J. Verhaeghe, S. Vandenberghe, S. Stroobants, S. Staelens, Performance evaluation of small-animal multipinhole μSPECT scanners for mouse imaging, Eur. J. Nucl. Med. Mol. Imaging 40 (2013) 744–758, https://doi.org/10.1007/s00259-012-2326-2.
[27] F. van der Have, O. Ivashchenko, M.C. Goorden, R.M. Ramakers, F.J. Beekman, High-resolution clustered pinhole 131Iodine SPECT imaging in mice, Nucl. Med. Biol. 43 (2016) 506–511, https://doi.org/10.1016/j.nucmedbio.2016.05.015.
[28] K. Van Audenhaege, R. Van Holen, S. Vandenberghe, C. Vanhove, S.D. Metzler, S.C. Moore, Review of SPECT collimator selection, optimization, and fabrication for clinical and preclinical imaging, Med. Phys. 42 (2015) 4796–4813, https://doi.org/10.1118/1.4927061.
[29] M. Lukas, A. Kluge, N. Beindorff, W. Brenner, Multi-Isotope Capabilities of a Small-Animal Multi-Pinhole SPECT System, J Nucl Med. 61 (2020) 152, https://doi.org/10.2967/jnumed.119.226027.
[30] G. Gnanasegaran, J.R. Ballinger, Molecular imaging agents for SPECT (and SPECT/CT), Eur J Nucl Med Mol Imaging. 41 (2014) 26–35, https://doi.org/10.1007/s00259-013-2643-0.
[31] M.C. Graham, K.S. Pentlow, O. Mawlawi, R.D. Finn, F. Daghighian, S.M. Larson, An investigation of the physical characteristics of ^{66}Ga as an isotope for PET imaging and quantification, Med. Phys. 24 (1997) 317–326, https://doi.org/10.1118/1.597924.
[32] K. Pentlow, Quantitative Imaging of Yttrium-86 with PET The Occurrence and Correction of Anomalous Apparent Activity in High Density Regions, Clinical Positron Imaging 3 (2000) 85–90, https://doi.org/10.1016/S1095-0397(00)00046-7.
[33] O.O. Peltek, A.R. Muslimov, M.V. Zyuzin, A.S. Timin, Current outlook on radionuclide delivery systems: from design consideration to translation into clinics, J. Nanobiotech. 17 (2019) 90, https://doi.org/10.1186/s12951-019-0524-9.
[34] C. Zeelen, C. Paus, D. Draper, S. Heskamp, A. Signore, F. Galli, C.M. Griessinger, E.H. Aarntzen, In-vivo imaging of tumor-infiltrating immune cells: implications for cancer immunotherapy, Quart. J. Nucl. Medi. Mole. Imag. 62 (2018) 56–77, https://doi.org/10.23736/S1824-4785.17.03052-7.
[35] Z. Li, K. Chen, Z. Wu, H. Wang, G. Niu, X. Chen, ^{64}Cu-Labeled polyethyleneimine (PEI) for cell trafficking and tumor imaging, J Nucl Med. 49 (2008) 415–423, https://doi.org/10.1007/s11307-009-0228-x.
[36] M. Hokland, M.S. Petersen, C.C. Fleischer, S.B. Hansen, H. Stüdkilde-Jürgensen, U. Skands, J. Marqversen, T. Blankenstein, H.J. Gundersen, R. Agger, Monitoring in vivo T cell traficking to tumors by positron emission tomography and magnetic resonance imaging, JCO 22 (2004), https://doi.org/10.1200/jco.2004.22.90140.2571 2571.
[37] M.L. Thakur, A.W. Segal, L. Louis, M.J. Welch, J. Hopkins, T.J. Peters, Indium-111-labeled cellular blood components: mechanism of labeling and intracellular location in human neutrophils, J. Nucl. Med. 18 (1977) 1022–1026.
[38] C. Jorgensen, I. Couret, C. Bologna, M. Rossi, J. Sany, Radiolabelled lymphocyte migration in rheumatoid synovitis, Ann. Rheum. Dis. 54 (1995) 39–44, https://doi.org/10.1136/ard.54.1.39.
[39] N. Adonai, K.N. Nguyen, J. Walsh, M. Iyer, T. Toyokuni, M.E. Phelps, T. McCarthy, D.W. McCarthy, S.S. Gambhir, Ex vivo cell labeling with 64Cu-pyruvaldehyde-bis(N4-methylthiosemicarbazone) for imaging cell trafficking in mice with positron-emission tomography, Proc. Natl. Acad. Sci. 99 (2002) 3030–3035, https://doi.org/10.1073/pnas.052709599.
[40] P. Afzelius, A.K. Alstrup, H.C. Schønheyder, P. Borghammer, S.B. Jensen, D. Bender, O.L. Nielsen, Utility of (11)C-methionine and (11)C-donepezil for imaging of Staphylococcus aureus induced osteomyelitis in a juvenile porcine model: comparison to autologous (111)In-labelled leukocytes, (99m) Tc-DPD, and (18)F-FDG, Am J Nucl Med Mol Imaging 6 (2016) 286–300.
[41] H. Ullman, K. Viragh, M. Thomas, C. Ni, 111In-Labeled White Blood Cell Uptake in the Urinary Bladder in Occult Urinary Tract Infection, Clin. Nucl. Med. 46 (2021), https://doi.org/10.1097/RLU.0000000000003446.
[42] A. Grabner, D. Kentrup, B. Edemir, Y. Sirin, H. Pavenstadt, E. Schlatter, O. Schober, M. Schafers, U. Schnockel, S. Reuter, PET with 18F-FDG-Labeled T Lymphocytes for Diagnosis of Acute Rat Renal Allograft Rejection, J. Nucl. Med. 54 (2013) 1147–1153, https://doi.org/10.2967/jnumed.112.109231.
[43] R. Meier, M. Piert, G. Piontek, M. Rudelius, R.A. Oostendorp, R. Senekowitsch-Schmidtke, T.D. Henning, W.S. Wels, C. Uherek, E.J. Rummeny, H.E. Daldrup-Link, Tracking of [18F]FDG-labeled natural killer cells to HER2/neu-positive tumors, Nucl. Med. Biol. 35 (2008) 579–588, https://doi.org/10.1016/j.nucmedbio.2008.02.006.
[44] B. Ma, K.D. Hankenson, J.E. Dennis, A.I. Caplan, S.A. Goldstein, M.R. Kilbourn, A simple method for stem cell labeling with fluorine 18, Nucl. Med. Biol. 32 (2005) 701–705, https://doi.org/10.1016/j.nucmedbio.2005.04.018.
[45] A. Bansal, M.K. Pandey, Y.E. Demirhan, J.J. Nesbitt, R.J. Crespo-Diaz, A. Terzic, A. Behfar, T.R. DeGrado, Novel 89Zr cell labeling approach for PET-based cell trafficking studies, EJNMMI Research. 5 (2015) 19, https://doi.org/10.1186/s13550-015-0098-y.
[46] T.T. Pham, Z. Lu, C. Davis, C. Li, F. Sun, J. Maher, R. Yan, Iodine-124 Based Dual Positron Emission Tomography and Fluorescent Labeling Reagents for *In Vivo* Cell Tracking, Bioconjugate Chem. 31 (2020) 1107–1116, https://doi.org/10.1021/acs.bioconjchem.9b00799.
[47] J.G. McAfee, G. Subramanian, G. Gagne, Technique of leukocyte harvesting and labeling: Problems and perspectives, Semin. Nucl. Med. 14 (1984) 83–106, https://doi.org/10.1016/S0001-2998(84)80023-9.
[48] M.F. Kircher, J.R. Allport, E.E. Graves, V. Love, L. Josephson, A.H. Lichtman, R. Weissleder, Vivo high resolution three-Dimensional Imaging of Antigen-Specific Cytotoxic T-Lymphocyte Trafficking to Tumors, Cancer Res 63 (2003) 6838–6846.
[49] E. Salmanoglu, S. Kim, M.L. Thakur, Currently Available Radiopharmaceuticals for Imaging Infection and the Holy Grail, Semin. Nucl. Med. 48 (2018) 86–99, https://doi.org/10.1053/j.semnuclmed.2017.10.003.

[50] S. Liu, The role of coordination chemistry in the development of target-specific radiopharmaceuticals, Chem. Soc. Rev. 33 (2004) 445–461, https://doi.org/10.1039/B309961J.
[51] T.J. Wadas, E.H. Wong, G.R. Weisman, C.J. Anderson, Coordinating Radiometals of Copper, Gallium, Indium, Yttrium, and Zirconium for PET and SPECT Imaging of Disease, Chem. Rev. 110 (2010) 2858–2902, https://doi.org/10.1021/cr900325h.
[52] D.S. MacPherson, K. Fung, B.E. Cook, L.C. Francesconi, B.M. Zeglis, A brief overview of metal complexes as nuclear imaging agents, Dalton Trans. 48 (2019) 14547–14565, https://doi.org/10.1039/C9DT03039E.
[53] J.G. McAfee, M.L. Thakur, Survey of Radioactive Agents for in Vitro Labeling of Phagocytic Leukocytes. I. Soluble Agents, J Nucl Med. 17 (1976) 480–487.
[54] A.W. Segal, R.N. Arnot, M.L. Thakur, J.P. Lavender, INDIUM-111-LABELLED LEUCOCYTES FOR LOCALISATION OF ABSCESSES, The Lancet. 308 (1976) 1056–1058, https://doi.org/10.1016/S0140-6736(76)90969-7.
[55] M.A. Green, J.C. Huffman, The molecular structure of indium oxine, J. Nucl. Med. 29 (1988) 417–420.
[56] C. Muller, C.C. Zielinski, W. Linkesch, Vivo Tracing of Indium- 111 Oxine-Labeled Human Peripheral Blood Mononuclear Cells in Patients with Lymphatic Malignancies, J Nucl Med 30 (1989) 1005–1011.
[57] N. Meidenbauer, J. Marienhagen, M. Laumer, S. Vogl, J. Heymann, R. Andreesen, A. Mackensen, Survival and Tumor Localization of Adoptively Transferred Melan-A-Specific T Cells in Melanoma Patients, J Immunol. 170 (2003) 2161–2169, https://doi.org/10.4049/jimmunol.170.4.2161.
[58] M.J. Pittet, J. Grimm, C.R. Berger, T. Tamura, G. Wojtkiewicz, M. Nahrendorf, P. Romero, F.K. Swirski, R. Weissleder, In vivo imaging of T cell delivery to tumors after adoptive transfer therapy, Proc. Natl. Acad. Sci. 104 (2007) 12457–12461, https://doi.org/10.1073/pnas.0704460104.
[59] A.C. Parente-Pereira, J. Burnet, D. Ellison, J. Foster, D.M. Davies, S. van der Stegen, S. Burbridge, L. Chiapero-Stanke, S. Wilkie, S. Mather, J. Maher, Trafficking of CAR-Engineered Human T Cells Following Regional or Systemic Adoptive Transfer in SCID Beige Mice, J Clin Immunol. 31 (2011) 710–718, https://doi.org/10.1007/s10875-011-9532-8.
[60] B.H. Beck, H.-G. Kim, H. Kim, S. Samuel, Z. Liu, R. Shrestha, H. Haines, K. Zinn, R.D. Lopez, Adoptively transferred ex vivo expanded γδ-T cells mediate in vivo antitumor activity in preclinical mouse models of breast cancer, Breast Cancer Res Treat. 122 (2010) 135–144, https://doi.org/10.1007/s10549-009-0527-6.
[61] M. Shapovalova, S.R. Pyper, B.S. Moriarity, A.M. LeBeau, The Molecular Imaging of Natural Killer Cells, Mol Imag. 17 (2018), https://doi.org/10.1177/1536012118794816.
[62] B. Meller, C. Frohn, J.-M. Brand, I. Lauer, L.F. Schelper, K. von Hof, H. Kirchner, E. Richter, M. Baehre, Monitoring of a new approach of immunotherapy with allogenic 111In-labelled NK cells in patients with renal cell carcinoma, Eur. J. Nucl. Med. Mol. Imaging 31 (2004) 403–407, https://doi.org/10.1007/s00259-003-1398-4.
[63] L. Matera, A. Galetto, M. Bello, C. Baiocco, I. Chiappino, G. Castellano, A. Stacchini, M.A. Satolli, M. Mele, S. Sandrucci, A. Mussa, G. Bisi, T.L. Whiteside, In vivo migration of labeled autologous natural killer cells to liver metastases in patients with colon carcinoma, Journal of Translational Medicine 4 (2006) 49, https://doi.org/10.1186/1479-5876-4-49.
[64] J. Cany, A.B. van der Waart, M. Tordoir, G.M. Franssen, B.N. Hangalapura, J. de Vries, O. Boerman, N. Schaap, R. van der Voort, J. Spanholtz, H. Dolstra, Natural Killer Cells Generated from Cord Blood Hematopoietic Progenitor Cells Efficiently Target Bone Marrow-Residing Human Leukemia Cells in NOD/SCID/IL2Rgnull Mice, PLoS ONE 8 (2013), https://doi.org/10.1371/journal.pone.0064384 e64384.
[65] H.M. Prince, D.M. Wall, D. Ritchie, D. Honemann, S. Harrrison, H. Quach, M. Thompson, R. Hicks, E. Lau, J. Davison, M. Loudovaris, J. Moloney, B. Loveland, J. Bartholeyns, A. Katsifis, L. Mileshkin, In Vivo Tracking of Dendritic Cells in Patients With Multiple Myeloma, J Immunother 31 (2008) 166–179, https://doi.org/10.1097/CJI.0b013e31815c5153.
[66] C. Martelli, M. Borelli, L. Ottobrini, V. Rainone, A. Degrassi, M. Russo, U. Gianelli, S. Bosari, C. Fiorini, D. Trabattoni, M. Clerici, G. Lucignani, In Vivo Imaging of Lymph Node Migration of MNP- and 111In-Labeled Dendritic Cells in a Transgenic Mouse Model of Breast Cancer (MMTV-Ras), Mol. Imag. Biol. 14 (2012) 183–196, https://doi.org/10.1007/s11307-011-0496-0.
[67] L. Mortelmans, A. Verbruggen, S. Malbrain, M.J. Heynen, C. de Bakkcr, M. Boogaerts, M. de Roo, Evaluation of 11 labelled white blood cells by in vitro functional tests and electron microscopy, Eur J Nucl Med 14 (1988) 159–164, https://doi.org/10.1007/BF00293542.
[68] D.S. Schauwecker, R.W. Burt, H.-M. Park, B.H. Mock, R.M. Witt, M.M. Tobolski, H.N. Weilman, Clinical Comparison of Indium-11, J. Nucl. Med. 27 (1986) 1675–1679.
[69] J.-T.-W. Wang, N.O. Hodgins, W.T. Al-Jamal, J. Maher, J.K. Sosabowski, K.T. Al-Jamal, Organ Biodistribution of Radiolabelled γδ T Cells Following Liposomal Alendronate Administration in Different Mouse Tumour Models 4 (2020) 12.
[70] D. Chroustová, N. El-Lababidi, J. Trnka, L. Černa, L. Lambert, Scintigraphy with 99mTc-HMPAO labeled leukocytes is still an accurate and convenient tool to rule out suspected inflammatory bowel disease in children, Nuclear Medicine Review 22 (2019) 69–73, https://doi.org/10.5603/NMR.2019.0017.
[71] E.F.J. de Vries, M. Roca, F. Jamar, O. Israel, A. Signore, Guidelines for the labelling of leucocytes with 99mTc-HMPAO, Eur J Nucl Med Mol Imaging 37 (2010) 842–848, https://doi.org/10.1007/s00259-010-1394-4.
[72] K. Uno, K. Yoshikawa, K. Imazeki, S. Minoshima, N. Arimizu, Technetium-99m HMPAO labeled leukocytes in inflammation imaging, Ann. Nucl. Med. 5 (1991) 77–81, https://doi.org/10.1007/BF03164618.
[73] J.H. Reynolds, D. Graham, F.W. Smith, Imaging inflammation with 99Tcm HMPAO labelled leucocytes, Clin. Radiol. 42 (1990) 195–198, https://doi.org/10.1016/S0009-9260(05)81933-6.
[74] A.M. Peters, The utility of [99mTc]HMPAO-leukocytes for imaging infection, Semin. Nucl. Med. 24 (1994) 110–127, https://doi.org/10.1016/S0001-2998(05)80226-0.
[75] J.C. Mansfield, M.H. Giaffer, W.B. Tindale, C.D. Holdsworth, Quantitative assessment of overall inflammatory bowel disease activity using labelled leucocytes: a direct comparison between indium-111 and technetium-99m HMPAO methods, Gut 37 (1995) 679–683, https://doi.org/10.1136/gut.37.5.679.
[76] S. Migliari, A. Sammartano, C. Cidda, G. Baldari, M. Scarlattei, G. Serreli, C. Ghetti, S. Pipitone, G. Lippi, L. Ruffini, Novel approach for quality assessment and improving diagnostic accuracy in cell-based infection imaging using 99mTc-HMPAO labeled leukocytes, Acta Biomed. 89 (2018) 355–364. https://doi.org/10.23750/abm.v89i3.7064.
[77] F.J. van Hemert, R. Thurlings, S.E. Dohmen, C. Voermans, P.P. Tak, B.L.F. van Eck-Smit, R.J. Bennink, Labeling of autologous monocytes with 99mTc–HMPAO at very high specific radioactivity, Nucl. Med. Biol. 34 (2007) 933–938, https://doi.org/10.1016/j.nucmedbio.2007.07.008.
[78] R.M. Thurlings, C.A. Wijbrandts, R.J. Bennink, S.E. Dohmen, C. Voermans, D. Wouters, E.S. Izmailova, D.M. Gerlag, B.L.F. van Eck-Smit, P.P. Tak, Monocyte Scintigraphy in Rheumatoid Arthritis: The Dynamics of Monocyte Migration in Immune-Mediated Inflammatory Disease, PLoS ONE 4 (2009), https://doi.org/10.1371/journal.pone.0007865 e7865.
[79] R.J. Bennink, R.M. Thurlings, F.J. van Hemert, C. Voermans, S.E. Dohmen, B.L. van Eck-Smit, P.P. Tak, E. Busemann-Sokole, Biodistribution and Radiation Dosimetry of ^{99m}Tc-HMPAO–Labeled Monocytes in Patients with Rheumatoid Arthritis, J Nucl Med. 49 (2008) 1380, https://doi.org/10.2967/jnumed.108.051755.
[80] P. Ruparelia, K.R. Szczepura, C. Summers, C.K. Solanki, K. Balan, P. Newbold, D. Bilton, A.M. Peters, E.R. Chilvers, Quantification of neutrophil migration into the lungs of patients with chronic obstructive pulmonary disease, Eur. J. Nucl. Med. Mol. Imaging 38 (2011) 911–919, https://doi.org/10.1007/s00259-010-1715-7.
[81] J.J. Lukawska, L. Livieratos, B.M. Sawyer, T. Lee, M. O'Doherty, P.J. Blower, M. Kofi, J.R. Ballinger, C.J. Corrigan, G. Gnanasegaran, E. Sharif-Paghaleh, G.E.D. Mullen, Real-time differential tracking of human neutrophil and eosinophil migration in vivo, Journal of Allergy and Clinical Immunology. 133 (2014) 233–239.e1, https://doi.org/10.1016/j.jaci.2013.06.031.
[82] J.J. Lukawska, L. Livieratos, B.M. Sawyer, T. Lee, M. O'Doherty, P.J. Blower, M. Kofi, J.R. Ballinger, C.J. Corrigan, G. Gnanasegaran, E. Sharif-Paghaleh, G.E.D. Mullen, Imaging Inflammation in Asthma: Real Time, Differential Tracking of Human Neutrophil and Eosinophil Migration in Allergen Challenged, Atopic Asthmatics in Vivo, EBioMedicine. 1 (2014) 173–180, https://doi.org/10.1016/j.ebiom.2014.10.014.
[83] N. Farahi, C. Loutsios, N. Tregay, A.K.A. Wright, R. Berair, L.S.C. Lok, D. Gillett, I. Cullum, R.P. Simmonds, C. Summers, A. Wong, C.K. Solanki, J. Buscombe, P.H. Pang, A. Thavakumar, A.M. Peters, C.E. Brightling, A.M. Condliffe, E.R. Chilvers, In vivo imaging reveals increased eosinophil uptake in the lungs of obese asthmatic patients, J Allergy Clin Immunol. 142 (2018) 1659–1662.e8, https://doi.org/10.1016/j.jaci.2018.07.011.
[84] B. MatthewR, PhilipJ Puncher, Blower,, Autoradiography and density gradient separation of technetium-99m-Exametazime (HMPAO) labelled leucocytes reveals selectivity for eosinophils, Eur. J. Nucl. Med. 21 (1994) 1175–1182, https://doi.org/10.1007/BF00182350.
[85] J. Pillay, N. Tregay, G. Juzenaite, L.M. Carlin, C. Pirillo, D.C.A. Gaboriau, N. Farahi, C. Summers, C. Lo Celso, E.R. Chilvers, S. Rankin, K. De Filippo, Effect of the CXCR4 antagonist plerixafor on endogenous neutrophil dynamics in the bone marrow, lung and spleen, J. Leukoc. Biol. 107 (2020) 1175–1185, https://doi.org/10.1002/JLB.1MA0420-571RR.
[86] E. Sharif-Paghaleh, J. Leech, K. Sunassee, N. Ali, P. Sagoo, R.I. Lechler, L.A. Smyth, G. Lombardi, G.E. Mullen, Monitoring the efficacy of dendritic cell vaccination by early detection of 99mTc-HMPAO-labelled CD4+ T cells, Eur. J. Immunol. 44 (2014) 2188–2191, https://doi.org/10.1002/eji.201344337.
[87] R. Ridolfi, A. Riccobon, R. Galassi, G. Giorgetti, M. Petrini, L. Fiammenghi, M. Stefanelli, L. Ridolfi, A. Moretti, G. Migliori, G. Fiorentini, Evaluation of in vivo labelled dendritic cell migration in cancer patients, Journal of Translational Medicine. 2 (2004) 27, https://doi.org/10.1186/1479-5876-2-27.
[88] T. Yamamoto, K. Yoneda, T. Osaki, N. Yoshimura, N. Akagi, Longer local retention of adoptively transferred T-LAK cells correlates with lesser adhesion molecule expression than NK-LAK cells, Clin Exp Immunol. 100 (1995) 13–20, https://doi.org/10.1111/j.1365-2249.1995.tb03597.x.
[89] N.J. Carter, C.N.P. Eustance, S.F. Barrington, M.J. O'Doherty, A.J. Coakley, Imaging of abdominal infection using 99mTc stannous fluoride colloid labelled leukocytes, Nuclear Medicine Communications 23 (2002) 153–160, https://doi.org/10.1097/00006231-200202000-00007.
[90] T. Mochizuki, E. Tsukamoto, Y. Kuge, K. Kanegae, S. Zhao, K. Hikosaka, M. Hosokawa, M. Kohanawa, N. Tamaki, FDG Uptake and Glucose Transporter Subtype Expressions in Experimental Tumor and Inflammation Models, J. Nucl. Med. (2001) 1551-5. PMID: 11585872.
[91] B. Doyle, B.J. Kemp, P. Chareonthaitawee, C. Reed, J. Schmeckpeper, P. Sorajja, S. Russell, P. Araoz, S.J. Riederer, N.M. Caplice, Dynamic Tracking During

Intracoronary Injection of 18F-FDG-Labeled Progenitor Cell Therapy for Acute Myocardial Infarction, J. Nucl. Med. 48 (2007) 1708–1714, https://doi.org/10.2967/jnumed.107.042838.
[92] D. Pellegrino, A.A. Bonab, S.C. Dragotakes, J.T. Pitman, G. Mariani, E.A. Carter, Inflammation and Infection: Imaging Properties of 18F-FDG–Labeled White Blood Cells Versus, J. Nucl. Med. 46 (2005) 1522-30. PMID: 16157536.
[93] L.A. Forstrom, B.P. Mullan, J.C. Hung, V.J. Lowe, L.M. Thorson, 18F-FDG labelling of human leukocytes, Nucl. Med. Commun. 4 (2000) 691–694, https://doi.org/10.1097/00006231-200007000-00014.
[94] B. Pio, Noninvasive quantification of bowel inflammation through positron emission tomography imaging of 2-deoxy-2-[18F]fluoro-D-glucose-labeled white blood cells, Mol. Imag. Biol. 5 (2003) 271–277, https://doi.org/10.1016/S1536-1632(03)00103-3.
[95] S. Yilmaz, A. Aliyev, O. Ekmekcioglu, M. Ozhan, L. Uslu, B. Vatankulu, S. Sager, M. Halaç, K. Sönmezoğlu, Comparison of FDG and FDG-labeled leukocytes PET/CT in diagnosis of infection, Nuklearmedizin. 54 (2015) 262–271, https://doi.org/10.3413/Nukmed-0724-15-02.
[96] A. Bhattacharya, R. Kochhar, S. Sharma, P. Ray, N. Kalra, N. Khandelwal, B.R. Mittal, PET/CT with 18F-FDG-Labeled Autologous Leukocytes for the Diagnosis of Infected Fluid Collections in Acute Pancreatitis, J. Nucl. Med. 55 (2014) 1267–1272, https://doi.org/10.2967/jnumed.114.137232.
[97] M. Meyer, N. Testart, M. Jreige, C. Kamani, M. Moshebah, B. Muoio, M. Nicod-Lalonde, N. Schaefer, L. Giovanella, J.O. Prior, G. Treglia, Diagnostic Performance of PET or PET/CT Using 18F-FDG Labeled White Blood Cells in Infectious Diseases: A Systematic Review and a Bivariate Meta-Analysis, Diagnostics 9 (2019) 60, https://doi.org/10.3390/diagnostics9020060.
[98] B. Taciak, M. Białasek, P. Kucharzewska-Siembieda, Ł. Kiraga, A. Szulc, E. Górka, M. Kubiak, Z. Pilch, K. Tonecka, Z. Sas, A. Braniewska, Ł. Cheda, Z. Rogulski, M. Godlewski, A. Boffi, T. Rygiel, M. Król, Abstract B24: The macrophage-drug conjugate (MDC) as a "Trojan horse" approach in cancer therapy, Cancer Immunol Res. 8 (2020) B24, https://doi.org/10.1158/2326-6074.TUMIMM18-B24.
[99] S. Lacroix, D. Egrise, G. Van Simaeys, G. Doumont, M. Monclus, F. Sherer, T. Herbaux, D. Leroy, S. Goldman, [18 F]-FBEM, a tracer targeting cell-surface protein thiols for cell trafficking imaging: [18 F]-FBEM, A TRACER FOR CELL TRAFFICKING IMAGING, Contrast Media & Molecular Imaging. 8 (2013) 409–416, https://doi.org/10.1002/cmmi.1540.
[100] B. Bondue, F. Sherer, G. Van Simaeys, G. Doumont, D. Egrise, Y. Yakoub, F. Huaux, M. Parmentier, S. Rorive, S. Sauvage, S. Lacroix, O. Vosters, P. De Vuyst, S. Goldman, PET/CT with 18F-FDG- and 18F-FBEM-Labeled Leukocytes for Metabolic Activity and Leukocyte Recruitment Monitoring in a Mouse Model of Pulmonary Fibrosis, J. Nucl. Med. 56 (2015) 127–132, https://doi.org/10.2967/jnumed.114.147421.
[101] K. Lim, J. Ropchan, D.O. Kiesewetter, X. Chen, Y. Huang, Automated radiosynthesis of [18F]FBEM, a sulfhydryl site specific labeling agent for peptides and proteins, Appl. Radiat. Isot. 140 (2018) 294–299, https://doi.org/10.1016/j.apradiso.2018.07.033.
[102] L. Kiru, T.J. Kim, B. Shen, F.T. Chin, G. Pratx, Single-cell imaging using radioluminescence microscopy reveals unexpected binding target for [18F] HFB, Mol Imaging Biol. 20 (2018) 378–387, https://doi.org/10.1007/s11307-017-1144-0.
[103] Y. Zhang, J.N. Dasilva, T. Hadizad, S. Thorn, D. Kuraitis, J.M. Renaud, A. Ahmadi, M. Kordos, R.A. Dekemp, R.S. Beanlands, E.J. Suuronen, M. Ruel, 18 F-FDG Cell Labeling May Underestimate Transplanted Cell Homing: More Accurate, Efficient, and Stable Cell Labeling with Hexadecyl-4-[18 F] Fluorobenzoate for in Vivo Tracking of Transplanted Human Progenitor Cells by Positron Emission Tomography, Cell Transplant. 21 (2012) 1821–1835, https://doi.org/10.3727/096368911X637416.
[104] B. Gutfilen, S. Souza, G. Valentini, Copper-64: a real theranostic agent, DDDT. 12 (2018) 3235–3245, https://doi.org/10.2147/DDDT.S170879.
[105] Y. Zhou, J. Li, X. Xu, M. Zhao, B. Zhang, S. Deng, Y. Wu, 64 Cu-based Radiopharmaceuticals in Molecular Imaging, Technol Cancer Res Treat 18 (2019), https://doi.org/10.1177/1533033819830758.
[106] M. Conti, L. Eriksson, Physics of pure and non-pure positron emitters for PET: a review and a discussion, EJNMMI Phys. 3 (2016) 8, https://doi.org/10.1186/s40658-016-0144-5.
[107] R.G. Pearson, Hard and Soft Acids and Bases, J. Am. Chem. Soc. 85 (1963) 3533–3539, https://doi.org/10.1021/ja00905a001.
[108] H. Taube, Rates and Mechanisms of Substitution in Inorganic Complexes in Solution, Chem. Rev. 50 (1952) 69–126, https://doi.org/10.1021/cr60155a003.
[109] L.E. McInnes, S.E. Rudd, P.S. Donnelly, Copper, gallium and zirconium positron emission tomography imaging agents: The importance of metal ion speciation, Coord. Chem. Rev. 352 (2017) 499–516, https://doi.org/10.1016/j.ccr.2017.05.011.
[110] K. Vermeulen, M. Vandamme, G. Bormans, F. Cleeren, Design and Challenges of Radiopharmaceuticals, Semin. Nucl. Med. 49 (2019) 339–356, https://doi.org/10.1053/j.semnuclmed.2019.07.001.
[111] E.W. Price, C. Orvig, Matching chelators to radiometals for radiopharmaceuticals, Chem. Soc. Rev. 43 (2014) 260–290, https://doi.org/10.1039/C3CS60304K.
[112] W. Wei, Z.T. Rosenkrans, J. Liu, G. Huang, Q.-Y. Luo, W. Cai, ImmunoPET: Concept, Design, and Applications, Chem. Rev. 120 (2020) 3787–3851, https://doi.org/10.1021/acs.chemrev.9b00738.
[113] Z. Cai, C.J. Anderson, Chelators for copper radionuclides in positron emission tomography radiopharmaceuticals, J. Label. Compd. Radiopharm. 57 (2014) 224–230, https://doi.org/10.1002/jlcr.3165.
[114] M. Shokeen, C.J. Anderson, Molecular Imaging of Cancer with Copper-64 Radiopharmaceuticals and Positron Emission Tomography (PET), Acc. Chem. Res. 42 (2009) 832–841, https://doi.org/10.1021/ar800255q.
[115] J.-J. Park, T.-S. Lee, J.-J. Son, K.-S. Chun, I.-H. Song, Y.-S. Park, K.-I. Kim, Y.-J. Lee, J.-H. Kang, Comparison of Cell-Labeling Methods with ^{124} I-FIAU and ^{64} Cu-PTSM for Cell Tracking Using Chronic Myelogenous Leukemia Cells Expressing HSV1-tk and Firefly Luciferase, Cancer Biother. Radiopharm. 27 (2012) 719–728, https://doi.org/10.1089/cbr.2012.1225.
[116] C.M. Griessinger, R. Kehlbach, D. Bukala, S. Wiehr, R. Bantleon, F. Cay, A. Schmid, H. Braumuller, B. Fehrenbacher, M. Schaller, M. Eichner, J.L. Sutcliffe, W. Ehrlichmann, O. Eibl, G. Reischl, S.R. Cherry, M. Rocken, B.J. Pichler, M. Kneilling, In Vivo Tracking of Th1 Cells by PET Reveals Quantitative and Temporal Distribution and Specific Homing in Lymphatic Tissue, J. Nucl. Med. 55 (2014) 301–307, https://doi.org/10.2967/jnumed.113.126318.
[117] K.K. Bhargava, R.K. Gupta, K.J. Nichols, C.J. Palestro, In vitro human leukocyte labeling with 64Cu: an intraindividual comparison with 111In-oxine and 18F-FDG, Nucl. Med. Biol. 36 (2009) 545–549, https://doi.org/10.1016/j.nucmedbio.2009.03.001.
[118] A. Socan, M. Petrik, P. Kolenc Peitl, M. Krošelj, C. Rangger, Z. Novy, U. Svajger, T. Gmeiner, C. Decristoforo, On-cartridge preparation and evaluation of 68Ga-, 89Zr- and 64Cu-precursors for cell radiolabelling, Nucl. Med. Biol. 71 (2019) 23–31, https://doi.org/10.1016/j.nucmedbio.2019.04.001.
[119] Leung K. 64Cu-Polyethylenimine. 2010 Apr 16 [Updated 2010 Jul 1]. In: Molecular Imaging and Contrast Agent Database (MICAD) [Internet]. Bethesda (MD): National Center for Biotechnology Information (US); 2004-2013. Available from: https://www.ncbi.nlm.nih.gov/books/NBK44815/
[120] Z. Wang, P. Huang, O. Jacobson, Z. Wang, Y. Liu, L. Lin, J. Lin, N. Lu, H. Zhang, R. Tian, G. Niu, G. Liu, X. Chen, Biomineralization-Inspired Synthesis of Copper Sulfide-Ferritin Nanocages as Cancer Theranostics, ACS Nano 10 (2016) 3453–3460, https://doi.org/10.1021/acsnano.5b07521.
[121] T. Zhao, S. Zhang, Y. Guo, Q. Wang, TiC 2: a new two-dimensional sheet beyond MXenes, Nanoscale. 8 (2016) 233–242, https://doi.org/10.1039/C5NR04472C.
[122] Ł Kiraga, Ł Cheda, Taciak, K Różańska, K Tonecka, A Szulc, K Kilian, E Górka, Z Rogulski, T.P. Rygiel, M. Król, Changes in hypoxia level of CT26 tumors during various stages of development and comparing different methods of hypoxia determination, PLOS ONE 13 (2018) e0206706, https://doi.org/10.1371/journal.pone.0206706.
[123] H.A. Watson, R.R.P. Durairaj, J. Ohme, M. Alatsatianos, H. Almutairi, R.N. Mohammed, M. Vigar, S.G. Reed, S.J. Paisey, C. Marshall, A. Gallimore, A. Ager, L-Selectin Enhanced T Cells Improve the Efficacy of Cancer Immunotherapy, Front Immunol. 10 (2019) 1321, https://doi.org/10.3389/fimmu.2019.01321.
[124] P. Kathirgamanathan, S. Surendrakumar, J. Antipan-Lara, S. Ravichandran, V. R. Reddy, S. Ganeshamurugan, M. Kumaraverl, V. Arkley, A.J. Blake, D. Bailey, Discovery of two new phases of zirconium tetrakis(8-hydroxyquinolinolate): synthesis, crystal structure and their electron transporting characteristics in organic light emitting diodes (OLEDs), J. Mater. Chem. 21 (2011) 1762–1771, https://doi.org/10.1039/C0JM02644A.
[125] T.J. Ferris, P. Charoenphun, L.K. Meszaros, G.E.D. Mullen, P.J. Blower, M.J. Went, Synthesis and characterisation of zirconium complexes for cell tracking with Zr-89 by positron emission tomography, Dalton Trans. 43 (2014) 14851–14857, https://doi.org/10.1039/C4DT01928H.
[126] P. Charoenphun, L.K. Meszaros, K. Chuamsaamarkkee, E. Sharif-Paghaleh, J.R. Ballinger, T.J. Ferris, M.J. Went, G.E.D. Mullen, P.J. Blower, [89Zr]Oxinate4 for long-term in vivo cell tracking by positron emission tomography, Eur. J. Nucl. Med. Mol. Imaging 42 (2015) 278–287, https://doi.org/10.1007/s00259-014-2945-x.
[127] N. Sato, H. Wu, K.O. Asiedu, L.P. Szajek, G.L. Griffiths, P.L. Choyke, ^{89} Zr-Oxine Complex PET Cell Imaging in Monitoring Cell-based Therapies, Radiology 275 (2015) 490–500, https://doi.org/10.1148/radiol.15142849.
[128] S.J. Paisey, J. Ohme, C. Marshall, A. Ager, Zr-89 Labelling of Immunotherapeutic Tumour Specific T-Cells to measure L-Selectin Dependent Homing in a Murine Cancer Model, Eur. J. Nucl. Med. Mol. Imaging. 43 (2016) S71–S71.
[129] F. Man, L. Lim, A. Volpe, A. Gabizon, H. Shmeeda, B. Draper, A.C. Parente-Pereira, J. Maher, P.J. Blower, G.O. Fruhwirth, R.T.M. de Rosales, In Vivo PET Tracking of 89Zr-Labeled Vγ9Vδ2 T Cells to Mouse Xenograft Breast Tumors Activated with Liposomal Alendronate, Mol. Ther. 27 (2019) 219–229, https://doi.org/10.1016/j.ymthe.2018.10.006.
[130] S. Krebs, M.M. Dacek, L.M. Carter, D.A. Scheinberg, S.M. Larson, CAR Chase, Where Do Engineered Cells Go in Humans?, Front Oncol 10 (2020) 577773, https://doi.org/10.3389/fonc.2020.577773.
[131] M.R. Weist, R. Starr, B. Aguilar, J. Chea, J.K. Miles, E. Poku, E. Gerdts, X. Yang, S. J. Priceman, S.J. Forman, D. Colcher, C.E. Brown, J.E. Shively, PET of Adoptively Transferred Chimeric Antigen Receptor T Cells with ^{89} Zr-Oxine, J Nucl Med. 59 (2018) 1531–1537, https://doi.org/10.2967/jnumed.117.206714.
[132] Y. Kurebayashi, P.L. Choyke, N. Sato, Imaging of cell-based therapy using (89) Zr-oxine ex vivo cell labeling for positron emission tomography, Nanotheranostics. 5 (2021) 27–35, https://doi.org/10.7150/ntno.51391.
[133] F. Man, A.A. Khan, A. Carrascal-Miniño, P.J. Blower, R.T.M. de Rosales, A kit formulation for the preparation of [89Zr]Zr(oxinate)4 for PET cell tracking: White blood cell labelling and comparison with [111In]In(oxinate)3, Nucl. Med. Biol. 90–91 (2020) 31–40, https://doi.org/10.1016/j.nucmedbio.2020.09.002.

[134] A.V.F. Massicano, J.L. Bartels, C.D. Jeffers, B.K. Crenshaw, H. Houson, C. Mueller, J.W. Younger, P. Knapp, J.E. McConathy, S.E. Lapi, Production of [89Zr]Oxinate4 and cell radiolabeling for human use, Journal of Labelled Compounds and Radiopharmaceuticals. 64 (2020) 209–216, https://doi.org/10.1002/jlcr.3901.
[135] N. Sato, K. Stringaris, J.K. Davidson-Moncada, R. Reger, S.S. Adler, C. Dunbar, P. L. Choyke, R.W. Childs, In Vivo Tracking of Adoptively Transferred Natural Killer Cells in Rhesus Macaques Using ^{89}Zirconium-Oxine Cell Labeling and PET Imaging, Clin Cancer Res. 26 (2020) 2573–2581, https://doi.org/10.1158/1078-0432.CCR-19-2897.
[136] N.B. Bhatt, D.N. Pandya, T.J. Wadas, Recent Advances in Zirconium-89 Chelator Development, Molecules 23 (2018) 638, https://doi.org/10.3390/molecules23030638.
[137] J.-K. Yoon, B.-N. Park, E.-K. Ryu, Y.-S. An, S.-J. Lee, Current Perspectives on 89Zr-PET Imaging, Int. J. Mol. Sci. 21 (2020) 4309, https://doi.org/10.3390/ijms21124309.
[138] J.R. Dilworth, S.I. Pascu, The chemistry of PET imaging with zirconium-89, Chem. Soc. Rev. 47 (2018) 2554–2571, https://doi.org/10.1039/C7CS00014F.
[139] S. Heskamp, R. Raavé, O. Boerman, M. Rijpkema, V. Goncalves, F. Denat, ^{89} Zr-Immuno-Positron Emission Tomography in Oncology: State-of-the-Art ^{89} Zr Radiochemistry, Bioconjugate Chem. 28 (2017) 2211–2223, https://doi.org/10.1021/acs.bioconjchem.7b00325.
[140] M.J.W.D. Vosjan, L.R. Perk, G.W.M. Visser, M. Budde, P. Jurek, G.E. Kiefer, G.A. M.S. van Dongen, Conjugation and radiolabeling of monoclonal antibodies with zirconium-89 for PET imaging using the bifunctional chelate p-isothiocyanatobenzyl-desferrioxamine, Nat. Protocols. 5 (2010) 739–743, https://doi.org/10.1038/nprot.2010.13.
[141] Ł Kiraga, G Cerutti, A Braniewska, D Strzemecki, Z Sas, A Boffi, C Savino, LC Montemiglio, D Turnham, G Seaton, A Bonamore, R Clarkson, A Dabkowski, S Paisey, B Taciak, P Kucharzewska, T.P. Rygiel, M Król, Biodistribution PET/CT Study of Hemoglobin-DFO-^{89}Zr Complex in Healthy and Lung Tumor-Bearing Mice, International Journal of Molecular Sciences 21 (2020) 4991, https://doi.org/10.3390/ijms21144991.
[142] S.H. Lee, H. Soh, J.H. Chung, E.H. Cho, S.J. Lee, J.-M. Ju, J.H. Sheen, H. Kim, S.J. Oh, S.-J. Lee, J. Chung, K. Choi, S.-Y. Kim, J.-S. Ryu, Feasibility of real-time in vivo 89Zr-DFO-labeled CAR T-cell trafficking using PET imaging, PLoS ONE 15 (2020), https://doi.org/10.1371/journal.pone.0223814 e0223814.
[143] A. Bansal, M.K. Pandey, S. Yamada, R. Goyal, N.R. Schmit, R. Jeon, J.J. Nesbitt, T. A. Witt, R.D. Singh, T.M. Gunderson, S. Boroumand, M. Li, R.J. Crespo-Diaz, M. L. Hillestad, A. Terzic, A. Behfar, T.R. DeGrado, [89Zr]Zr-DBN labeled cardiopoietic stem cells proficient for heart failure, Nucl. Med. Biol. 90–91 (2020) 23–30, https://doi.org/10.1016/j.nucmedbio.2020.09.001.
[144] M. Fairclough, C. Prenant, B. Ellis, H. Boutin, A. McMahon, G. Brown, P. Locatelli, A.K.P. Jones, A new technique for the radiolabelling of mixed leukocytes with zirconium-89 for inflammation imaging with positron emission tomography: Radiolabelling leukocytes with ^{89} Zr for inflammation imaging with PET, J. Label Compd. Radiopharm. 59 (2016) 270–276, https://doi.org/10.1002/jlcr.3392.
[145] M. Wilks, D. Albrecht, H. Yuan, G. El Fakhri, P. Brugarolas, M. Normandin, ^{89}Zr-Nanoparticle Based PET Imaging of B-cell Trafficking in a Murine Model of Multiple Sclerosis, J Nucl Med. 59 (2018) 264.
[146] M. Wilks, P. Reeves, H. Yuan, F. Kools, K. Takahashi, C. Kaittanis, G. El Fakhri, L. Josephson, M. Poznansky, M. Normandin, In vivo PET imaging of T-cell trafficking by ^{89}Zr-radiolabeled nanoparticles, J Nucl Med. 58 (2017) 622.
[147] M. Wilks, P. Reeves, H. Yuan, K. Takahashi, C. Yang, M. Poznansky, L. Josephson, G. El Fakhri, M. Normandin, Nanoparticle-Based PET Imaging of T-cell Trafficking in Immuno-Competent Murine Tumor Models, J Nucl Med. 61 (2020) 1207.
[148] J.-S. Choi, A.J. Berdis, Nucleoside transporters: biological insights and therapeutic applications, Future Med. Chem. 4 (2012) 1461–1478, https://doi.org/10.4155/fmc.12.79.
[149] R.G. Richards, L.C. Sowers, J. Laszlo, W.D. Sedwick, The occurrence and consequences of deoxyuridine in DNA, Adv. Enzyme Regul. 22 (1984) 157–185, https://doi.org/10.1016/0065-2571(84)90013-X.
[150] H. Williams, P. Julyan, M. Ranson, J. Zweit, J. Gillies, D. Hastings, Does 124Iodo-deoxyuridine measure cell proliferation in NSCLC?, Initial investigations with PET imaging and radio-metabolite analysis, European Journal of Nuclear Medicine and Molecular Imaging. 34 (2007) 301–303, https://doi.org/10.1007/s00259-006-0107-5.
[151] I. Guenther, L. Wyer, E.J. Knust, R.D. Finn, J. Koziorowski, R. Weinreich, Radiosynthesis and Quality Assurance of 5-[124I]Iodo-2′-deoxyuridine for Functional PET Imaging of Cell Proliferation, Nucl. Med. Biol. 25 (1998) 359–365, https://doi.org/10.1016/S0969-8051(97)00220-5.
[152] K.O. Jung, T.J. Kim, J.H. Yu, S. Rhee, W. Zhao, B. Ha, K. Red-Horse, S.S. Gambhir, G. Pratx, Whole-body tracking of single cells via positron emission tomography, Nat. Biomed. Eng. 4 (2020) 835–844, https://doi.org/10.1038/s41551-020-0570-5.
[153] X. Wang, Y. Wang, Q. Wu, J. Liu, Y. Liu, D. Pan, W. Qi, L. Wang, J. Yan, Y. Xu, G. Wang, L. Miao, L. Yu, M. Yang, Feasibility study of 68Ga-labeled CAR T cells for in vivo tracking using micro-positron emission tomography imaging, Acta Pharmacol. Sin. 42 (2020) 824–831, https://doi.org/10.1038/s41401-020-00511-5.
[154] J. Barbet, M. Bardiès, M. Bourgeois, J.-F. Chatal, M. Chérel, F. Davodeau, A. Faivre-Chauvet, J.-F. Gestin, F. Kraeber-Bodéré, Radiolabeled Antibodies for Cancer Imaging and Therapy, in: P. Chames (Ed.), Antibody Engineering, Humana Press, Totowa, NJ, 2012, pp. 681–697, https://doi.org/10.1007/978-1-61779-974-7_38.
[155] P. Kręcisz, K. Czarnecka, L. Królicki, E. Mikiciuk-Olasik, P. Szymański, Radiolabeled Peptides and Antibodies in Medicine, Bioconjugate Chem. 32 (2021) 25–42, https://doi.org/10.1021/acs.bioconjchem.0c00617.
[156] A.H. Alnahwi, S. Ait-Mohand, V. Dumulon-Perreault, Y.L. Dory, B. Guérin, Promising Performance of 4HMS, a New Zirconium-89 Octadendate Chelator, ACS Omega 5 (2020) 10731–10739, https://doi.org/10.1021/acsomega.0c00207.
[157] B.A. Rhodes, P.O. Zamora, K.D. Newell, E.F. Valdez, Technetium-99m labeling of murine monoclonal antibody fragments, Journal of Nuclear Medicine : Official Publication, Society of Nuclear Medicine 27 (1986) 685–693.
[158] C.H. Paik, L.N.B. Phan, J.J. Hong, M.S. Sahami, S.C. Heald, R.C. Reba, J. Steigman, W.C. Eckelman, The labeling of high affinity sites of antibodies with 99mTc, Int. J. Nucl. Med. Biol. 12 (1985) 3–8, https://doi.org/10.1016/0047-0740(85)90004-X.
[159] E. Hawkins, K. Pant, B. Rhodes, Resistance of direct Tc-99m-protein bond to transchelation, Antibody Immunoconj. Radiopharm. 3 (1990) 17–25.
[160] B.A. Rhodes, Direct labeling of proteins with 99mTc, International Journal of Radiation Applications and Instrumentation, Part B. Nuclear Medicine and Biology. 18 (1991) 667–676, https://doi.org/10.1016/0883-2897(91)90004-5.
[161] A.E. Martell, R.D. Hancock, R.J. Motekaitis, Factors affecting stabilities of chelate, macrocyclic and macrobicyclic complexes in solution, Coord. Chem. Rev. 133 (1994) 39–65, https://doi.org/10.1016/0010-8545(94)80056-1.
[162] D Goldenberg, R Sharkey, Novel radiolabeled antibody conjugates, Oncogene 26 (2007) 3734–3744, https://doi.org/10.1038/sj.onc.1210373.
[163] B. Hendriks, D. Gaddy, Radiolabeled Antibody-Based Imaging in Clinical Oncology: Fundamentals, Drug Development, and Clinical Outcomes to Target Cancer, in (2016) 431–472, https://doi.org/10.1002/9781119060727.ch17.
[164] N. Pandit-Taskar, M.A. Postow, Immune-Directed Molecular Imaging Biomarkers, Semin. Nucl. Med. 50 (2020) 584–603, https://doi.org/10.1053/j.semnuclmed.2020.06.005.
[165] P. Mondello, S. Cuzzocrea, M. Navarra, M. Mian, 90 Y-ibritumomab tiuxetan: a nearly forgotten opportunity, Oncotarget. 7 (2016) 7597–7609. 10.18632/oncotarget.6531.
[166] H. Kawashima, Radioimmunotherapy: A Specific Treatment Protocol for Cancer by Cytotoxic Radioisotopes Conjugated to Antibodies, The Scientific World Journal. 2014 (2014) 1–10, https://doi.org/10.1155/2014/492061.
[167] G. Malviya, C. D'Alessandria, E. Bonanno, V. Vexler, R. Massari, C. Trotta, F. Scopinaro, R. Dierckx, A. Signore, Radiolabeled Humanized Anti-CD3 Monoclonal Antibody Visilizumab for Imaging Human T-Lymphocytes, J. Nucl. Med. 50 (2009) 1683–1691, https://doi.org/10.2967/jnumed.108.059485.
[168] S. Krebs, A. Ahad, L.M. Carter, J. Eyquem, C. Brand, M. Bell, V. Ponomarev, T. Reiner, C.F. Meares, S. Gottschalk, M. Sadelain, S.M. Larson, W.A. Weber, Antibody with Infinite Affinity for In Vivo Tracking of Genetically Engineered Lymphocytes, J Nucl Med. 59 (2018) 1894–1900, https://doi.org/10.2967/jnumed.118.208041.
[169] E.Yu. Grigor'eva, Yu.V. Stukalov, A.V. Smirnova, E. Yu. Koldaeva, N.S. Kalygina, V.N. Kulakov, A.Yu. Baryshnikov, Cytotoxicity of Conjugates of 188Re-Labeled Dendrimers and Monoclonal Antibodies Anti-ICO-25 (MUC1) and Anti-ICO-80 (CD5) Against SKOV-3 (Ovary Cancer) and Jurkat Tumor Cell Lines (T-Lymphoblstic Lymphoma), Pharm Chem J. 52 (2018) 681–684, https://doi.org/10.1007/s11094-018-1880-8.
[170] S.H.L. Hoffmann, D.I. Reck, A. Maurer, B. Fehrenbacher, J.E. Sceneay, M. Poxleitner, H.H. Öz, W. Ehrlichmann, G. Reischl, K. Fuchs, M. Schaller, D. Hartl, M. Kneilling, A. Möller, B.J. Pichler, C.M. Griessinger, Visualization and quantification of *in vivo* homing kinetics of myeloid-derived suppressor cells in primary and metastatic cancer, Theranostics. 9 (2019) 5869–5885, https://doi.org/10.7150/thno.33275.
[171] D.M. Goldenberg, Targeted Therapy of Cancer with Radiolabeled Antibodies, J. Nucl. Med. 43 (2002) 693-713. PMID: 11994535.
[172] M.F. Leahy, J.H. Turner, Radioimmunotherapy of relapsed indolent non-Hodgkin lymphoma with 131I-rituximab in routine clinical practice: 10-year single-institution experience of 142 consecutive patients, Blood 117 (2011) 45–52, https://doi.org/10.1182/blood-2010-02-269753.
[173] Jh. Turner, P. Calais, Standard Operating Procedure for Prospective Individualised Dosimetry for $^{[131]}$ I-rituximab Radioimmunotherapy of Non-Hodgkin's Lymphoma, World J Nucl Med. 11 (2012) 110, https://doi.org/10.4103/1450-1147.103409.
[174] G.W. Kang, H.J. Kang, D.-Y. Shin, H.R. Gu, H.S. Choi, S.M. Lim, Radioimmunotherapy with 131I-Rituximab in a Patient with Diffuse Large B-Cell Lymphoma Relapsed After Treatment with 90Y-Ibritumomab Tiuxetan 47 (2013) 281–284, https://doi.org/10.1007/s13139-013-0229-1.
[175] T.M. Illidge, M. Bayne, N.S. Brown, S. Chilton, M.S. Cragg, M.J. Glennie, Y. Du, V. Lewington, J. Smart, J. Thom, M. Zivanovic, P.W.M. Johnson, Phase 1/2 study of fractionated 131I-rituximab in low-grade B-cell lymphoma: the effect of prior rituximab dosing and tumor burden on subsequent radioimmunotherapy, Blood 113 (2009) 1412–1421, https://doi.org/10.1182/blood-2008-08-175653.

[176] G.L. DeNardo, D.L. Kukis, S. Shen, D.A. DeNardo, C.F. Meares, S.J. DeNardo, 67Cu- versus 131I-Labeled Lym-1 Antibody: Comparative Pharmacokinetics and Dosimetry in Patients with Non-Hodgkin's Lymphoma, Clin Cancer Res. 5 (1999) 533-41, PMID: 10100704.
[177] G.L. DeNardo, S.J. DeNardo, R.T. O'Donnell, L.A. Kroger, D.L. Kukis, C.F. Meares, D.S. Goldstein, S. Shen, Are Radiometal-Labeled Antibodies Better Than Iodine- 131–Labeled Antibodies: Comparative Pharmacokinetics and Dosimetry of Copper-67–, Iodine-131–, and Yttrium-90–Labeled Lym-1 Antibody in Patients with Non-Hodgkin's Lymphoma, Clin Lymphoma 1 (2000) 118–126, https://doi.org/10.3816/clm.2000.n.010.
[178] G.L. Griffiths, S.V. Govindan, R.M. Sharkey, D.R. Fisher, D.M. Goldenberg, 90Y-DOTA-hLL2: An Agent for Radioimmunotherapy of Non-Hodgkin's Lymphoma, J. Nucl. Med. 44 (2003) 77-84, PMID: 12515879.
[179] R.M. Sharkey, A. Brenner, J. Burton, G. Hajjar, S.P. Toder, A. Alavi, A. Matthies, D.E. Tsai, S.J. Schuster, E.A. Stadtmauer, M.S. Czuczman, D. Lamonica, F. Kraeber-Bodere, B. Mahe, J.-F. Chatal, A. Rogatko, G. Mardirrosian, D.M. Goldenberg, Radioimmunotherapy of Non-Hodgkin's Lymphoma with 90Y-DOTA Humanized Anti-CD22 IgG (90Y-Epratuzumab): Do Tumor Targeting and Dosimetry Predict Therapeutic Response? J. Nucl. Med. 44 (2003) 2000-18. PMID: 14660727.
[180] T.E. Witzig, M.B. Tomblyn, J.G. Misleh, E.A. Kio, R.M. Sharkey, W.A. Wegener, D.M. Goldenberg, Anti-CD22 90Y-epratuzumab tetraxetan combined with anti-CD20 veltuzumab: a phase I study in patients with relapsed/refractory, aggressive non-Hodgkin lymphoma, Haematologica 99 (2014) 1738–1745, https://doi.org/10.3324/haematol.2014.112110.
[181] D.V. Gold, T. Cardillo, D.M. Goldenberg, R.M. Sharkey, Localization of pancreatic cancer with radiolabeled monoclonal antibody PAM4, Critical Reviews in Oncology/Hematology. 39 (2001) 147–154, https://doi.org/10.1016/S1040-8428(01)00114-7.
[182] G. Sgouros, B.M. Mehta, R.D. Finn, S.M. Larson, D.A. Scheinberg, Pharmacokinetics and Dosimetry of an a-Particle Emitter Labeled Antibody: 213Bi-HuM195 (Anti-CD33) in Patients with Leukemia, J. Nucl. Med. 40 (1999) 1935-46, PMID: 10565792.
[183] T.L. Rosenblat, M.R. McDevitt, D.A. Mulford, N. Pandit-Taskar, C.R. Divgi, K.S. Panageas, M.L. Heaney, S. Chanel, A. Morgenstern, G. Sgouros, S.M. Larson, D. A. Scheinberg, J.G. Jurcic, Sequential Cytarabine and α-Particle Immunotherapy with Bismuth-213–Lintuzumab (HuM195) for Acute Myeloid Leukemia, Clin Cancer Res. 16 (2010) 5303–5311, https://doi.org/10.1158/1078-0432.CCR-10-0382.
[184] J.G. Jurcic, T.L. Rosenblat, Targeted Alpha-Particle Immunotherapy for Acute Myeloid Leukemia, American Society of Clinical Oncology Educational Book. (2014) e126–e131, https://doi.org/10.14694/EdBook_AM.2014.34.e126.
[185] S. Abedin, G.S. Guru Murthy, L. Runaas, L.C. Michaelis, E.L. Atallah, M. Hamadani, A.M. Harrington, K. Carlson, Lintuzumab Ac-225 in Combination with CLAG-M Chemotherapy in Relapsed/Refractory AML: Interim Results of a Phase I Study, Blood. 134 (2019) 2605–2605. https://doi.org/10.1182/blood-2019-122487.
[186] J. Burke, P. Caron, E. Papadopoulos, C. Divgi, G. Sgouros, K. Panageas, S. Larson, R. O'Reilly, D. Scheinberg, J. Jurcic, Cytoreduction with iodine-131-anti-CD33 antibodies before bone marrow transplantation for advanced myeloid leukemias, Bone Marrow Transplant 32 (2003) 549–556, https://doi.org/10.1038/sj.bmt.1704201.
[187] C. Bailly, S. Gouard, F. Guérard, B. Chalopin, T. Carlier, A. Faivre-Chauvet, P. Remaud-Le Saëc, M. Bourgeois, N. Chouin, L. Rbah-Vidal, R. Tripier, F. Haddad, F. Kraeber-Bodéré, C. Bodet-Milin, M. Chérel, What is the Best Radionuclide for Immuno-PET of Multiple Myeloma? A Comparison Study Between 89Zr- and 64Cu-Labeled Anti-CD138 in a Preclinical Syngeneic Model, IJMS. 20 (2019) 2564, https://doi.org/10.3390/ijms20102564.
[188] M. Cherel, S. Gouard, J. Gaschet, C. Sai-Maurel, F. Bruchertseifer, A. Morgenstern, M. Bourgeois, J.-F. Gestin, F.K. Bodere, J. Barbet, P. Moreau, F. Davodeau, 213Bi Radioimmunotherapy with an Anti-mCD138 Monoclonal Antibody in a Murine Model of Multiple Myeloma, J. Nucl. Med. 54 (2013) 1597–1604, https://doi.org/10.2967/jnumed.112.111997.
[189] C. Rousseau, L. Ferrer, S. Supiot, M. Bardiès, F. Davodeau, A. Faivre-Chauvet, P. Baumgartner, J. Wijdenes, M. Lacombe, J. Barbet, T. Guillaume, P. Moreau, J.L. Harousseau, F. Kraeber-Bodéré, M. Cherel, Dosimetry results suggest feasibility of radioimmunotherapy using anti-CD138 (B-B4) antibody in multiple myeloma patients, Tumor Biol. 10 (2012) 679–688, https://doi.org/10.1007/s13277-012-0362-y.
[190] N. Bander, Targeted systemic therapy of prostate cancer with a monoclonal antibody to prostate-specific membrane antigen, Semin. Oncol. 30 (2003) 667–676, https://doi.org/10.1016/S0093-7754(03)00358-0.
[191] E.K. Fung, S.M. Cheal, S.B. Fareedy, B. Punzalan, V. Beylergil, J. Amir, S. Chalasani, W.A. Weber, D.E. Spratt, D.R. Veach, N.H. Bander, S.M. Larson, P.B. Zanzonico, J.R. Osborne, Targeting of radiolabeled J591 antibody to PSMA-expressing tumors: optimization of imaging and therapy based on non-linear compartmental modeling, EJNMMI Res. 6 (2016) 7, https://doi.org/10.1186/s13550-016-0164-0.
[192] L.R. Perk, G.W.M. Visser, B.M. Tijink, C.R. Leemans, 89Zr as a PET Surrogate Radioisotope for Scouting Biodistribution of the Therapeutic Radiometals 90Y and 177Lu in Tumor-Bearing Nude Mice After Coupling to the Internalizing Antibody Cetuximab, J. Nucl. Med. 46 (2005) 1898-906, PMID: 16269605
[193] P.J. Perik, M.N. Lub-De Hooge, J.A. Gietema, W.T.A. van der Graaf, M.A. de Korte, S. Jonkman, J.G.W. Kosterink, D.J. van Veldhuisen, D.T. Sleijfer, P.L. Jager, E.G.E. de Vries, Indium-111–Labeled Trastuzumab Scintigraphy in Patients With Human Epidermal Growth Factor Receptor 2–Positive Metastatic Breast Cancer, JCO. 24 (2006) 2276–2282, https://doi.org/10.1200/JCO.2005.03.8448.
[194] S.B.M. Gaykema, J.R. de Jong, P.J. Perik, A.H. Brouwers, C.P. Schröder, T.H.O. Munnink, A.H.H. Bongaerts, E.G.E. de Vries, M.N.L. Hooge, 111 In-Trastuzumab Scintigraphy in HER2-Positive Metastatic Breast Cancer Patients Remains Feasible during Trastuzumab Treatment, Mol Imaging 13 (2014), https://doi.org/10.2310/7290.2014.00011.
[195] C.M.B. Holloway, Phase I trial of intraoperative detection of tumor margins in patients with HER2-positive carcinoma of the breast following administration of 111In-DTPA-trastuzumab Fab fragments, Nucl. Med. Biol. 8 (2013) 630–637, https://doi.org/10.1016/j.nucmedbio.2013.03.005.
[196] J. Sorensen, D. Sandberg, M. Sandstrom, A. Wennborg, J. Feldwisch, V. Tolmachev, G. Astrom, M. Lubberink, U. Garske-Roman, J. Carlsson, H. Lindman, First-in-Human Molecular Imaging of HER2 Expression in Breast Cancer Metastases Using the 111In-ABY-025 Affibody Molecule, J. Nucl. Med. 55 (2014) 730–735, https://doi.org/10.2967/jnumed.113.131243.
[197] A. Orlova, V. Tolmachev, R. Pehrson, M. Lindborg, T. Tran, M. Sandstrom, F.Y. Nilsson, A. Wennborg, L. Abrahmsen, J. Feldwisch, Synthetic Affibody Molecules: A Novel Class of Affinity Ligands for Molecular Imaging of HER2-Expressing Malignant Tumors, Cancer Res. 10 (2007) 2178–2186, https://doi.org/10.1158/0008-5472.CAN-06-2887.
[198] T. Tran, T. Engfeldt, A. Orlova, M. Sandström, J. Feldwisch, L. Abrahmsén, A. Wennborg, V. Tolmachev, A.E. Karlström, 99mTc-maEEE-ZHER2:342, an Affibody Molecule-Based Tracer for the Detection of HER2 Expression in Malignant Tumors, Bioconjug Chem 18 (2007) 1956–1964, https://doi.org/10.1021/bc7002617.
[199] V. Tolmachev, F.Y. Nilsson, C. Widstrom, K. Andersson, D. Rosik, L. Gedda, A. Wennborg, A. Orlova, 111In-Benzyl-DTPA–ZHER2:342, an Affibody-Based Conjugate for In Vivo Imaging of HER2 Expression in Malignant Tumors, J. Nucl. Med. 47 (2006) 846-53. PMID:16644755.
[200] G. Kramer-Marek, D.O. Kiesewetter, L. Martiniova, E. Jagoda, S.B. Lee, J. Capala, [18F]FBEM-ZHER2:342-Affibody molecule—a new molecular tracer for in vivo monitoring of HER2 expression by positron emission tomography, Eur J Nucl Med Mol Imaging. 35 (2008) 1008–1018, https://doi.org/10.1007/s00259-007-0658-0.
[201] M. D'Huyvetter, J. De Vos, C. Xavier, M. Pruszynski, Y.G.J. Sterckx, S. Massa, G. Raes, V. Caveliers, M.R. Zalutsky, T. Lahoutte, N. Devoogdt, ^{131} I-labeled Anti-HER2 Camelid sdAb as a Theranostic Tool in Cancer Treatment, Clin Cancer Res. 23 (2017) 6616–6628, https://doi.org/10.1158/1078-0432.CCR-17-0310.
[202] C.D. Martins, C. Da Pieve, T.A. Burley, R. Smith, D.M. Ciobota, L. Allott, K.J. Harrington, W.J.G. Oyen, G. Smith, G. Kramer-Marek, HER3-Mediated Resistance to Hsp90 Inhibition Detected in Breast Cancer Xenografts by Affibody-Based PET Imaging, Clin Cancer Res. 24 (2018) 1853–1865, https://doi.org/10.1158/1078-0432.CCR-17-2754.
[203] S. Shibata, A. Raubitschek, L. Leong, M. Koczywas, L. Williams, J. Zhan, J.Y.C. Wong, A Phase I Study of a Combination of Yttrium-90-Labeled Anti-Carcinoembryonic Antigen (CEA) Antibody and Gemcitabine in Patients with CEA-Producing Advanced Malignancies, Clin. Cancer Res. 15 (2009) 2935–2941, https://doi.org/10.1158/1078-0432.CCR-08-2213.
[204] J.Y.C. Wong, S. Shibata, L.E. Williams, C.S. Kwok, A. Liu, D.Z. Chu, D.M. Yamauchi, S. Wilczynski, D.N. Ikle, A.M. Wu, P.J. Yazaki, J.E. Shively, J.H. Doroshow, A.A. Raubitschek, A Phase I Trial of 90Y-Anti-Carcinoembryonic Antigen Chimeric T84.66 Radioimmunotherapy with 5-Fluorouracil in Patients with Metastatic Colorectal Cancer, Clin Cancer Res. 1 (2003) 5842-52, PMID: 14676105.
[205] J.Y.C. Wong, D.Z. Chu, L.E. Williams, A. Liu, J. Zhan, D.M. Yamauchi, S. Wilczynski, A.M. Wu, P.J. Yazaki, J.E. Shively, L. Leong, A.A. Raubitschek, A Phase I Trial of ^{90}Y-DOTA-Anti-CEA Chimeric T84.66 (cT84.66) Radioimmunotherapy in Patients with Metastatic CEA-Producing Malignancies, Cancer Biother. Radiopharm. 21 (2006) 88–100, https://doi.org/10.1089/cbr.2006.21.88.
[206] J.Y.C. Wong, G.E. Thomas, D. Yamauchi, L.E. Williams, T.L. Odom-Maryon, A. Liu, J.M. Esteban, M. Neumaier, S. Dresse, A.M. Wu, F.J. Primus, J.E. Shively, Clinical Evaluation of Indium- 111-Labeled Chimeric Anti-CEA Monoclonal Antibody, J. Nucl. Med. 38 (1997) 1951-9, PMID: 9430476.
[207] T. Meyer, A.M. Gaya, G. Dancey, M.R.L. Stratford, S. Othman, S.K. Sharma, D. Wellsted, N.J. Taylor, J.J. Stirling, L. Poupard, L.K. Folkes, P.-s Chan, R.B. Pedley, K.A. Chester, K. Owen, J.A. Violet, A. Malaroda, A.J. Green, J. Buscombe, A.R. Padhani, G.J. Rustin, R.H. Begent, A Phase I Trial of Radioimmunotherapy with 131I–A5B7 Anti-CEA Antibody in Combination with Combretastatin-A4-Phosphate in Advanced Gastrointestinal Carcinomas, Clin. Cancer Res. 15 (2009) 4484–4492, https://doi.org/10.1158/1078-0432.CCR-09-0035.
[208] J.L. Casey, R.B. Pedley, D.J. King, A.J. Green, G.T. Yarranton, R.H.J. Begent, Dosimetric evaluation and radioimmunotherapy of anti-tumour multivalent Fab′ fragments, Br J Cancer. 81 (1999) 972–980, https://doi.org/10.1038/sj.bjc.6690795.
[209] V. Rajkumar, V. Goh, M. Siddique, M. Robson, G. Boxer, R.B. Pedley, G.J.R. Cook, Texture analysis of 125I–A5B7 anti-CEA antibody SPECT differentiates metastatic colorectal cancer model phenotypes and anti-vascular therapy response, Br J Cancer. 112 (2015) 1882–1887, https://doi.org/10.1038/bjc.2015.166.
[210] T.A. Burley, C. Da Pieve, C.D. Martins, D.M. Ciobota, L. Allott, W.J.G. Oyen, K.J. Harrington, G. Smith, G. Kramer-Marek, Affibody-Based PET Imaging to Guide EGFR-Targeted Cancer Therapy in Head and Neck Squamous Cell Cancer Models, J Nucl Med. 60 (2019) 353–361, https://doi.org/10.2967/jnumed.118.216069.

[211] E. Nordberg, A. Orlova, M. Friedman, V. Tolmachev, S. Ståhl, F. Nilsson, B. Glimelius, J. Carlsson, In vivo and in vitro uptake of 111In, delivered with the affibody molecule (ZEGFR:955)2, in EGFR expressing tumour cells, Oncol Rep. 19 (2008) 853–857, https://doi.org/10.3892/or.19.4.853.
[212] J. Mohammadnejad, M.J. Rasaee, M.H. Babaei, M. Paknejad, Z.M. Hasan, M. Salouti, M. Gandomkar, K. Sadri, Radioimmunotherapy of MCF7 breast cancer cell line with 131I-PR81 monoclonal antibody against MUC1: Comparison of direct and indirect radioiodination methods, HAB. 19 (2010) 15–25, https://doi.org/10.3233/HAB-2010-0216.
[213] M. Salouti, H. Rajabi, M. Babaei, M. Rassaee, R. Najafi, M. Paknejad, M. Hasan, T. Altarihi, J. Nejad, A new monoclonal antibody radiopharmaceutical for radioimmunoscintigraphy of breast cancer: Direct labeling of antibody and its quality control, Daru, Journal of Faculty of Pharmacy, Tehran University of Medical Sciences. 14 (2006) 51–56.
[214] S.H.L. Hoffmann, A. Maurer, D.I. Reck, G. Reischl, B.J. Pichler, M. Kneilling, C.M. Griessinger, Murine Lymphocyte Labeling by ^{64}Cu-Antibody Receptor Targeting for In Vivo Cell Trafficking by PET/CT, JoVE. (2017) 55270, https://doi.org/10.3791/55270.
[215] H.J. Schroth, E. Oberhausen, R. Berberich, Cell labelling with colloidal substances in whole blood, Eur J Nucl Med. 6 (1981), https://doi.org/10.1007/BF00252805.
[216] E.J. Keliher, J. Yoo, M. Nahrendorf, J.S. Lewis, B. Marinelli, A. Newton, M.J. Pittet, R. Weissleder, ^{89} Zr-Labeled Dextran Nanoparticles Allow in Vivo Macrophage Imaging, Bioconjugate Chem. 22 (2011) 2383–2389, https://doi.org/10.1021/bc200405d.
[217] M.H. Kim, Y.J. Lee, J.H. Kang, Stem Cell Monitoring with a Direct or Indirect Labeling Method, Nuclear Medicine and Molecular Imaging. 50 (2016) 275–283, https://doi.org/10.1007/s13139-015-0380-y.
[218] D.J. Ellis, Silencing and Variegation of Gammaretrovirus and Lentivirus Vectors, Hum. Gene Ther. 16 (2005) 1241–1246, https://doi.org/10.1089/hum.2005.16.1241.
[219] M. Krishnan, J.M. Park, F. Cao, D. Wang, R. Paulmurugan, J.R. Tseng, M.L. Gonzalgo, S.S. Gambhir, J.C. Wu, Effects of epigenetic modulation on reporter gene expression: implications for stem cell imaging, FASEB j. 20 (2006) 106–108, https://doi.org/10.1096/fj.05-4551fje.
[220] A. De, X.Z. Lewis, S.S. Gambhir, Noninvasive imaging of lentiviral-mediated reporter gene expression in living mice, Mol. Ther. 7 (2003) 681–691, https://doi.org/10.1016/S1525-0016(03)00070-4.
[221] N. Emami-Shahri, J. Foster, R. Kashani, P. Gazinska, C. Cook, J. Sosabowski, J. Maher, S. Papa, Clinically compliant spatial and temporal imaging of chimeric antigen receptor T-cells, Nat Commun. 9 (2018) 1081, https://doi.org/10.1038/s41467-018-03524-1.
[222] A.M. Hamilton, P.J. Foster, J.A. Ronald, Evaluating Nonintegrating Lentiviruses as Safe Vectors for Noninvasive Reporter-Based Molecular Imaging of Multipotent Mesenchymal Stem Cells, Hum. Gene Ther. 29 (2018) 1213–1225, https://doi.org/10.1089/hum.2018.111.
[223] M. Li, Y. Wang, M. Liu, X. Lan, Multimodality reporter gene imaging: Construction strategies and application, Theranostics. 8 (2018) 2954–2973, https://doi.org/10.7150/thno.24108.
[224] A.P. Lam, D.A. Dean, Progress and prospects: nuclear import of nonviral vectors, Gene Ther. 17 (2010) 439–447, https://doi.org/10.1038/gt.2010.31.
[225] P.K. Nguyen, J. Riegler, J.C. Wu, Stem Cell Imaging: From Bench to Bedside, Cell Stem Cell 14 (2014) 431–444, https://doi.org/10.1016/j.stem.2014.03.009.
[226] C. Ashmore-Harris, M. Iafrate, A. Saleem, G.O. Fruhwirth, Non-invasive Reporter Gene Imaging of Cell Therapies, including T Cells and Stem Cells, Mol. Ther. 28 (2020) 1392–1416, https://doi.org/10.1016/j.ymthe.2020.03.016.
[227] J.-J. Min, S.S. Gambhir, Molecular Imaging of PET Reporter Gene Expression, in: W. Semmler, M. Schwaiger (Eds.), Molecular Imaging II, Springer, Berlin Heidelberg, Berlin, Heidelberg, 2008, pp. 277–303, https://doi.org/10.1007/978-3-540-77496-9_12.
[228] J.T. Lee, H. Zhang, M.A. Moroz, Y. Likar, L. Shenker, N. Sumzin, J. Lobo, J. Zurita, J. Collins, R.M. van Dam, V. Ponomarev, Comparative Analysis of Human Nucleoside Kinase-Based Reporter Systems for PET Imaging, Mol. Imag. Biol. 19 (2017) 100–108, https://doi.org/10.1007/s11307-016-0981-6.
[229] G. Koehne, M. Doubrovin, E. Doubrovina, P. Zanzonico, H.F. Gallardo, A. Ivanova, J. Balatoni, J. Teruya-Feldstein, G. Heller, C. May, V. Ponomarev, S. Ruan, R. Finn, R.G. Blasberg, W. Bornmann, I. Riviere, M. Sadelain, R.J. O'Reilly, S.M. Larson, J.G. Gelovani Tjuvajev, Serial in vivo imaging of the targeted migration of human HSV-TK-transduced antigen-specific lymphocytes, Nat Biotechnol. 21 (2003) 405–413, https://doi.org/10.1038/nbt805.
[230] S.S. Yaghoubi, M.C. Jensen, N. Satyamurthy, S. Budhiraja, D. Paik, J. Czernin, S. S. Gambhir, Noninvasive detection of therapeutic cytolytic T cells with 18F–FHBG PET in a patient with glioma, Nat Rev Clin Oncol. 6 (2009) 53–58, https://doi.org/10.1038/ncponc1278.
[231] K.V. Keu, T.H. Witney, S. Yaghoubi, J. Rosenberg, A. Kurien, R. Magnusson, J. Williams, F. Habte, J.R. Wagner, S. Forman, C. Brown, M. Allen-Auerbach, J. Czernin, W. Tang, M.C. Jensen, B. Badie, S.S. Gambhir, Reporter gene imaging of targeted T cell immunotherapy in recurrent glioma, Sci. Transl. Med. 9 (2017) eaag2196, https://doi.org/10.1126/scitranslmed.aag2196.
[232] Q. Liang, N. Satyamurthy, J. Barrio, T. Toyokuni, M. Phelps, S. Gambhir, H. Herschman, Noninvasive, quantitative imaging in living animals of a mutant dopamine D2 receptor reporter gene in which ligand binding is uncoupled from signal transduction, Gene Ther. 8 (2001) 1490–1498, https://doi.org/10.1038/sj.gt.3301542.
[233] Y. Likar, J. Zurita, K. Dobrenkov, L. Shenker, S. Cai, A. Neschadim, J.A. Medin, M. Sadelain, H. Hricak, V. Ponomarev, A New Pyrimidine-Specific Reporter Gene: A Mutated Human Deoxycytidine Kinase Suitable for PET During Treatment with Acycloguanosine-Based Cytotoxic Drugs, J. Nucl. Med. 51 (2010) 1395–1403, https://doi.org/10.2967/jnumed.109.074344.
[234] H. Zhang, M.A. Moroz, I. Serganova, T. Ku, R. Huang, J. Vider, H.R. Maecke, S.M. Larson, R. Blasberg, P.M. Smith-Jones, Imaging Expression of the Human Somatostatin Receptor Subtype-2 Reporter Gene with 68Ga-DOTATOC, J. Nucl. Med. 52 (2011) 123–131, https://doi.org/10.2967/jnumed.110.079004.
[235] Y. Vedvyas, E. Shevlin, M. Zaman, I.M. Min, A. Amor-Coarasa, S. Park, S. Park, K.-W. Kwon, T. Smith, Y. Luo, D. Kim, Y. Kim, B. Law, R. Ting, J. Babich, M.M. Jin, Longitudinal PET imaging demonstrates biphasic CAR T cell responses in survivors, JCI Insight. 1 (2016), https://doi.org/10.1172/jci.insight.90064 e90064.
[236] Alan R. Penheiter, Stephen J. Russell, Stephanie K. Carlson, The Sodium Iodide Symporter (NIS) as an Imaging Reporter for Gene, Viral, and Cell-based Therapies, CGT. 12 (2012) 33–47, https://doi.org/10.2174/156652312799789235.
[237] S.B. Lee, H.W. Lee, H. Lee, Y.H. Jeon, S.-W. Lee, B.-C. Ahn, J. Lee, S.Y. Jeong, Tracking dendritic cell migration into lymph nodes by using a novel PET probe 18F-tetrafluoroborate for sodium/iodide symporter, EJNMMI Res. 7 (2017) 32, https://doi.org/10.1186/s13550-017-0280-5.
[238] M.M. Doubrovin, E.S. Doubrovina, P. Zanzonico, M. Sadelain, S.M. Larson, R.J. O'Reilly, In vivo Imaging and Quantitation of Adoptively Transferred Human Antigen-Specific T Cells Transduced to Express a Human Norepinephrine Transporter Gene, Cancer Res. 67 (2007) 11959–11969, https://doi.org/10.1158/0008-5472.CAN-07-1250.
[239] M.A. Moroz, I. Serganova, P. Zanzonico, L. Ageyeva, T. Beresten, E. Dyomina, E. Burnazi, R.D. Finn, M. Doubrovin, R.G. Blasberg, Imaging hNET Reporter Gene Expression with 124I-MIBG, J. Nucl. Med. 48 (2007) 827–836, https://doi.org/10.2967/jnumed.106.037812.
[240] A.Y. Zhao, A.F. Brooks, D.M. Raffel, J. Stauff, J. Arteaga, P.J.H. Scott, X. Shao, Fully Automated Radiosynthesis of [11C]Guanidines for Cardiac PET Imaging, ACS Med. Chem. Lett. 11 (2020) 2325–2330, https://doi.org/10.1021/acsmedchemlett.0c00479.
[241] E. Sharif-Paghaleh, K. Sunassee, R. Tavaré, K. Ratnasothy, A. Koers, N. Ali, R. Alhabbab, P.J. Blower, R.I. Lechler, L.A. Smyth, G.E. Mullen, G. Lombardi, In Vivo SPECT Reporter Gene Imaging of Regulatory T Cells, PLoS ONE 6 (2011), https://doi.org/10.1371/journal.pone.0025857 e25857.
[242] M.A. Moroz, H. Zhang, J. Lee, E. Moroz, J. Zurita, L. Shenker, I. Serganova, R. Blasberg, V. Ponomarev, Comparative Analysis of T Cell Imaging with Human Nuclear Reporter Genes, J. Nucl. Med. 56 (2015) 1055–1060, https://doi.org/10.2967/jnumed.115.159855.
[243] W. Wei, D. Jiang, E.B. Ehlerding, Q. Luo, W. Cai, Noninvasive PET Imaging of T cells, Trends in Cancer. 4 (2018) 359–373, https://doi.org/10.1016/j.trecan.2018.03.009.
[244] M. Thunemann, B.F. Schörg, S. Feil, Y. Lin, J. Voelkl, M. Golla, A. Vachaviolos, U. Kohlhofer, L. Quintanilla-Martinez, M. Olbrich, W. Ehrlichmann, G. Reischl, C. M. Griessinger, H.F. Langer, M. Gawaz, F. Lang, M. Schäfers, M. Kneilling, B.J. Pichler, R. Feil, Cre/lox-assisted non-invasive in vivo tracking of specific cell populations by positron emission tomography, Nat Commun. 8 (2017) 444, https://doi.org/10.1038/s41467-017-00482-y.
[245] S.S. Yaghoubi, S.S. Gambhir, PET imaging of herpes simplex virus type 1 thymidine kinase (HSV1-tk) or mutant HSV1-sr39tk reporter gene expression in mice and humans using [18F]FHBG, Nat Protoc. 1 (2006) 3069–3074, https://doi.org/10.1038/nprot.2006.459.
[246] M.N. McCracken, D.N. Vatakis, D. Dixit, J. McLaughlin, J.A. Zack, O.N. Witte, Noninvasive detection of tumor-infiltrating T cells by PET reporter imaging, J. Clin. Invest. 125 (2015) 1815–1826, https://doi.org/10.1172/JCI77326.
[247] S.-B. Ahn, S.B. Lee, T.D. Singh, S.J. Cho, S.K. Kim, I.-K. Lee, S.Y. Jeong, B.-C. Ahn, J. Lee, S.-W. Lee, Y.H. Jeon, Multimodality Imaging of Bone Marrow-Derived Dendritic Cell Migration and Antitumor Immunity, Transl. Oncol. 10 (2017) 262–270, https://doi.org/10.1016/j.tranon.2017.01.003.
[248] A. Volpe, C. Lang, L. Lim, F. Man, E. Kurtys, C. Ashmore-Harris, P. Johnson, E. Skourti, R.T.M. de Rosales, G.O. Fruhwirth, Spatiotemporal PET Imaging Reveals Differences in CAR-T Tumor Retention in Triple-Negative Breast Cancer Models, Mol. Ther. 28 (2020) 2271–2285, https://doi.org/10.1016/j.ymthe.2020.06.028.
[249] I. Minn, D.J. Huss, H.-H. Ahn, T.M. Chinn, A. Park, J. Jones, M. Brummet, S.P. Rowe, P. Sysa-Shah, Y. Du, H.I. Levitsky, M.G. Pomper, Imaging CAR T cell therapy with PSMA-targeted positron emission tomography, Sci Adv. 5 (2019) eaaw5096, https://doi.org/10.1126/sciadv.aaw5096.
[250] J.W.M. Bulte, H.E. Daldrup-Link, Clinical Tracking of Cell Transfer and Cell Transplantation: Trials and Tribulations, Radiology 289 (2018) 604–615, https://doi.org/10.1148/radiol.2018180449.
[251] GE Healthcare, Medi-Physics, Inc. Arlington Heights, IL 60004 U.S.A. INDIUM In 111 OXYQUINOLINE SOLUTION For the Radiolabeling of Autologous Leukocytes Rx ONLY Diagnostic; URL: https://www.gehealthcare.com/-/media/09213f4199d04b119331e5088bf73f1e.pdf (accessed 15 March 2021).
[252] R.J.M. ten Berge, A.T. Natarajan, M.R. Hardeman, E.A. van Royen, P.Th.A. Schellekens, Labeling with Indium-111 has Detrimental Effects on Human Lymphocytes: Concise Communication, J Nucl Med. 24 (1983) 615.
[253] S. Ebbe, S. Taylor, H. Maurer, B. Kullgren, Uptake of Indium-111-Labeled Platelets and Indium-111 Oxine by Murine Kidneys after Total-Body Irradiation, Radiat. Res. 146 (1996) 216–222, https://doi.org/10.2307/3579593.

[254] H. Kobayashi, C. Wu, M.-K. Kim, C.H. Paik, J.A. Carrasquillo, M.W. Brechbiel, Evaluation of the in Vivo Biodistribution of Indium-111 and Yttrium-88 Labeled Dendrimer-1B4M-DTPA and Its Conjugation with Anti-Tac Monoclonal Antibody, Bioconjugate Chem. 10 (1999) 103–111, https://doi.org/10.1021/bc980091d.
[255] INTERNATIONAL ATOMIC ENERGY AGENCY, Radiolabelled Autologous Cells: Methods and Standardization for Clinical Use, Human Health Series No. 5, IAEA, Vienna (2015).
[256] L. Hendershott, R. Gentilcore, F. Ordway, J. Fletcher, R. Donati, Tropolone: A lipid solubilizing agent for cationic metals, Eur. J. Nucl. Med. 7 (1982) 234–236, https://doi.org/10.1007/BF00256471.
[257] Health Products Regulatory Summary of Product Characteristics (Ceretec 500 micrograms kit for radiopharmaceutical preparation); URL: https://www.hpra.ie/img/uploaded/swedocuments/Licence_PA0735-013-001_30042019131219.pdf (accessed 15 March 2021).
[258] C. Tsopelas, E. Smith, P.A. Drew, F.D.L. Bartholomeusz, Preparation and biological evaluation of99mTc-stannous fluoride colloid-labelled-leucocytes in rats99mTc-stannous fluoride-labelled-leucocytes in rats, J. Labelled Cpd. Radiopharm. 46 (2003) 751–763, https://doi.org/10.1002/jlcr.715.
[259] F.Z. Ahmed, J. James, M.J. Memmott, P. Arumugam, Radionuclide Imaging of Cardiovascular Infection, Cardiol. Clin. 34 (2016) 149–165, https://doi.org/10.1016/j.ccl.2015.06.004.
[260] F. Jamar, J. Buscombe, A. Chiti, P.E. Christian, D. Delbeke, K.J. Donohoe, O. Israel, J. Martin-Comin, A. Signore, EANM/SNMMI Guideline for ^{18}F-FDG Use in Inflammation and Infection, J Nucl Med. 54 (2013) 647, https://doi.org/10.2967/jnumed.112.112524.
[261] FDA: NDA 21-870: Fludeoxyglucose F 18 Injection. https://www.accessdata.fda.gov/drugsatfda_docs/label/2005/021870lbl.pdf, 2021 (accessed March 15, 2021).
[262] M.A. Green, A potential copper radiopharmaceutical for imaging the heart and brain: Copper-labeled pyruvaldehyde bis(N4-methylthiosemicarbazone), International Journal of Radiation Applications and Instrumentation, Part B. Nuclear Medicine and Biology. 14 (1987) 59–61, https://doi.org/10.1016/0883-2897(87)90162-0.
[263] S. Thompson, M. Rodnick, P. Scott, B. Viglianti, Automated Synthesis of [^{68}Ga] Gallium Oxine (KP-46) and Preparation of ^{68}Ga-labelled Erythrocytes for Imaging the Vasculature, J Nucl Med. 58 (2017) 481.
[264] M.N. McCracken, R. Tavaré, O.N. Witte, A.M. Wu, Chapter Five - Advances in PET Detection of the Antitumor T Cell Response, in: F.W. Alt (Ed.), Advances in Immunology, Academic Press, 2016, pp. 187–231, https://doi.org/10.1016/bs.ai.2016.02.004.
[265] Z.-B. Li, K. Chen, Z. Wu, H. Wang, G. Niu, X. Chen, 64Cu-Labeled PEGylated Polyethylenimine for Cell Trafficking and Tumor Imaging, Mol. Imag. Biol. 11 (2009) 415, https://doi.org/10.1007/s11307-009-0228-x.
[266] Z. Yuan, J. Li, D. Zhu, X. Sun, T. Gong, Z. Zhang, Enhanced accumulation of low-molecular-weight chitosan in kidneys: a study on the influence of N-acetylation of chitosan on the renal targeting, Null. 19 (2011) 540–551, https://doi.org/10.3109/1061186X.2010.521158.
[267] W.-P. Deng, W.K. Yang, W.-F. Lai, R.-S. Liu, J.-J. Hwang, D.-M. Yang, Y.-K. Fu, H.-E. Wang, Non-invasive in vivo imaging with radiolabelled FIAU for monitoring cancer gene therapy using herpes simplex virus type 1 thymidine kinase and ganciclovir, Eur. J. Nucl. Med. Mol. Imaging 31 (2004) 99–109, https://doi.org/10.1007/s00259-003-1269-z.
[268] S.V. Selivanova, É. Lavallée, H. Senta, L. Caouette, A.J.B. McEwan, B. Guérin, R. Lecomte, É. Turcotte, Clinical Trial with Sodium ^{99m}Tc-Pertechnetate Produced by a Medium-Energy Cyclotron: Biodistribution and Safety Assessment in Patients with Abnormal Thyroid Function, J Nucl Med. 58 (2017) 791, https://doi.org/10.2967/jnumed.116.178509.
[269] E. Bombardieri, F. Giammarile, C. Aktolun, R.P. Baum, A. Bischof Delaloye, L. Maffioli, R. Moncayo, L. Mortelmans, G. Pepe, S.N. Reske, M.R. Castellani, A. Chiti, 131I/123I-Metaiodobenzylguanidine (mIBG) scintigraphy: procedure guidelines for tumour imaging, Eur. J. Nucl. Med. Mol. Imaging 37 (2010) 2436–2446, https://doi.org/10.1007/s00259-010-1545-7.
[270] S. Vallabhajosula, A. Nikolopoulou, Radioiodinated Metaiodobenzylguanidine (MIBG): Radiochemistry, Biology, and Pharmacology, Seminars in Nuclear Medicine. 41 (2011) 324–333, https://doi.org/10.1053/j.semnuclmed.2011.05.003.
[271] E. Bombardieri, V. Ambrosini, C. Aktolun, R.P. Baum, A. Bishof-Delaloye, S. Del Vecchio, L. Maffioli, L. Mortelmans, W. Oyen, G. Pepe, A. Chiti, 111In-pentetreotide scintigraphy: procedure guidelines for tumour imaging, Eur. J. Nucl. Med. Mol. Imaging 37 (2010) 1441–1448, https://doi.org/10.1007/s00259-010-1473-6.
[272] M.G. Stabin, P.P.M. Kooij, W.H. Bakker, T. Inoue, K. Endo, J. Coveney, R. de Jong, A. Minegishi, Radiation Dosimetry for Indium-111-Pentetreotide, J. Nucl. Med. 38 (1997) 1919-22, PMID: 9430470.
[273] A. Jacobs, I. Bräunlich, R. Graf, M. Lercher, T. Sakaki, J. Voges, V. Hesselmann, W. Brandau, K. Wienhard, W.-D. Heiss, Quantitative Kinetics of [^{124}I]FIAU in Cat and Man, J Nucl Med. 42 (2001) 467.
[274] X.M. Zhang, H.H. Zhang, P. McLeroth, R.D. Berkowitz, M.A. Mont, M.G. Stabin, B.A. Siegel, A. Alavi, T.M. Barnett, J. Gelb, C. Petit, J. Spaltro, S.Y. Cho, M.G. Pomper, J.J. Conklin, C. Bettegowda, S. Saha, [124I]FIAU: Human dosimetry and infection imaging in patients with suspected prosthetic joint infection, Nucl. Med. Biol. 43 (2016) 273–279, https://doi.org/10.1016/j.nucmedbio.2016.01.004.
[275] L.A. Diaz Jr., C.A. Foss, K. Thornton, S. Nimmagadda, C.J. Endres, O. Uzuner, T. M. Seyler, S.D. Ulrich, J. Conway, C. Bettegowda, N. Agrawal, I. Cheong, X. Zhang, P.W. Ladenson, B.N. Vogelstein, M.A. Mont, S. Zhou, K.W. Kinzler, B. Vogelstein, M.G. Pomper, Imaging of Musculoskeletal Bacterial Infections by [124I]FIAU-PET/CT, PLoS ONE 2 (2007), https://doi.org/10.1371/journal.pone.0001007 e1007.
[276] S. Yaghoubi, J.R. Barrio, M. Dahlbom, M. Iyer, M. Namavari, N. Satyamurthy, R. Goldman, H.R. Herschman, M.E. Phelps, S.S. Gambhir, Human Pharmacokinetic and Dosimetry Studies of [^{18}F]FHBG: A Reporter Probe for Imaging Herpes Simplex Virus Type-1 Thymidine Kinase Reporter Gene Expression, J Nucl Med. 42 (2001) 1225.
[277] A. Ruggiero, P. Brader, I. Serganova, P. Zanzonico, S. Cai, N.S. Lipman, H. Hricak, R.G. Blasberg, Different strategies for reducing intestinal background radioactivity associated with imaging HSV1-tk expression using established radionucleoside probes, Mol Imaging. 9 (2010) 47–58.
[278] D.O. Campbell, S.S. Yaghoubi, Y. Su, J.T. Lee, M.S. Auerbach, H. Herschman, N. Satyamurthy, J. Czernin, A. Lavie, C.G. Radu, Structure-guided Engineering of Human Thymidine Kinase 2 as a Positron Emission Tomography Reporter Gene for Enhanced Phosphorylation of Non-natural Thymidine Analog Reporter Probe*, J. Biol. Chem. 287 (2012) 446–454, https://doi.org/10.1074/jbc.M111.314666.
[279] H. Jiang, N.R. Schmit, A.R. Koenen, A. Bansal, M.K. Pandey, R.B. Glynn, B.J. Kemp, K.L. Delaney, A. Dispenzieri, J.N. Bakkum-Gamez, K.-W. Peng, S.J. Russell, T.M. Gunderson, V.J. Lowe, T.R. DeGrado, Safety, pharmacokinetics, metabolism and radiation dosimetry of (18)F-tetrafluoroborate ((18)F-TFB) in healthy human subjects, EJNMMI Res. 7 (2017) 90–90. https://doi.org/10.1186/s13550-017-0337-5.
[280] C.-L. Lee, H. Wahnishe, G.A. Sayre, H.-M. Cho, H.-J. Kim, M. Hernandez-Pampaloni, R.A. Hawkins, S.F. Dannoon, H.F. VanBrocklin, M. Itsara, W.A. Weiss, X. Yang, D.A. Haas-Kogan, K.K. Matthay, Y. Seo, Radiation dose estimation using preclinical imaging with 124I-metaiodobenzylguanidine (MIBG) PET, Med Phys. 37 (2010) 4861–4867, https://doi.org/10.1118/1.3480965.
[281] N. Pandit-Taskar, P.B. Zanzonico, K.D. Staton, J.A. Carrasquillo, D. Reidy-Lagunes, S.K. Lyashchenko, E. Burnazi, H. Zhang, J.S. Lewis, R. Blasberg, S.M. Larson, W.A. Weber, S. Modak, Biodistribution and dosimetry of 18F-Meta Fluorobenzyl Guanidine (MFBG): A first-in-human PET-CT imaging study of patients with neuroendocrine malignancies, J Nucl Med 59 (2017) 147–153, https://doi.org/10.2967/jnumed.117.193169.
[282] M. Sandström, I. Velikyan, U. Garske-Román, J. Sörensen, B. Eriksson, D. Granberg, H. Lundqvist, A. Sundin, M. Lubberink, Comparative Biodistribution and Radiation Dosimetry of ^{68}Ga-DOTATOC and ^{68}Ga-DOTATATE in Patients with Neuroendocrine Tumors, J Nucl Med. 54 (2013) 1755, https://doi.org/10.2967/jnumed.113.120600.
[283] S.A. Esfahani, S. Salcedo, P. Heidari, O.A. Catalano, R. Pauplis, J. Hesterman, J.F. Kronauge, U. Mahmood, A phase one, single-dose, open-label, clinical safety and PET/MR imaging study of (68)Ga-DOTATOC in healthy volunteers, Am J Nucl Med Mol Imaging. 7 (2017) 53–62.
[284] G. Ferreira, A. Iravani, M.S. Hofman, R.J. Hicks, Intra-individual comparison of (68)Ga-PSMA-11 and (18)F-DCFPyL normal-organ biodistribution, Cancer Imaging. 19 (2019) 23–23. https://doi.org/10.1186/s40644-019-0211-y.
[285] Z. Szabo, E. Mena, S.P. Rowe, D. Plyku, R. Nidal, M.A. Eisenberger, E.S. Antonarakis, H. Fan, R.F. Dannals, Y. Chen, R.C. Mease, M. Vranesic, A. Bhatnagar, G. Sgouros, S.Y. Cho, M.G. Pomper, Initial Evaluation of [18F] DCFPyL for Prostate-Specific Membrane Antigen (PSMA)-Targeted PET Imaging of Prostate Cancer, Mol. Imag. Biol. 17 (2015) 565–574, https://doi.org/10.1007/s11307-015-0850-8.
[286] G.A.M.S. van Dongen, R. Boellaard, D.J. Vugts, In vivo tracking of single cells with PET, Nat. Biomed. Eng. 4 (2020) 765–766, https://doi.org/10.1038/s41551-020-0598-6.